The potential of renewable energy sources for powering of trolleybus grids - An Arnhem case-study

by

Bram Scheurwater

in partial fulfilment of the requirements for the degree of

Master of Science in Sustainable Energy Technology
Track: Autonomous energy systems

at the Delft University of Technology,
Faculty of Electrical Engineering, Mathematics & Computer Science,
to be defended on 6 November 2020

Supervision:
ir. I. Diab
dr. ir. G.R Chandramouli
Prof. dr. ir. P. Bauer
Dr. P. Manganiello

TU Delft

Preface

I did my bachelor in Chemical Engineering because I was interested in solving technical problems. When I started my masters in Sustainable Energy Technologies this interested evolved from solving technical problems to a passion for increasing the renewable energy in the world to reduce the devastating effects of climate change.

When Ibrahim offered me the opportunity to work with him on solving the sustainability issues of trolley grids, I did not have to wait long to make the decision. I am glad that I could help with creating a framework for mapping trolley bus loads and showing the potential for solar PV to increase the renewable energy share. My hope is that other students at the TU Delft and elsewhere can continue this work and renew trolley grids all around the world to solve one small piece in the puzzle against climate change.

First of all, I am grateful for the support that I received from Ibrahim throughout this thesis. He was always present to answer any question on short notice and I have learned alot from him. Next, I would like to thank dr.ir. Gautham Chandra Mouli for the support and creative ideas that he showed in the monthly meetings. I would also like to thank Prof. dr. ir P. Bauer for his input in the midterm and for granting me with the green light to defend my work. Last but certainly not least, I would like to thank my friends, family and my girlfriend Minne for listening to my boring monologues for hours. This thesis wouldn't be possible without their support. Thank you all.

With warm regards,

Bram

Summary

Trolleybuses use electricity for movement. This electricity may be generated in a non-renewable way, contributing to the devastating effects of climate change [1]. In this work, a case-study on the Arnhem trolley grid is executed to reach the following objective:

Investigating the attainable renewable energy share of the Arnhem trolleybus grid while minimizing the need for seasonal storage.

The research is limited to the use of PhotoVoltaics (PV) and wind energy as energy sources.

First a model for the trolley grid load must be established. In this work, the year-round bus loads on the substations are constructed with a bottom-up approach. Velocity and power measurements for each bus line are combined with the timetables of the buses to construct the location and magnitude of the bus loads in the Arnhem grid throughout the year. Next, the bus loads are separated into the different grid sections. Finally, the grid sections are combined into substations.

Initially, the PV was placed on the substations (between the transformer and the rectifier) to allow grid dump into the AC-grid. The sizes of the PV systems were optimized on the basis of a net social benefit criterion. It was found that 13 of the 18 substations should not have PV installed and that the remaining substations should only have a few percent of an energy neutral system installed (maximum 23%). The overall increase in renewable energy share (RES) with this approach is 8.2%. Simply increasing the PV size and curtailing the excess PV to limit grid dump is not a successful strategy to improve the RES due to the inconsistent stream of bus traffic under the substations. The extra installed PV will send a larger power share to the AC-grid.

To increase the RES further, stationary energy storage was sized. It was found that for a substation with a constant stream of traffic and for a substation with inconsistent traffic, two PV and storage combinations have potential. A 50% energy neutral system with 10 KWh of storage can be an affordable option that can increase the RES to 35% while using the Arnhem grid to provide seasonal storage for 25% of the PV (for both substations). To increase the RES further, an 80% energy neutral PV system could be installed with 0.5 to 1 MWh of storage for the constant traffic substation and between 200 and 400 kWh for the inconsistent traffic substation. In both cases, the PV utilization increases to 55-60% while the grid dump is 25-30% for the constant traffic substation and 18-24% for the in consistent traffic substation. It makes sense that the constant traffic substation needs more storage, since the PV system is six times larger. Increasing the PV system with 20% increases the RES by 5-10% while the grid dump increases by 10-15%. Increasing the storage size would make the systems too expensive.

Finally, a third approach was suggested. Instead of sizing the PV systems for the individual substations, an energy system is sized for the combined grid load. In this way the base load is higher, and the peaks are reduced. Furthermore, the PV system is combined with a wind system. Wind has a better seasonal fit with the grid load while PV has a better daily fit. It was found that a system with 49% wind and 51% PV has the highest power utilization by the buses (55%). For this system – and a 100% PV and 100% wind system – the power utilization with varying storage sizes was investigated. It was found that a PV system has a higher power utilization up to 30 MWh of storage. Furthermore, the hybrid system outperforms both the wind and the PV systems up to 100 MWh of storage, if more storage is installed the wind system is the better option. The most promising option is to install the hybrid system with 5-10 MWh of storage. This system could power 72% to 78% of the Arnhem grid directly, while using the AC grid for 22% to 28% as seasonal storage. Moreover, with this system the CO_2 emissions could be decreased by 80% over a 30-year span.

Contents

Chapter 1: Introduction

In this introduction, first the working principle of the trolleybuses and their power systems (combined trolley systems) are explained. Second, the challenges within these trolley systems are described and finally how the work in this thesis can contribute to solving these challenges.

1.1 What is the trolley system?

The scientific interest in buses powered with overhead lines (trolleybuses) has sparked in the last years and with it the challenges that it faces [2, 3, 4]. To understand the challenges in the trolley grids, the trolleybus grid itself should be understood first. Therefore, in this section the essentials of the trolleybus grid are explained. A trolleybus is similar to a regular bus except for its energy supply, see figure 1.1.

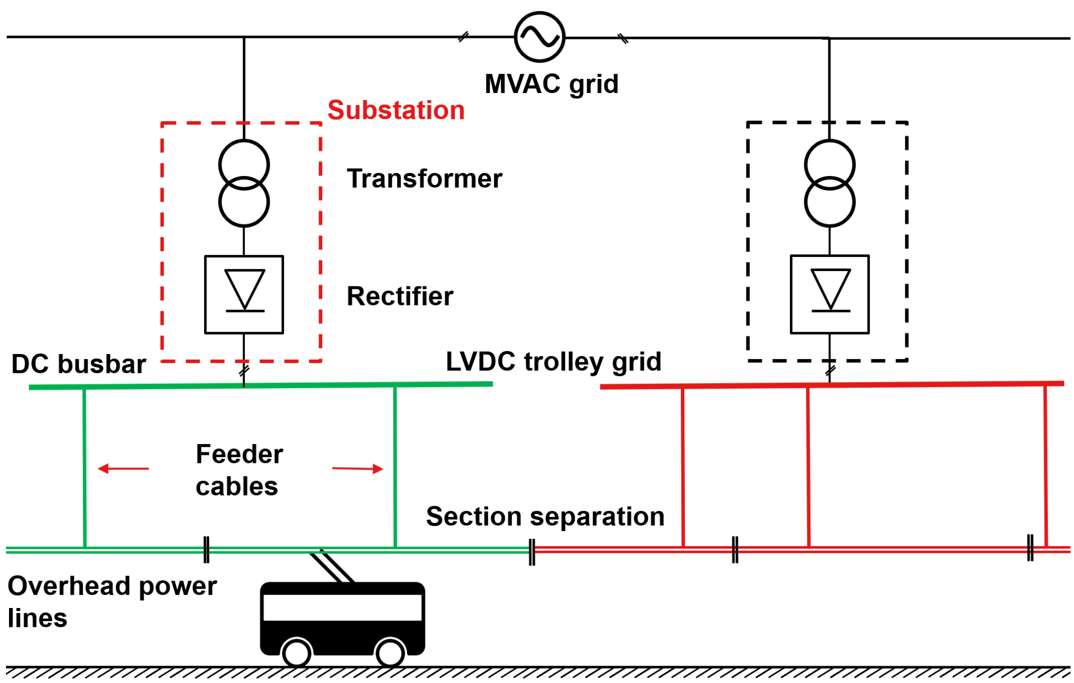

Figure 1.1: Schematic of the trolley system

Trolleybuses are fed power through the pantograph on top of the bus that connects to overhead power lines. The sections are colored in different colors to illustrate which substation powers what sections. One line is powered by the traction substation via the DC busbar and the feeder cables. The other line forms the return path for the current. A substation can power multiple sections with its feeder lines, but not all sections are powered by the same substation. Where one substation stops powering the overhead lines from one side, another substation will - after a physical separation of the overhead lines - start powering the other side of the overhead lines. This physical separation is called the *section separation*. This section separation is necessary to protect the remaining sections of the grid when failures on one section occurs. The momentum of the bus transports the bus across the section separation. The grid operator can decide to connect sections from different substations together. In this case the sections are physically connected. However, it is up to the grid operator to make the trade-off between grid safety and the possibility for substations to assist each other.

The concept of trolleybuses and their respective grids are very old. The first trolleybus was already in operation in 1882 [5]. However, the fact that the grids are old, does not mean that they are outperformed by diesel or battery buses. To understand why the interest in trolley systems has gone up, the trolley system has to be compared with it competitors.

It is well known that diesel-powered buses cause air pollution in their immediate environment and contribute to the rising CO_2 concentrations and consequently, climate change [6]. As a replacement for diesel-powered buses, many cities are starting to introduce battery-powered buses [7]. However, due to the high energy and power demands of the buses, the batteries must be large and consequently heavy and expensive. Moreover, the battery-powered buses need to be charged at a slow rate to maximize the battery lifespan. The buses might need to be charged throughout the day, resulting in lower operational times. Moreover, in special cases when the buses need to be used for extended periods, this will be more difficult (e.g. public holidays, defective buses etc.)

Trolleybuses omit these problems, but come with the problem of being less flexible with regards to overtaking other buses and taking detours. Besides, the interconnecting of multiple cities is a lot more difficult. Finally, the investment into the infrastructure of the trolley grids is costly.

However, a recent technological development called *In-Motion-Charging* (IMC) helps to overcome these drawbacks. IMC is a technology that combines the benefits of battery-powered buses with trolleybuses, as illustrated in figure 1.2.

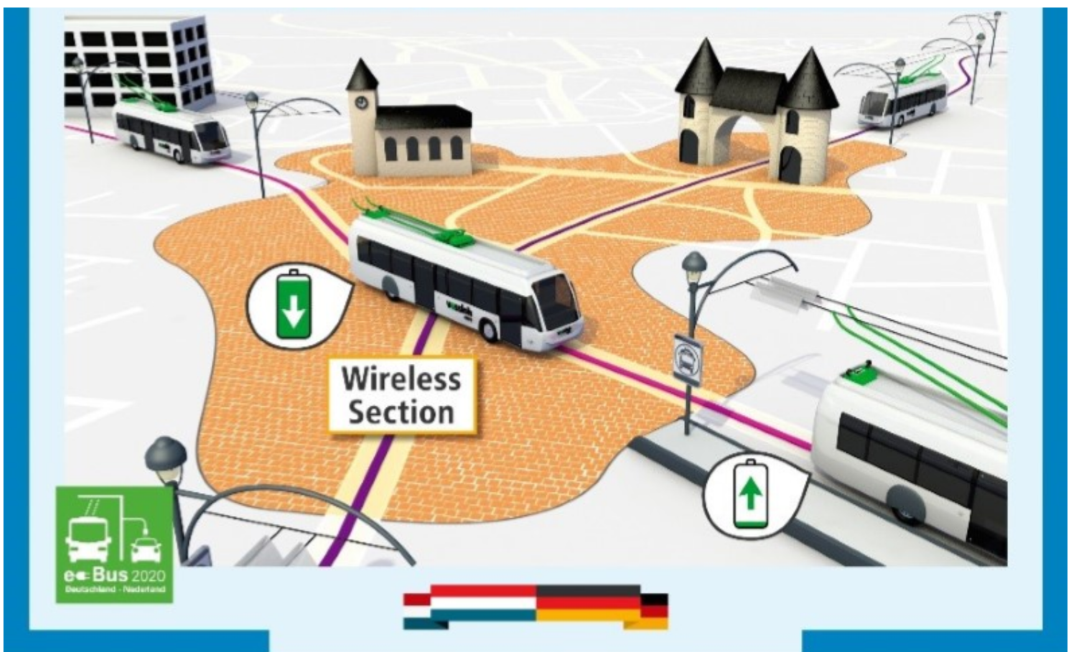

Figure 1.2: Schematic of In-Motion-Charging [8]

The buses are equipped with small (light and cheap) batteries, that are discharged when the bus is driving without overhead lines and are charged when the buses are driving with overhead lines. Therefore, the bus can easily overtake other vehicles, take detours, drive to other nearby cities with a trolleybus grid without local air pollution and possibly without CO_2 emissions. Because of these benefits, research is devoted to IMC [3, 4, 9].

There is also a reason for the renewed interest in the old grids. This has to do with changes in our energy loads and generation and the fact that trolley grids are DC powered.

Back in the day when the grid was installed, the main loads where candescent light bulbs and motors, both of which can be AC powered. Moreover, the energy supply was taken care of solely by traditional electricity plants - like coal or gas plants - that use steam generators to produce AC power. However, nowadays, most household loads are DC powered and more and more electricity is generated decentralized using solar photovoltaics (PV) which generates DC power [10]. An example of the powering of a low voltage DC (LVDC) load by solar PV via the medium voltage AC (MVAC) grid is provided in figure 1.3. In figure 1.4, the same PV is connected in a DC grid to power the LVDC load. It is evident from the examples that the connection into the DC grid results in higher efficiency operation. The inverter, power correction unit and the rectifier add significantly to the overall system cost and efficiency.

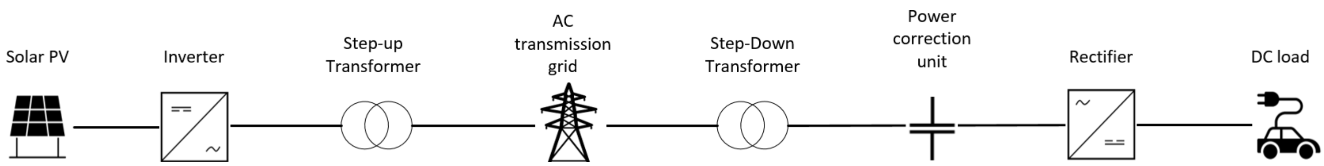

Figure 1.3: PV connected into HVAC tranmission grid powering a DC load

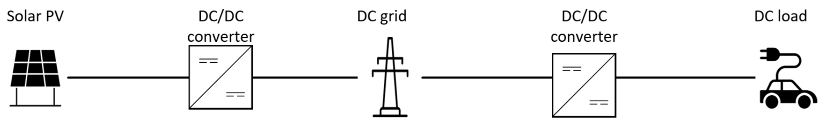

Figure 1.4: PV connected into DC grid powering a DC load

Since the grid is DC-based and the load and generation are also DC-based, the trolley grids are prime candidates to be used for more applications than moving buses. Using the grid for other applications than transporting buses is called *grid multi-functionality*. Examples of multi-functionality are integration of electric vehicle (EV) charging poles and street lightning into the LVDC grid directly [9, 11]. From an energy efficiency standpoint this makes sense, because the batteries in the EV's are DC powered. In [11], K.A Smith et al. compares the integration of EV charging points on the existing street lightning network of the UK (LVAC) and compares it to the integration of EV charging in a LVDC grid. Their main conclusions are; distribution losses are lower and energy efficiency of the charger is higher.

In many places, some form of multi-functionality is considered for the existing trolley grid infrastructure. In Arnhem, Solingen, Prague, Gdynia, Eberswalde, Szeged and possibly many more cities are considering intergating some form of grid multi-functionality in their trolley grids [8]. Now that we understand why interest in the trolley systems is renewed, it is important to understand the challenges that the systems face.

1.2 Challenges in trolleybus systems

The main motivation for this work is the energy use of these trolley grids. Especially with the developments in the trolley systems (eg. larger buses, IMC buses, grid multi-funcitionality) the electricity demand is increasing. Unfortunately, the majority of this power is still regenerated in a non-renewable way, contributing to global warming and to climate change [12, 13]. Furthermore, the grids are low voltage and due to the large load peaks, large voltage drops occur. This results in increased transmission losses and may cause the currents to exceed the rated current of the overhead lines. Moreover, this may hinder the developments of the trolley grids. More information about how these voltages drops occur and an example of voltage drop in the trolley grid in Arnhem, the Netherlands can be found in appendix B. In this work however, the focus is not on improving the robustness of voltage the overhead lines, but rather on increasing the renewable energy share of trolley grids.

To see how large the CO_2 contribution of trolley systems are, the emissions of the trolley grid in Arnhem, the Netherlands have been approximated. The average energy use per km in Eberswalde, Germany is 2 kWh per km [14]. Similar values were later found for the trolleybuses in Arnhem, the Netherlands. These values are presented in the figure below.

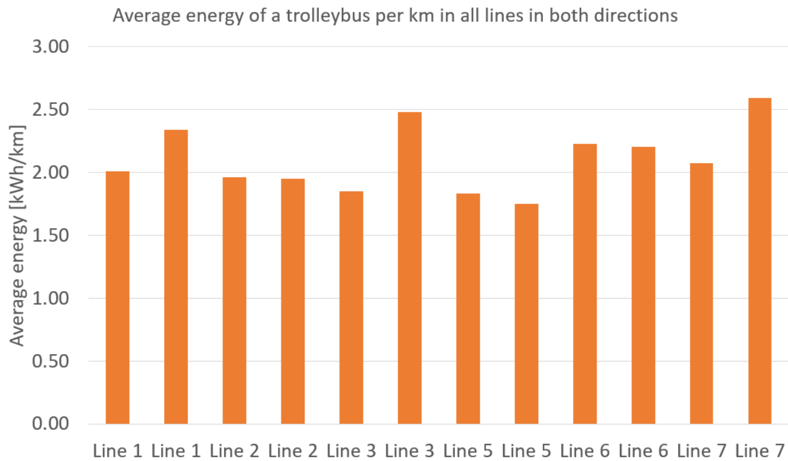

Figure 1.5: Energy per km for trolleybuses in Arnhem, the Netherlands

The observant reader may have noticed that line 4 is not shown in the figure. The reason for this is because the line was discontinued in 1950. For Arnhem, the trolley grid the annual energy consumption is around 6 GWh [15]. In the Netherlands, the average electricity consumption per household is around 2800 kWh, therefore the trolley grid has an electric energy demand equivalent to over 2000 households. Now that we have established that the Arnhem trolley grid consumes a substantial amount of energy, the energy use has to be related to CO_2 emissions. In the Netherlands, the electricity is mostly generated in a non-renewable way. The energy mix for electricity generation by source is shown in figure 1.6 [16].

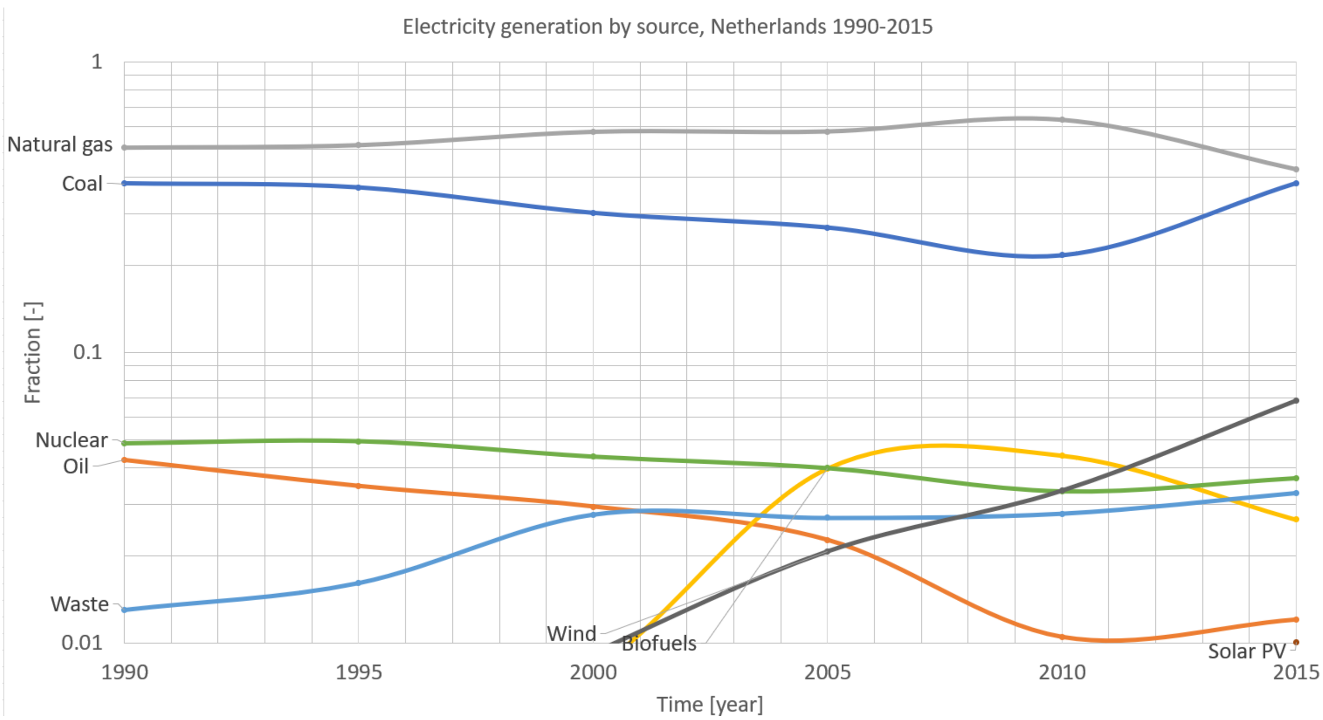

Figure 1.6: Energy mix for the Netherlands [16].

To find the CO_2 impact of the electricity generation, the sources have to be linked to their emissions.

The emissions per energy source are shown in table 1.1 [17].

Table 1.1: CO2 emissions per source [17]

Source	kg CO2eq/ kWh
Coal	820
Oil	820
Natural gas	490
Biofuels	740
Waste	Varying
Nuclear	12
Hydro	24
Solar PV	48
Wind	11

By combining the energy mix with its carbon footprint, the CO_2 emissions for the Arhem grid are estimated at around 3300 Mton. The final step is to relate the CO_2 emissions with impact on global warming and climate change. It has long been established that CO_2 emissions have effect on climate change [18]. Moreover, it was found that human-induced climate change results in global warming, which brings along massive costs due to humans having to adapt to the new environment [1]. Furthermore, it was found that anthropogenic CO_2 has irreversible effects on climate change [13]. The importance of sustainable electricity is listed seventh of the 17 most important goals for the 21^{st} century by the United Nations [19].

There are two ways to reduce the CO_2 emissions of the trolley systems. The first is to reduce the energy consumption. This could be done by reducing the consumption of the buses or by reducing the transmission losses. Alternatively, a renewable energy source could be used to decrease the use of non-renewable energy. Reducing the energy consumption of trolleybuses could be done by installing on-board energy storage. In [20] Stana et al. size on-board supercapacitors (SC) to reduce distribution losses and optimize braking energy recuperation. In their conclusions they state that up to 50% of the power demands during acceleration can be supplied by SC's, thereby limiting the distribution losses between 19.31% and 24.25% on a distance up to 2km. In this work, however, the focus is on introducing a renewable energy source to reduce the CO_2 emissions.

1.3 Problem statement

Sizing a renewable energy system gives a trade-off between power utilization by trolleybuses and dump to the surrounding grid. It is important to minimize this dump, because of technical, economic and contractual reasons. For technical reason, it could be that the old connections to the MVAC grid are not physically capable of exporting the power. In this case, the power export is physically limited. Moreover, since the PV or wind systems are likely to be large, offsetting does not apply anymore rather a feed-in-tariff may apply. By offsetting, the imported and exported energy are subtracted from each other and the consumer only pays for the left over imported energy. With a feed-in-tariff, the prices between the exported and imported power are different. If there is no sun and or no wind, the price difference can be significant. Finally, the operator of the grid has to be in agreement with the distribution grid operator about the export of energy. This may also limit the export of PV or wind. To make the work practical, the focus is entirely on the trolley grid of Arnhem, the Netherlands.

1.4 Research Objectives

The main research objective is:

Investigating the attainable renewable energy share of the Arnhem trolleybus grid while minimizing the need for seasonal storage.

The below table shows an overview of the research questions and where they are answered in this work.

Category		Question	Answered in:
Design of the renewable energy system	RQ 1:	Is wind or solar energy better suitable for increasing the renewable energy share?	Literature review and Results (CH2 & CH6)
	RQ 2:	Where should the wind or PV system be connected to the trolley grid?	Literature review (CH2)
	RQ 3:	What size should the system be?	Results (CH4 & CH6)
Performance of the system	RQ 4:	What fraction of the PV or wind output is directly utilized by the trolleybuses?	Results (CH4)
	RQ 5:	How does the PV or wind utilization improve with varying storage sizes?	Results (CH5 & CH6)

Figure 1.7: Research questions

First a renewable energy source should be selected. Next, it should be decided where the energy system is connected to the trolley system. This could be on the DC-side (DC- busbar or sections) or on the AC-side (substation). Next, the size of the energy system should be established. After the system is designed, the system performance should be analysed. The first questions is about the fraction of energy that is directly utilized by the PV. This question shows how large the mismatch between generation and bus load is and motivates the use of energy storage. For the last question, the generation is coupled with storage to quantify the effects on energy utilization.

1.5 Research Scope

This work is about sizing and placement of renewable energy in the Arnhem trolley grid with the aim of increasing the renewable energy share. The analysis is purely technical. Investigating ways to reduce the trolleybus loads or decrease transmission losses are not part of this research. Furthermore, power flow calculations across the overhead lines are also not executed. These calculations require a detailed topology of the overhead lines, which was not shared with the TU Delft at the time of writing. Rather, a constant energy loss of 16.7% was conservatively assumed for power flow on the overhead lines. Moreover, the effects of IMC, grid multi-functionality and bilateral connects are not researched. Finally, the research is focused only on the trolley grid of Arnhem. Therefore, city-specific parameters cannot be compared and the conclusions are limited to the Arnhem grid.

1.6 Project workflow and report organization

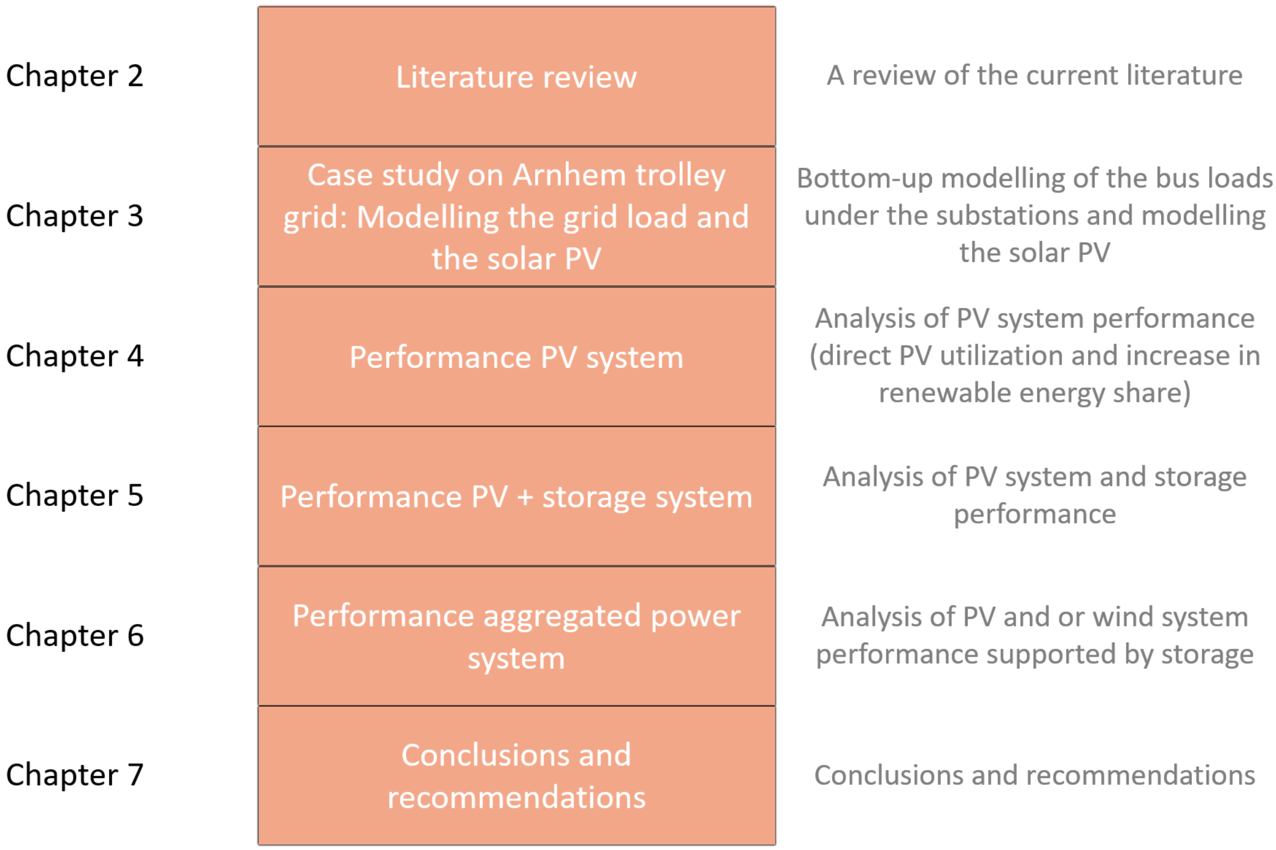

Chapter 2: Literature Review

The bus load and the bus traffic must be modeled as well as the energy generation and storage systems. In this chapter, literature on which the research is based is discussed. The gaps in the literature are identified, establishing the ground for this research.

2.1 Bus load

First realistic bus load profiles need to be established. These profiles form the basis of the load on the substations. In literature a standard bus velocity cycle is often used, see figure 2.1. [21, 22, 23, 24]

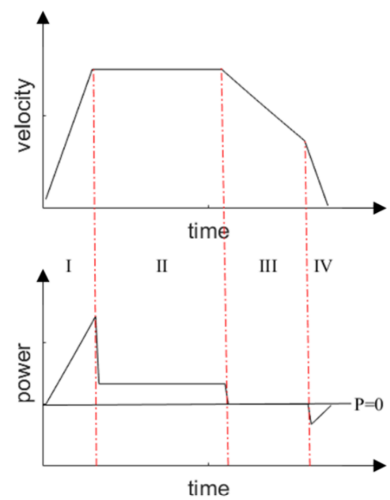

Figure 2.1: Bus velocity and power profile [21]

In this profile four different stages are considered; I) *acceleration, II) constant speed, III) coasting and IV) braking*. For the acceleration stage, Newton's second law is considered.

$$F_{\mathrm{T}} = m \cdot a + F_{\mathrm{R}} \tag{2.1}$$

Here F_{T} is the traction force, m and a are the mass and the acceleration of the bus, respectively. F_{R} are the resistive forces acting on the bus. These resistive forces consist of the roll force, drag force and the gradient force. The roll resistance is approximated by the deformation or abrasion of the tires [25]. The drag force is caused by air friction. The gradient forces are the gravitational forces om the bus, depending on the incline of the road.

For the *constant velocity* stage, the acceleration is set to zero. For the *coasting* stage, the traction force is set to zero. For the *braking* stage, the bus is assumed to decelerate as quickly as it accelerates (0.5 m/s^2).

To make the profiles more realistic, in [21], speed reduction and standstill time are are varied with the traffic conditions. Four levels of traffic are considered: no traffic, low traffic, medium traffic and high traffic. These traffic conditions are assigned to times in the day and impact the probability that buses are delayed by nodes on the route. How the authors constructed these traffic conditions was not published.

To my knowledge, the modelled bus velocity and power has not been compared with measurements on the bus. For illustration, in figure 2.2, measurements from an Arnhem trolleybus are shown.

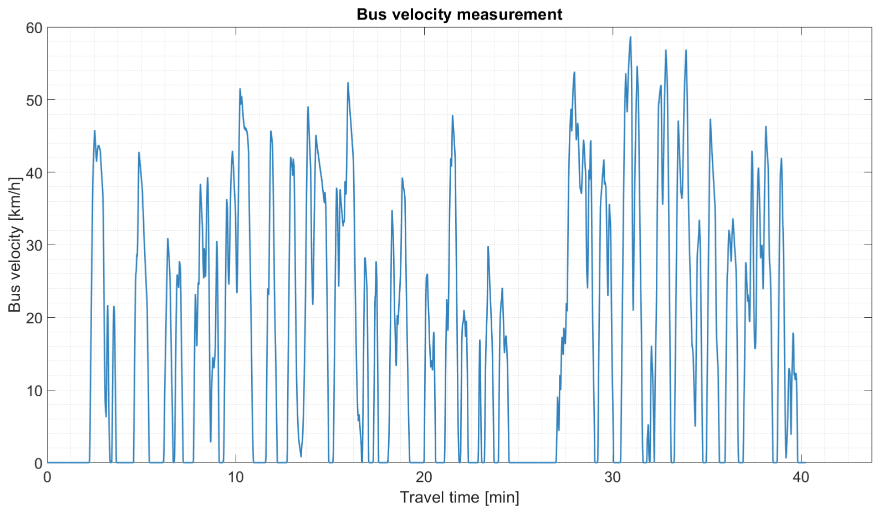

Figure 2.2: Sample of bus velocity measurement

It is evident that the velocity profile shown in figure 2.1 gives a too simplistic image of the actual velocity. In figure 2.3a and 2.3b the computed and measured power profiles are compared.

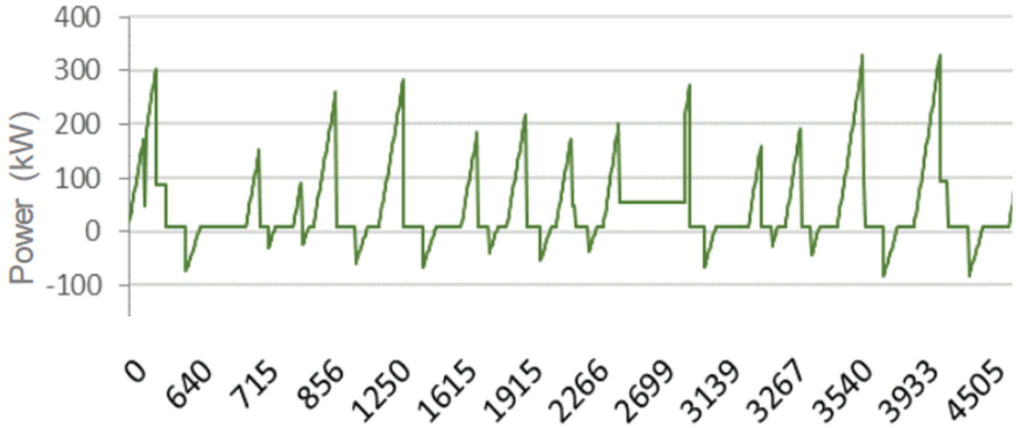

(a) Example bus load computed [9]

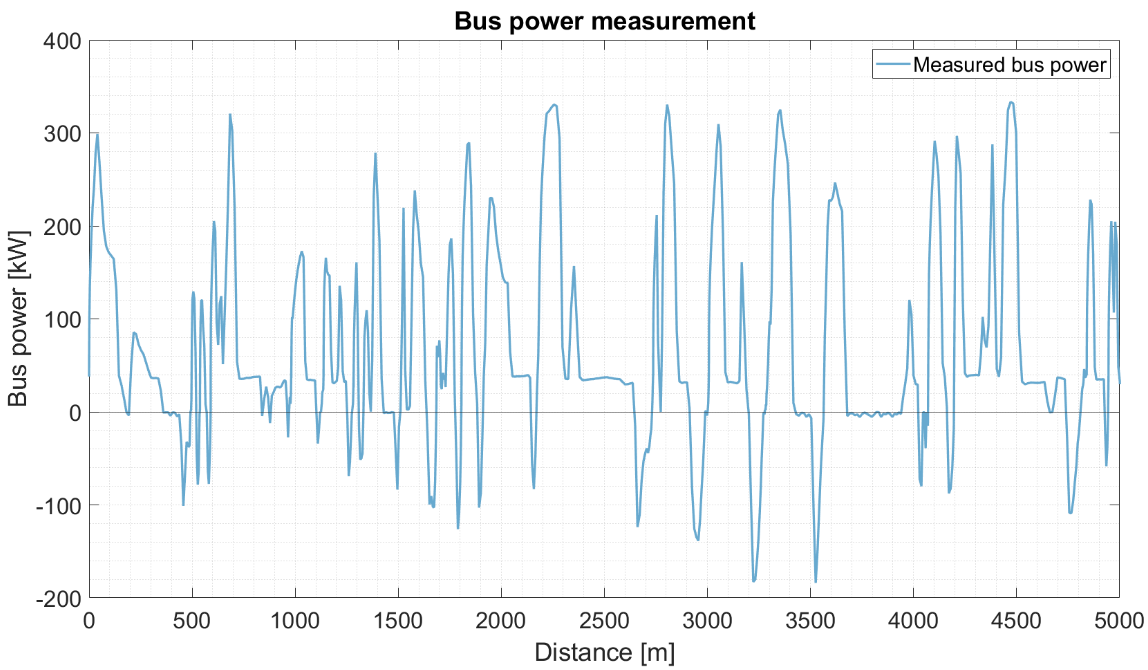

(b) Example bus load measured in Arnhem

Figure 2.3: Comparison between calculated and measured bus loads.

From these figures, two things are apparent. First, the simple power model does not capture the dynamics of the real bus load. Second, the simple power model does not include power for the heating, ventilation and AC (HVAC) of the buses. In figure 2.3b, the fraction of the loads of the HVAC are visible as the power plateaus at around 40 kW. The fraction of the bus load to support the HVAC can be up to 35% in the summer and up to 43% in the winter [14]. To accurately model the bus loads, the HVAC loads can therefore not be ignored.

In this work, the modeled velocity and power profiles are replaced by measured profiles for all the bus routes. The velocity measurements are used as input for a bus load model [26]. The calculation of the bus power profiles was already done by researchers of the HAN university and shared with TU Delft.

2.2 Bus traffic

The bus traffic must be incorporated to compute the loads under each substation. In literature, no instances have been found of a complete modeling of the bus loads for an entire trolley grid.

In [27], the authors aim to optimize the design for stationary supercapacitors for train systems. In their approach, they go in detail about how the voltage of the trains and the current in the overhead lines can be calculated, see figure 2.4.

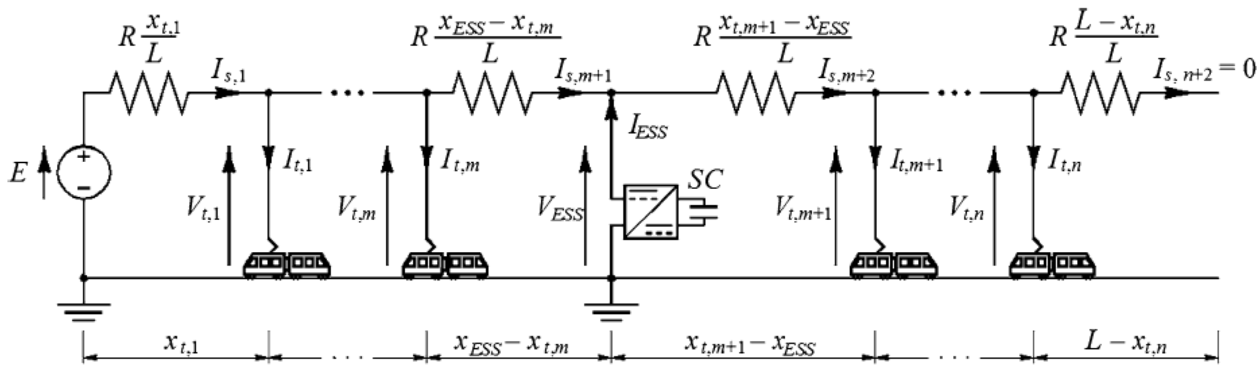

Figure 2.4: Equivalent circuit of single side DC contact line [27]

The approach suggested in this paper can be useful for computing the voltages and currents for all the nodes in the Arnhem trolley grid. It is important to note that trolley buses do not have a low resistance return path at the ground. Therefore, the current in the overhead lines should be doubled. However, power flow calculations in the overhead lines are not part of this work. In the paper, the authors account for two buses on a single section which may leave at varying times. Furthermore, they assume that the mean value of the power drawn by each train for each position can be identified by a probabilistic analysis [28]. A probability analysis for bus loads is a lot more difficult than for trains, since the load is a less predictable. Furthermore, in the Arnhem grid, often more than two buses are on a single section (see figure 3.9).

There are publications with more than two trolley buses on a single section. In [29], the authors compare seven buses on a single line to investigate the effects of energy-saving due to battery-assisted buses recuperating the braking energy. An even more complex traffic scenario can be found in a paper from the Wuppertal university. In this work, they explore the loads on the substations for a future trolley grid (with EV charging, PV and battery-assisted buses). The authors consider 46 conventional trolleybuses with an additional five battery-assisted trolleybuses on one line for the Monday bus schedule [23]. This paper resembles the aim of this thesis the best.

However, this paper does not capture the complexity proposed in this work. In this thesis, the bus traffic for seven bus lines are considered with buses from multiple lines that may be crossing. Moreover, the bus traffic shall be simulated for the entire year instead of a single day. Besides, in [21], the simplified velocity and power profile (figure 2.1) are used.

To recap, this work aims to expand upon the current literature by using measured bus velocity and power values instead of simplified profiles. In addition, the bus traffic for all buses in the Arnhem grid for the whole year shall be computed. To my knowledge, this has never been done before for trolley systems.

Now that the literature on the modelling of the bus loads and the traffic has been scrutinized, it is important to do the same for renewable energy integration in these systems.

2.3 Renewable energy integration in low voltage transit grids

In this thesis, wind and PV energy are both considered as the renewable energy source. In figure 2.6, the advantages and disadvantages of each source are listed. Below each category is discussed.

Category	Wind	PV
Type of current	😐	😐
Daily power profile match	☹	🙂
Seasonal power profile match	🙂	☹
Placement	😐	🙂
Modularity	☹	🙂
Price	🙂	🙂

Figure 2.5: Advantages and disadvantages of PV and wind integration in trolley grids.

PV produces DC-power and wind produces AC-power. Both may have their advantages in a trolley system. The PV has a higher energy efficiency if its placed on the DC-side and wind has the advantage if it is placed on the AC-side (connected to the MVAC grid). PV has a better diurnal generation profile than wind, because the solar profile matches the load profile of the grid better. Therefore, less short-term energy storage is required. Moreover, PV is more urban-friendly than wind, the wind characteristics may be affected a lot by the city. Therefore, wind energy cannot be harvested close to the sections, which leads to transmission losses. In addition, PV can be scaled better by adding more panels.

The benefit of wind energy as source are more specific to the location of the trolley grid. In the Netherlands, wind energy has the benefit of a better fitting seasonal profile because the energy consumption of trolleybuses rises (due to heating) in the winter. Moreover, the Arnhem grid has summer bus schedules that have a reduced number of bus trips. The wind potential is the also highest in the winter. The last category is cost. In figure 2.6, the trends for the Levelized Cost of Electricity (LCoE) and the action prices for onshore wind, offshore wind and PV are shown.

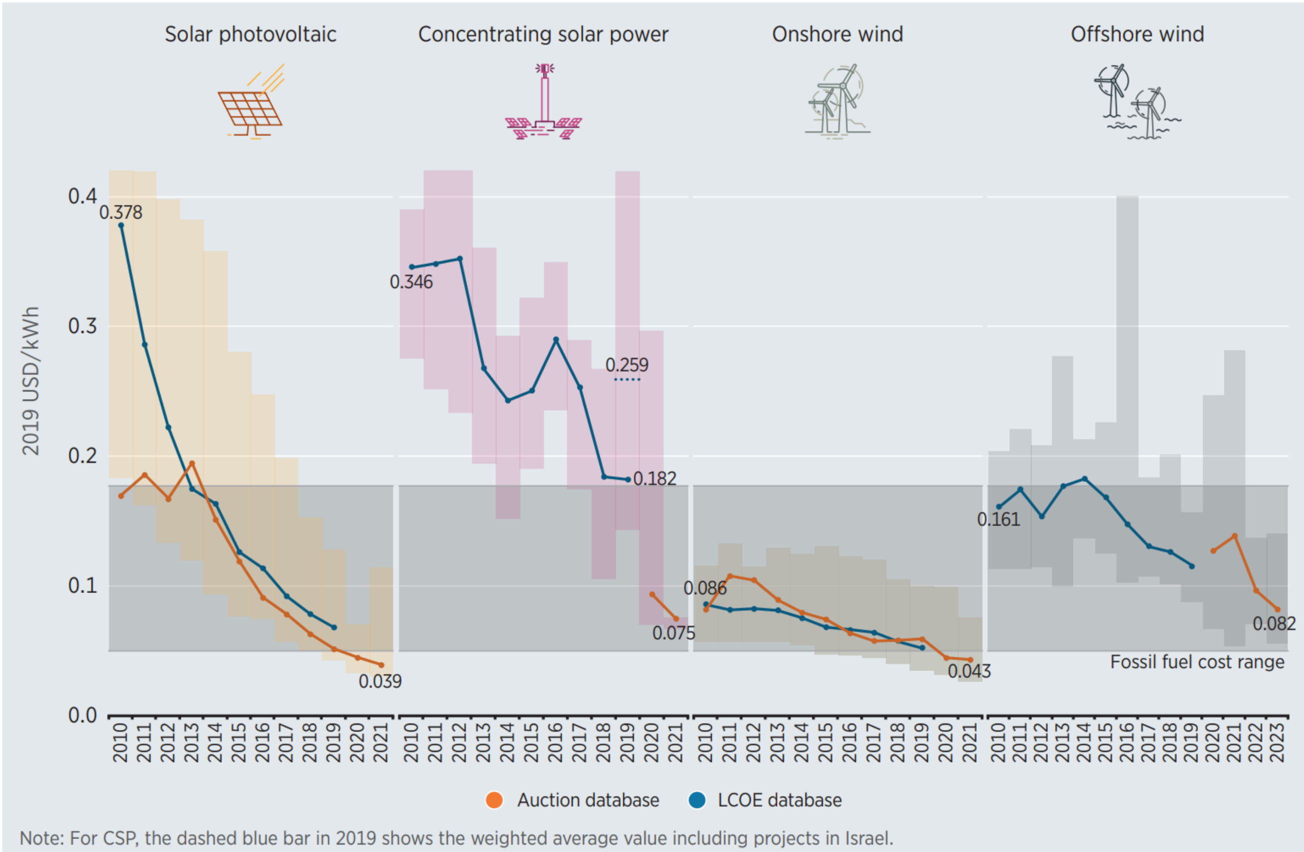

Figure 2.6: Price trends for onshore wind, offshore wind and PV [30].

Globally, the costs for onshore wind are equal to that of PV. However, the price drop for PV is steeper. In the Netherlands, the LCoE is lower for onshore wind than for solar PV in the Netherlands [31]. The cost for offshore wind is higher than the cost for PV.

Despite the lower cost for wind (in the Netherlands), the preferred renewable energy source is PV. This is because the PV is modular and urban-friendly. It can be placed close to the trolley grid at multiple locations. Furthermore, if needed, the PV system can easily be expanded. Later it was found that the seasonal mismatch between PV generation and bus load is large, the PV system is then expanded with a wind system.

PV has succesfully be integrated into LVDC grids before in the form of microgrids [32]. A microgrid is a group of interconnected loads and distributed energy resources within clearly defined electrical boundaries that acts as a single controllable entity with respect to the grid. A microgrid can connect and disconnect from the grid to enable it to operate in both grid-connected or island-mode. In this way a microgrid is similar to a trolley grid. However, one crucial difference between solar PV integration in microgrids and trolleygrids is the unpredicability of the position of the loads on top of the unpredictability of the time occurrence of the loads and generation. Therefore it is much more difficult to size and place the solar PV and stationary storage for trolleybus grids than microgrids. This is the main challenge with integrating solar PV in trolley grids.

PV is has also been integrated in transit grids before. Publications on integration of solar PV into train networks were found [33, 34, 35, 36]. However, often the PV was placed on top of the train, which is different from the stationary placement proposed in this work [33, 34, 35]. Only one paper proposed to place the PV on the station [36]. For train grids, the traffic and load are easily modelled because they are predictable. Therefore, non of the papers go into detail about how they accomplished this. Furthermore, the main aim of the papers is not to increase the renewable energy share as much as possible, rather it is to power auxiliary power (eg. lightning, EV's at the train station). Therefore, these papers only vaguely resemble the aim of this paper.

Integration of PV into tram networks was described by [37]. Insights from this paper are interesting for increasing the voltage profile robustness and thereby reducing transmission losses. Moreover, tram systems are comparable to trolley systems as they are both DC-powered at low voltage (600 to 900 VDC in this article). Given their identical power requirements, the voltage drops experienced by both systems are comparable. In this paper, the PV is sized based on the available area on the tram shelters. The PV is combined with supercapacitors to supply the peak power demands of the trams. The aim of the article is to find an economic optimum for the amount of supercapacitors connected in parallel and series for each tram stop. For this a *random searching optimization problem* was established. This is an algorithm that based on some initial guesses tries to minimize an objective function by trial and error. The objectives in this function are the costs associated with: the energy stored into the SC's, the energy losses and the energy produced by the PV. The results show that the system remains within the voltage and current ranges for all simulation times, however the voltage drops to almost 600V at one time. This suggests that the economically optimum found in this paper does not yield the best setup for reducing voltage drops. Moreover, the effects of the SC integration on the power demands of the trams shows that the SC's hardly make a difference for the power demands of the trams. This is likely because the size of the PV is only 12 kWp, which is very small in comparison to the loads of the trams. Moreover, the PV profile proposed in this paper is a perfect profile for a summer and a winter day. These profiles are in practice unrealistic, see figure 2.7.

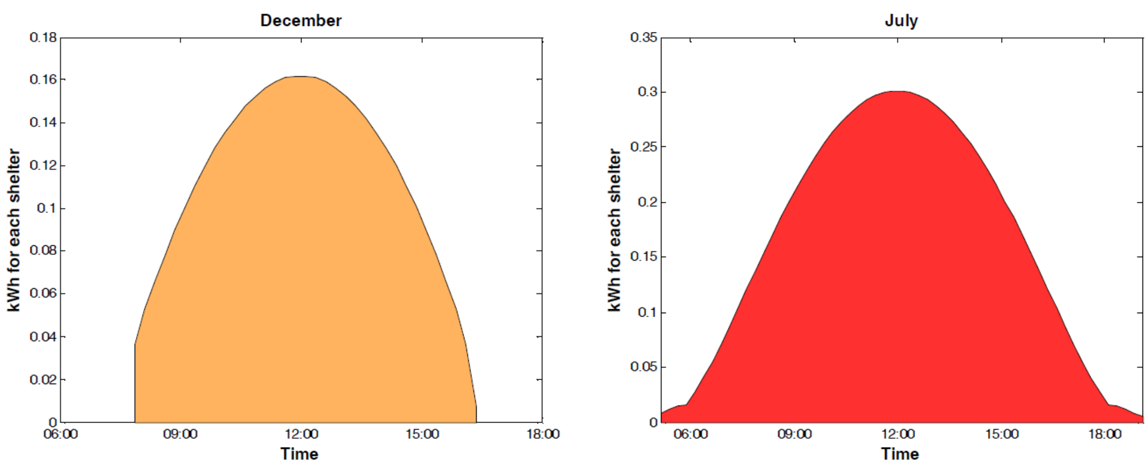

Figure 2.7: PV power profiles December and July [37]

The optimization in this paper is aimed at making a cost effective energy storage which may help to make the voltage profile more robust and reduce transmission losses. However, for increasing the renewable energy share the storage has little impact. Furthermore, only one line of 1.8 km was simulated with a single tram for 5 minutes. Therefore, a lot of the challenges for this work are not adressed in this paper.

PV integration in metro systems is also already investigated [38, 39]. In [38], the authors perform a feasibility study on the M1 light metro line in Istanbul to use PV on top of metros in combination with batteries and new LED lamps to replace the energy inefficient fluorescent lights. Their objective was to show that PV and storage on metros can perform niche power applications (like replace the lighting). They estimate that their system has a payback time of 7.5 years, which - considering the lifetime of the system - make it a cost effective investment.

In [39], PV is integrated on a larger scale into a MVAC network (35kV) after inverting. With their work, the authors aim to improve the power factor of the AC power that is rectified for the metros. They do this by using the inverter of the PV to generate a reactive power. This reactive power cancels the reactive power of the grid and therefore increases the power factor from 0.9 to 0.96. However, the trolley grid is DC powered and therefore has a power factor of one. The aim of this paper thus only vaguely resembles the aim of this work.

Integrating PV into trolley grids has been proposed before by researchers of the Univerisity of Wuppertal, Germany. In [9] M. Salih et al. apply an adapted Newton Raphson power flow algorithm (ANR) that they developed in [40] to the nearby Solingen trolleybus grid to determine the electrical state (voltage across the nodes and power flow towards the nodes) of all grid nodes (components connected to the grid) at all times. In this NRA they include, trolleybuses with IMC, solar PV and grid multi functionality (EV charging). The approach suggested here may be interesting for the Arnhem grid if the PV is placed on the sections. However, to compute power flow calculations the topology of the overhead lines need to be known. At the time of writing, the topology of the Arnhem grid has not been shared with TU Delft. Therefore, power flow calculations are not possible. The method for power flow calculations and methods for PV placement on sections is placed in the final section of this literature study called future research.

Moreover, in [9], the authors modeling approach for the solar PV is rather simplistic. In short, they create a 'realistic' solar profile, based on a prefect solar profile for the coordinates of Solingen and the introduction of a semi-randomized cloud factor (between 0 and 1), which depends on the seasons. See figure 2.8.

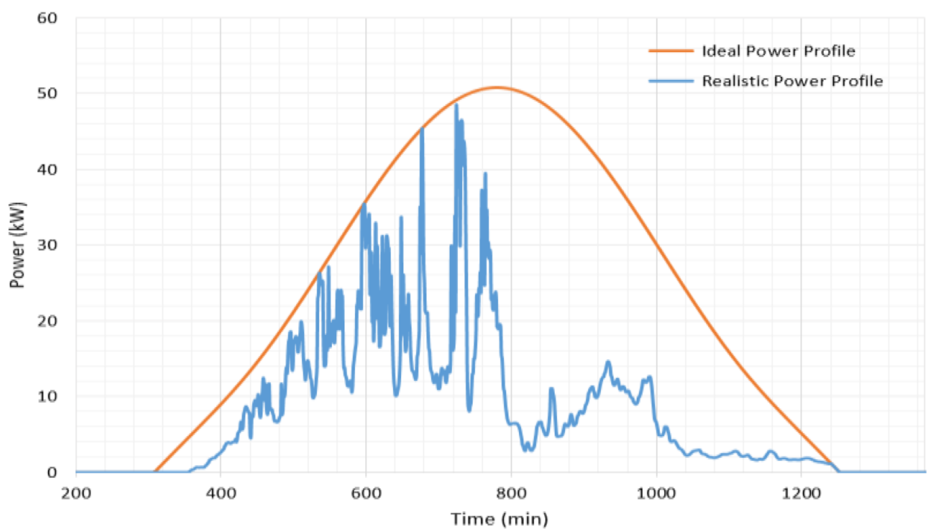

Figure 2.8: Ideal and realistic PV power profiles [24]

The reduction factor is based on a fit with data from the 2016-2017 data set for Wuppertal, Germany. In the paper, the authors do not go into detail about how good the profile fits the measured data.

In this thesis, a different approach is selected. Measured data from nearby KNMI stations have been interpolated and used as input for a stochastic model to create realistic solar data. This was automatically excucted by Meteonorm [41]. Now that the renewable energy source is selected, the location where the energy system connects to the trolley system should be decided.

2.4 Placement of the PV system

Before the PV and storage can be sized, it is important to analyse the possible locations where the PV and storage systems could be placed. In this work, the assumption is made that PV and storage are placed at the same location. Therefore, are three possible combinations where PV and storage can be placed; on the substation (AC-side) or on the DC-busbar or section (DC-side). The three options are shown in figures 2.9, 2.10 and 2.11, .

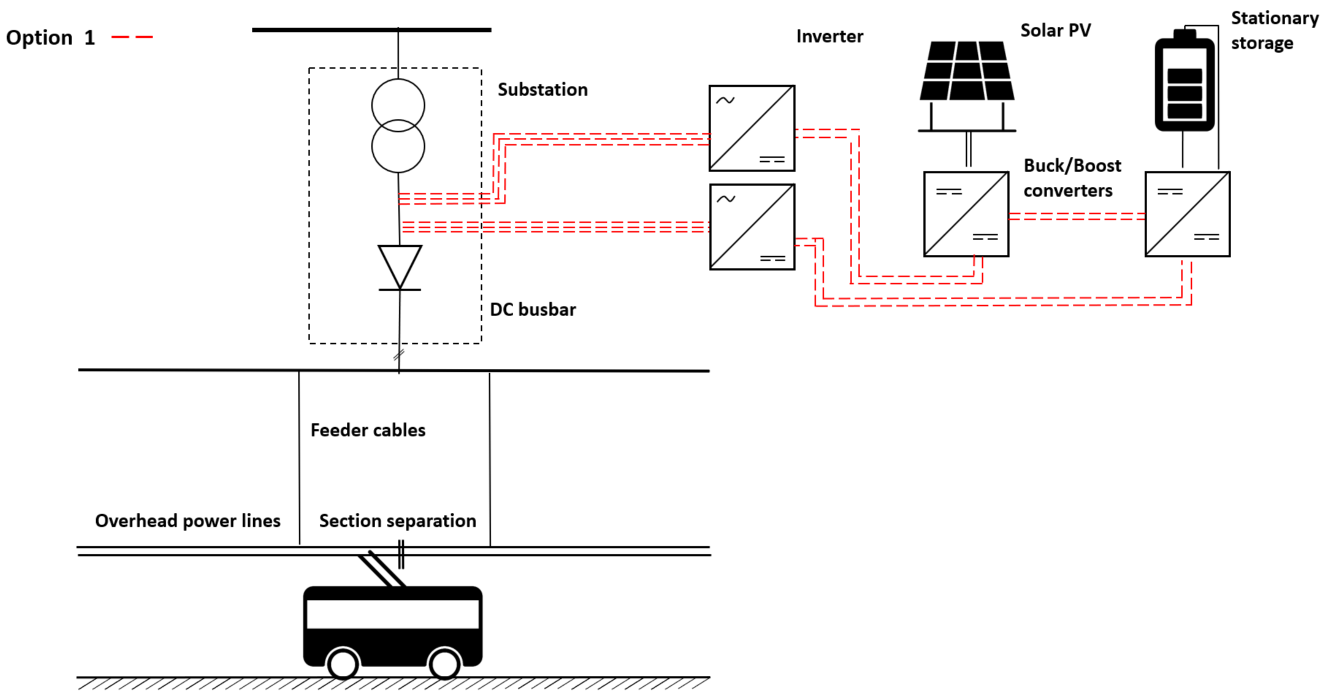

Figure 2.9: Option 1: PV and storage at the substation

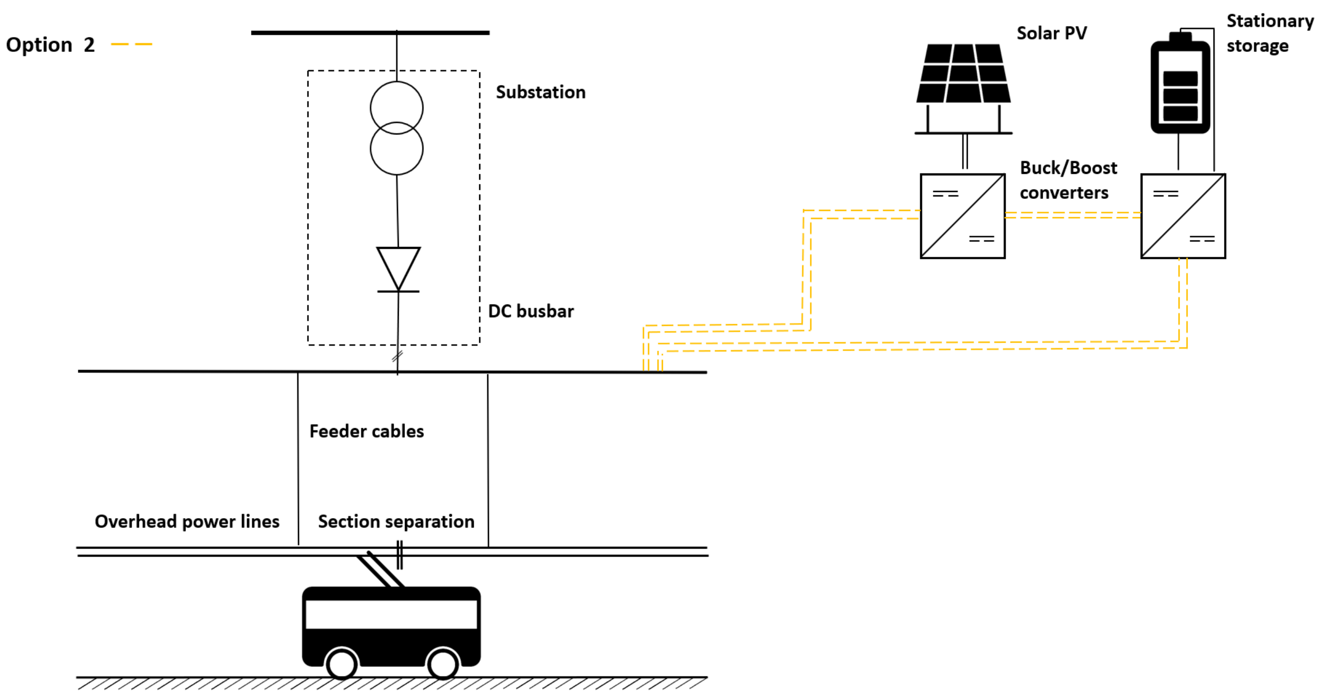

Figure 2.10: Option 2: PV and storage on the DC-busbar

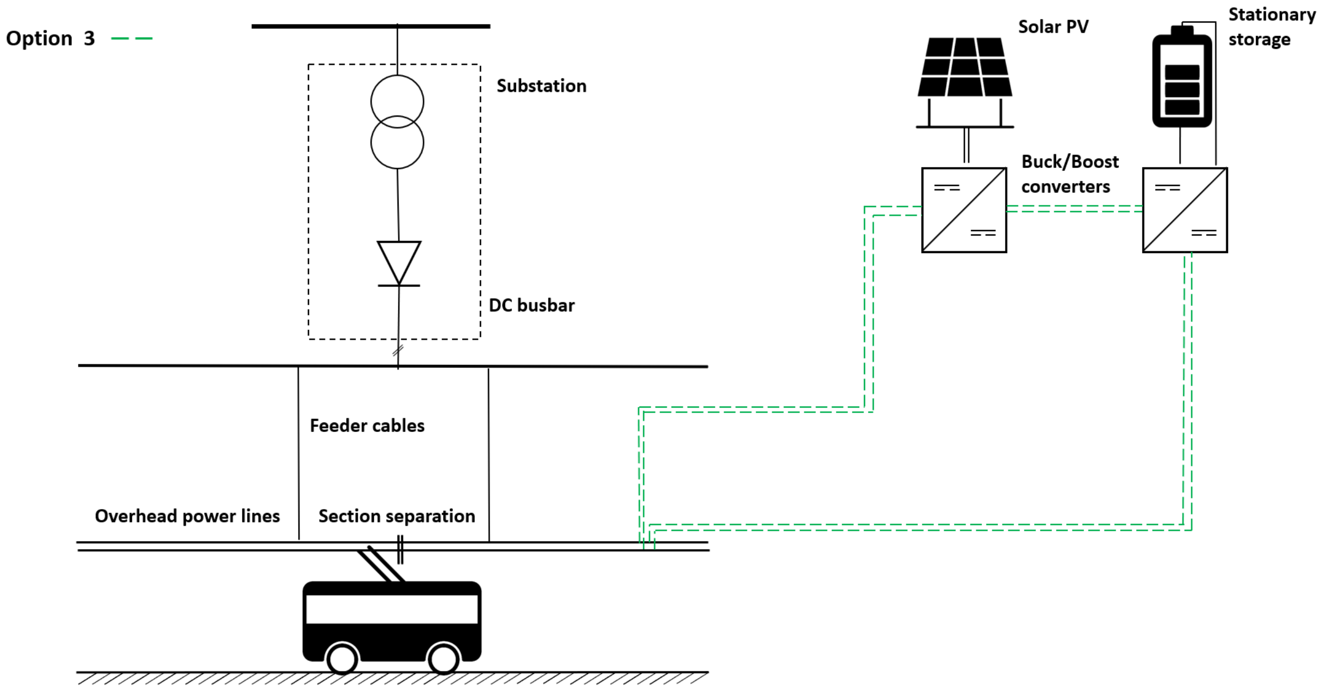

Figure 2.11: Option 3: PV and storage on the section

In literature, PV is often placed directly on the overhead lines (DC-side) [9, 22, 24]. Placement of PV on the sections results in more sources from which the buses can be powered and consequently lower voltage drops and transmission losses in the overhead lines (see appendix B). Placement of PV on the DC-busbar results in lower resistance transmission between the sections. Moreover, DC-side placement has the advantage over AC-side placement when it comes to energy efficiency. However, DC-side placement has important disadvantages compared to AC-side placement. If - for a substation - the PV generation is larger than the bus load, the excess PV cannot be send to the AC-grid due to the rectifier. This power either has to be stored or wasted. By placing PV on the DC-side, a significant part of the PV power may be wasted.

Since the objective of this work is to increase the renewable energy share, AC-side placement has been selected. Another reason to choose the AC-side was the requirement for a grid topology. Placement of PV on the DC-side requires power flow computations in the overhead lines, for this purpose the amount of parallel overhead lines should be known. For the AC-side, the topology is also necessary to do the power flow calculations, however in this work a constant power flow loss of 16.7% is assumed for transmission over the overhead lines. Energy storage should be included to reduce the mismatch between generation and load. There are two positions where the energy storage could be located; on the trolleybuses or on the ground. If the storage were to be placed on the trolleybuses, the storage cannot be used to reliably store the renewable energy. If the bus drives from one section to a section that is isolated, the intermittent source cannot use it to store power anymore. In addition, the storage size on a bus is limited due to the mass and size constraints. This limits the amount of PV that can utilized by buses. In this work, the main aim is to increase the renewable energy share of the trolleybuses as much as possible. Therefore, stationary storage was selected.

2.5 Research gap

This thesis aims to expand upon the current literature by simulating the bus loads on a complete trolley grid for a whole year with measured bus and PV data. In the current literature, simplistic and inaccurate models have been used to calculate the bus load and PV generation. The velocity profiles and power profiles shown in literature do not represent the actual profiles accurately. Moreover, the simplistic bus power profiles do not account for the HVAC power requirements. In practice, the HVAC requires a significant share of the overall bus power.

This work aims to further expand on the way bus traffic is modelled. Thus far the trolleybus traffic has only been simulated for one line maximum for a single day. In this thesis, seven bus lines with interconnected sections shall be simulated for an entire year.

Finally, integrating solar PV into trolley grids has been proposed before. However, the methods for simulating the PV are based on an ideal PV profile that receives a semi-random reduction factor based on the seasons. In this work, the PV shall be modelled using data from the nearby weather stations. Furthermore, the PV temperature and efficiency calculations shall be done on the basis of a fluid dynamic model for actual solar panels[42]. In this way, this research provides a more thorough way to simulate the PV that has not been applied to trolley grids before.

Chapter 3: Models

In the previous chapter, we have established that a model is necessary that simulate the bus loads for the entire Arnhem grid year-round. In this chapter this model is described in detail. Afterwards, a model is described for the PV. However, first the Arnhem trolley grid is introduced.

3.1 Research method: A case-study on the Arnhem grid

To answer the research questions the work has to take a pragmatic turn. Therefore, the Arnhem trolley grid is used for a case-study. In this section an overview of the Arnhem trolley grid is presented and the case-study is explained in detail.

The Arnhem trolley grid is the one of the largest trolley grids in West-Europe and is the only trolley grid in the Benelux that is still operational. Furthermore, the Arnhem trolley grid is one of the grids that is selected for the trolley2.0 project and will therefore support IMC buses in the future[8]. Also, there are plans to add grid multi-functionally to the Arnhem grid. The load on the Arnhem grid will therefore increase in the coming years. An overview of the trolleybus grid of Arnhem is shown in figure 3.1.

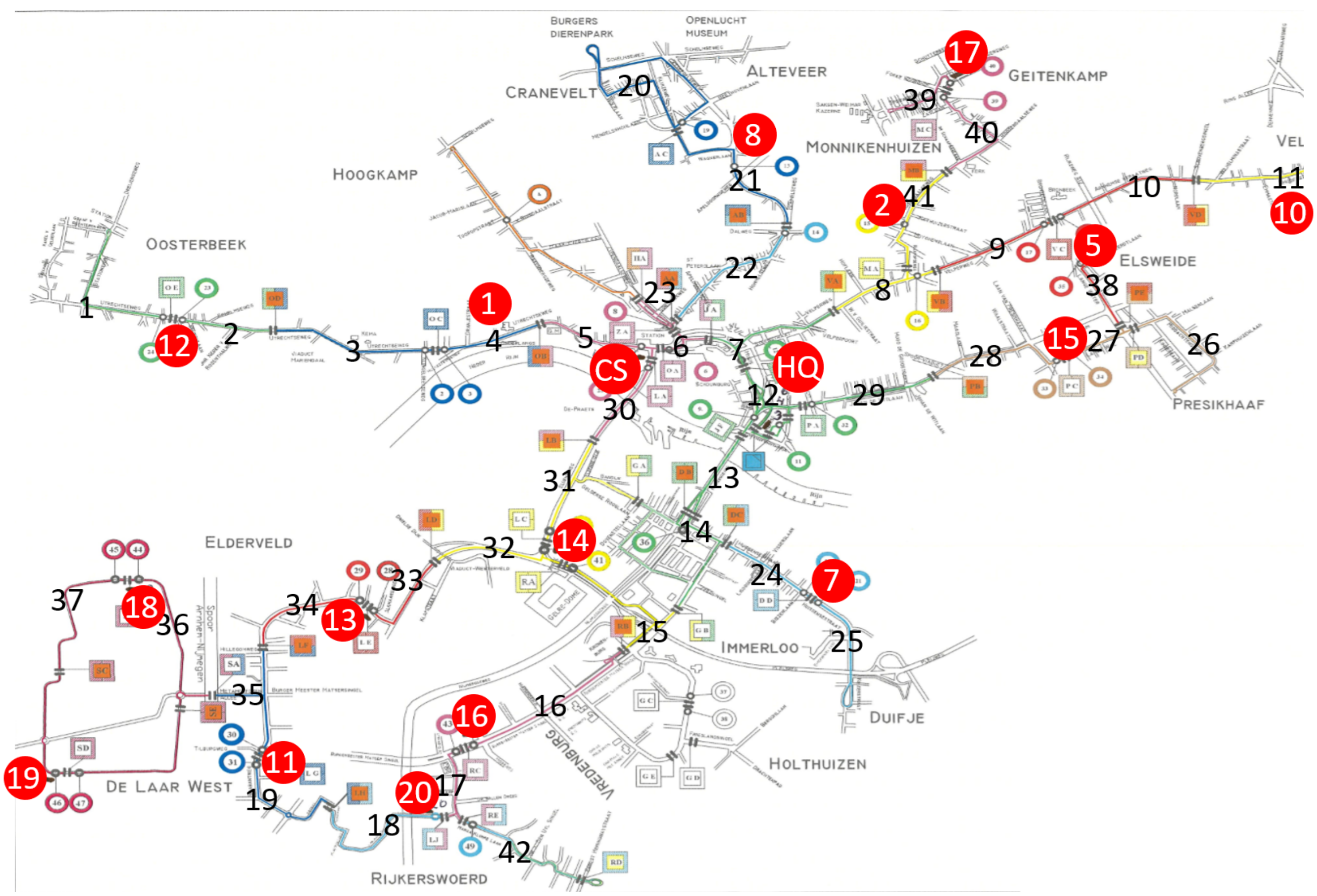

Figure 3.1: Arnhem grid overview

There are seven trolleybus lines in Arnhem (lines 1,2,3,5,6,7 and 9). Only lines 1,2,3,5,6 and 7 have been modeled, as there was no data available for line 9. This is because line 9 is a new line that has been operation only since December 2017. This line may be modeled if data from this line becomes available.

The remaining lines are divided into 44 sections. Furthermore, there are 18 substations, which are indicated by the red dots. The CS substations are the substations near the central station and are a collective of substation 4, 9 & 21. The HQ substations are the substations near the head quarters of connexxion and are comprised of substation 3 6. The connection of the feeder cables with the overhead lines is poorly visible in the graph and is not relevant for AC-side placement, since the PV is placed on the substations and not the sections.

It has been confirmed by Connexxion that there are bilateral connections in the Arnhem grid, however the precise topology of the grid has not been shared with TU Delft. Therefore, it was decided to model the grid as being unilateral (the substation can only feed the sections its connected to with the feeder cables). Bilateral connectivity may be added to the model later, the insights of this model may still be useful at locations with unilateral connections. Although the grid may differ in size from other trolley grids, the general topology of the grid is similar. Therefore it is reasonable to assume that the model proposed here can be extrapolate to other trolley grids.

3.2 Bus data

Kiepe Electric GmbH - the electrical component supplier of the trolleybuses - has collected data on the trolleybuses as commissioned by the HAN university. These measurements have been executed from December 2018 to January 2019 while the buses where in normal operation. Table 3.1, shows the number of measurements per line and the distance of that line.

Table 3.1: Bus measurements by HAN university [26]

Line No.	Source to destination	No. of trips	Length of one trip [km]
1	Velp to Oosterbeek	11	11.5
1	Oosterbeek to Velp	12	11.5
2	Arnhem Central to De Laar West	10	8.5
2	De Laar West to Arnhem Central	8	8.3
3	Het Duifje to Burger Zoo	8	9.8
3	Burger Zoo to Het Duifje	11	10.3
5	Presikhaaf to De Zeis	8	14
5	De Zeis to Preshikhaaf	8	14
6	De Laar West to HAN	7	12
6	HAN to De Laar West	7	11.5
7	Rijkerswoerd to Geitenkamp	8	12.6
7	Geitenkamp to Rijkerswoerd	8	12.6

At the time of writing, not all this data was made available to TU Delft. For each line in both directions, the measurements with the highest average bus power and the lowest average bus power were accessible to TU Delft for the use of bus load simulations. Furthermore, the monthly energy output of the substations is provided for the years 2016, 2017 and 2018. To construct the bus loads for each substation year-round, the raw power measurement data needs to be processed and in combination with the traffic data used to construct the power output of the substations. The aim is to emulate the measured substation output while preserving realistic bus power profiles. How this was done is described in detail in section .

In this chapter the various models that are used in this work are discussed in detail. First the *bus power model* is explained, followed by the *PV model* and finally the *storage model* is discussed.

3.3 Modelling the bus load under the substations

First a model for the bus power demand under each substation must be established, without this model the case-study cannot take place. The grid model is constructed from a bottom-up approach; measured data from the buses in combination with bus schedules is used to build up the power demands on each section and subsequently on each substation. Before the model is explained in detail it is important to scrutinize the input data for the model first.

As input data for the grid model, power and velocity measurements on the trolleybuses as well as the bus schedules have been used. In Arnhem there are six trolley lines that each operate on a different bus schedule in both directions. In addition, there are five different bus schedules depending on the day of the year. Namely, a workday, Saturday, Sunday, summer-workday and summer-Saturday bus schedule. The summer bus schedules are active from 30 June to 17 August 2019. The Sunday schedules remain unchanged throughout the year. These schedules can be found online [15]. From the bus schedules, the time that the bus arrives at the first bus stop has been used as input for the model, the bus movement is based on the measured data.

In figure 3.2, the bus velocity - as measured by Kiepe Gbmt - is shown. In the bus trip of around 40 minutes the bus is often changing velocity, this is expected because of the varying traffic situations, the road topology and the bus stops. In figure 3.3, it is clear that these accelerations have a major impact on the bus power consumption. The first few minutes of the measurement the velocity of the bus is zero. Since we would like to use this profile to indicate the bus movement *from the moment when the bus leaves the first stop*, the zero-velocity measurements at the beginning were removed. Of course, it could be that buses are standing still for an extended period of time at the first stop, however this behaviour was deemed unrealistic for normal bus operation.

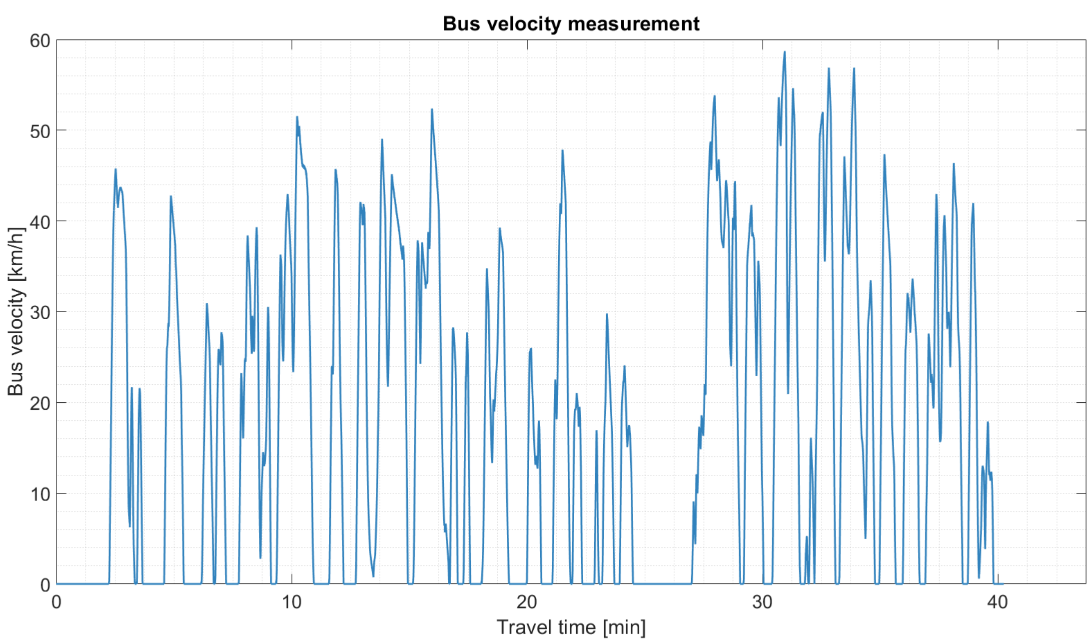

Figure 3.2: Sample of bus velocity measurement

In figure 3.3, the power of a bus has been plotted.

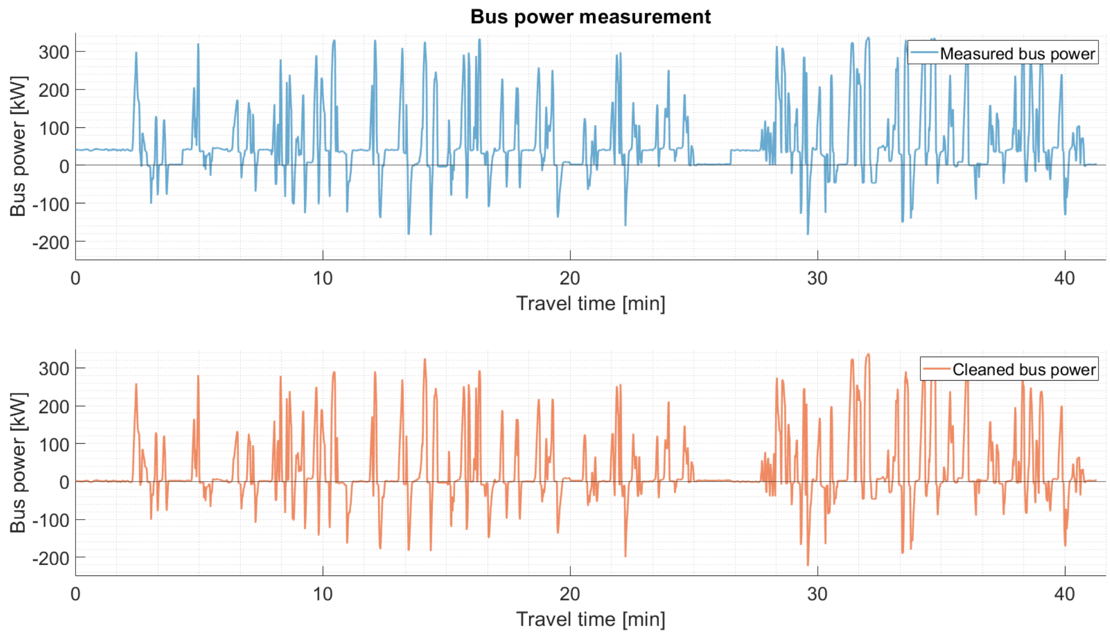

Figure 3.3: Sample of bus power measurement

From this plot we can see that the continuous accelerating and braking has a major impact on the power profile. When the bus is braking the power drops below zero. At these times, the bus is functioning like a generator that is trying to send power back to the overhead lines. When there is another bus under the same substation that requires power - or in case of bilateral connections even under another substation - the bus can transfer its braking power to that bus. However, when there is no recipient of the bus power, the power gets fed to braking resistors and wasted as heat.

Another thing that should be noted from the plot are the power plateaus at around 40 kW. These plateaus are the result of the Heating,Ventilation and Air-Conditioning (HVAC) and auxiliary power requirements of the bus when the bus is not using power for movement. The climate control in the bus is operated based on a temperature sensor(s) that measure whether the temperature inside the bus is within the set temperature range. If the temperature is not within the range, the climate control will power the HVAC at 38.4kW to correct the temperature. It is therefore clear that the HVAC demands most of the non-movement power and that this power is not negligible. Especially on cold days the HVAC energy can be significant, amounting to almost 50% of the total bus energy [26]. The auxiliary power is only one or two kW and is therefore negligible. Unfortunately, the measurements were carried out from December 2018 to January 2019 [26]. Since the aim is to use the measured power data sets to compute the power of the substations year-round, the power data had to be corrected for the HVAC power.

First the HVAC power had to be removed from the measured data. The HVAC power profile was recreated by multiplying the HVAC trigger signal (0 or 1) with the HVAC power of 38.4kW. This profile was then subtracted from the measured data to yield the *clean power profiles*, see figure 3.3. Here again the first few minutes of measured data were removed. It was later found that the HVAC power is also set to zero if the bus load is higher than 300 kW to prevent overheating of the overhead lines, however this is not considered in this work. The impact of this assumption is not likely to have a large effect on the bus load profile. From figure 3.3 it can be seen that the 300 kW only happens in the acceleration peaks of the bus and are only sustained for small duration.

The idea behind the model is to use the power and velocity data from the buses to determine where in the grid the bus is drawing what power. Later on, the PV is sized according to the energy and power demands of the substations. The steps below give a simplified illustration of the logic behind the grid power model.

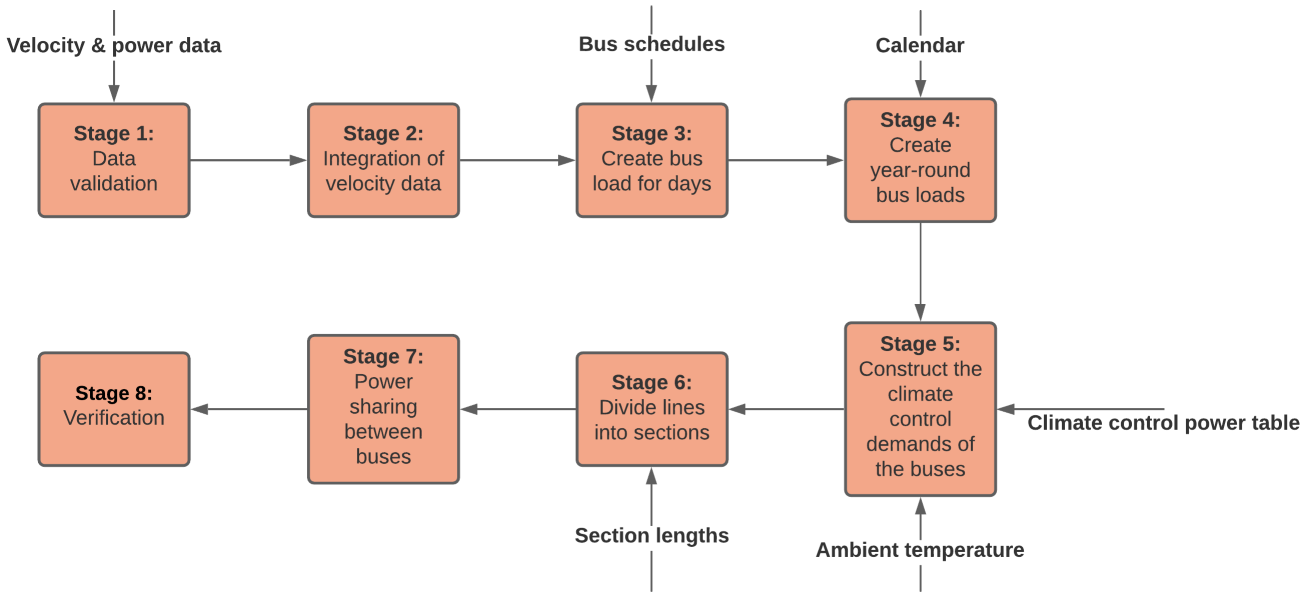

Figure 3.4: Stages of the grid load model

The first stage has already been discussed in section 3.3 and the second stage is trivial. Therefore, the explanation shall continue from stage three on-wards.

3.3.1 Stage 3: Create bus loads for days

Initially, the simulation was carried out for each line in both directions and for each bus schedule. A matrix was established with alternating bus location and bus power data columns. The values from all the buses cannot be put into the same two columns because if there are multiple buses on the same line at the same time the last bus to be computed will override the values of the previously computed bus. The bus values can also not be added together in the same two columns because the locations of the buses will then not be accurate anymore and they cannot be grouped into sections later on. Moreover, the power values can also not be added together because this mean that the buses are sharing power in the whole line without considering transmission losses. Of course, power sharing in the whole line is not realistic, especially if you take into account the assumption of unilateral connections. To save on computational time, it was checked for each bus if a set of the earlier used columns was available (eg. that earlier bus is no longer active for that trip) and if this was the case the new bus was put into that set of columns. According to the bus schedules, not all buses drive the entire line. Some buses start at the central station (CS) and drive to the end of the line, while others begin at the first bus stop and stop at CS. In this work, it was assumed that measurements are used till the time that they enter the CS or from the time that they leave the CS. The waiting time of the buses is unknown, because it is not clear how the buses transition from one line to another at the CS. In this transition time, the buses may be heated or cooled, but this is not taken into account in the model. This approach resulted in a matrix for each line for each day with a different bus schedule.

3.3.2 Stage 4: Creating year-round bus loads

The bus values for each line for the days with different bus schedules were now made into year matrices for each line. This was done by appending the rows of the bus data from different days according to the calendar. Making year matrices out of day matrices increases the computational burden considerably. However it was still decided to do it early on in the model because of the chosen approach for incorporating the HVAC power demands of the buses. This approach is discussed in the next step.

3.3.3 Stage 5: Construct the climate control power demands of the buses

The process for creating the HVAC profiles is shown in figure 3.5.

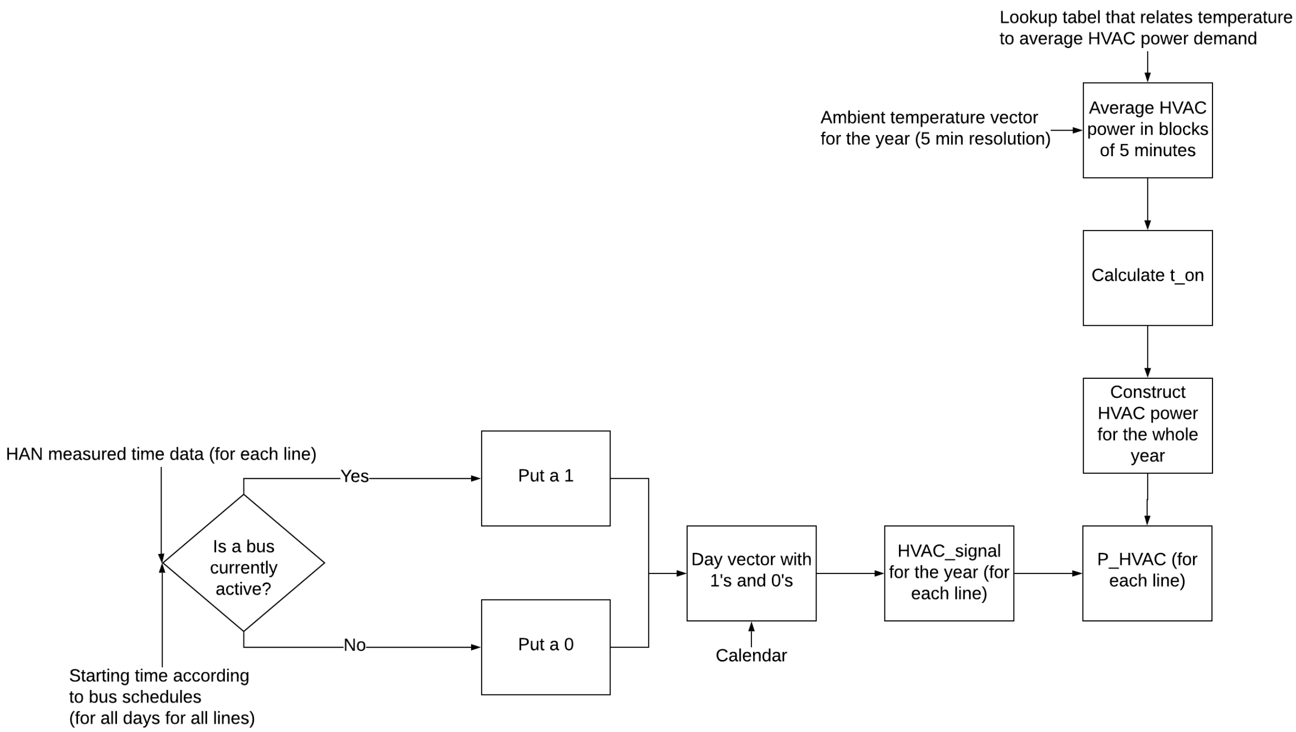

Figure 3.5: HVAC power construction logic

Starting from the left, the bus schedules in combination with the measurements are used to see if a bus is currently active on that line. To clarify, by active a bus that undertakes a trip is meant. If this is the case a 1 is placed in the first column of matrix for that instance in time. If there is no bus a 0 is placed in that location instead. Similar to the structuring of the bus locations and powers, if multiple buses are active at the same time the next column receives the 1 and so on. Year matrices can be constructed with the use of the year calendar. These new matrices contain the signal for when the HVAC could be on. But as we have seen in figure 3.3, it does not mean that the HVAC is active when the bus is active.

To compute the actual HVAC power, the logic continues at the top-right of the logic chart. It was observed from the power measurements that the HVAC operates in cycles of approximately five minutes. In these five minute blocks the climate control turns on the HVAC for a fraction of the time. If a lot of HVAC power is required, the on-time is close to the cycle time. HVAC power reuirements are low, the on-time is close to zero. This observation lead to the approach for estimating the HVAC power without the need to establish a thermodynamic model, which would be outside of the scope of this work.

In [26], the researchers try to construct an energy-balance for the Arnhem trolleybuses but conclude that all but one variables are trip specific and relate to each other. Therefore it would be difficult to get an accurate general HVAC power model. The researchers continue by correlating the average HVAC power with the ambient temperature, since this is the only parameter that is not trip specific. This is shown in figure 3.6. Here, the black dots show the average HVAC power for the each bus trip as a function of the ambient temperature. However, since the measurements are conducted in the winter the ambient temperature range is only between -1 °and 12 °. Therefore, the fit is not usable for the entire year.

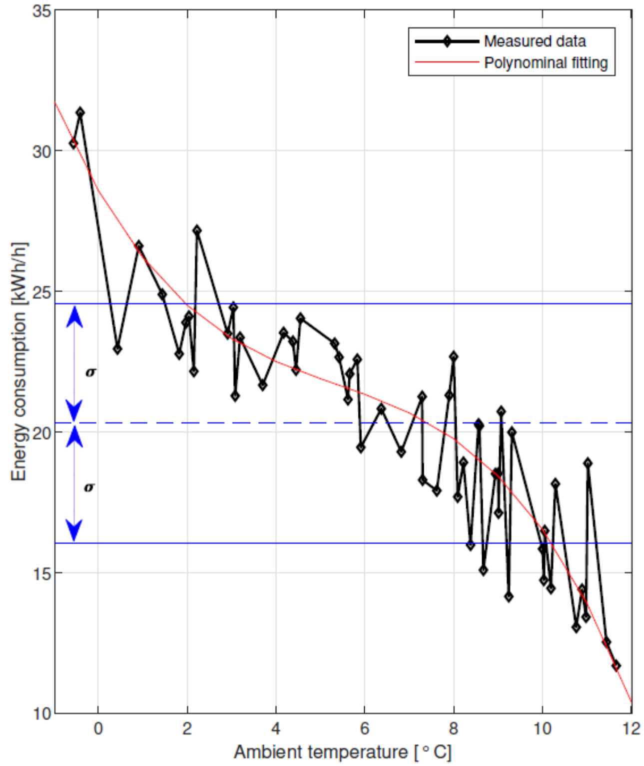

Figure 3.6: Average HVAC power as a function of ambient temperature [26].

To get a better approximation of the HVAC power, formula 3.1 was used to come up with a general power balance across the bus has been constructed for ambient temperatures in the range of -20 °to 40 °Celsius [26].

$$\dot{Q}_{\text{net}} = U \cdot A \cdot (T_{\text{amb}} - T_{\text{cab}}) + \dot{m}_{\text{freshair}} \cdot (e_{\text{amb}} - e_{\text{cab}}) + \dot{m}_{\text{doorair}} \cdot (e_{\text{amb}} - e_{\text{cab}}) \cdot n_{\text{do}} + n_{\text{p}} \cdot \dot{Q}_{\text{p}} \tag{3.1}$$

In this formula $\dot{Q}_{\text{net}}$ is the net heat flowing in and out of the bus. The first term represents the heat losses through the vehicle body, here U is the overall heat transfer coefficient of the bus, A is the area of the bus, T_{amb} and T_{cab} are the ambient temperature and the cabin temperature, respectively. The second term represents the heat exchange due to fresh air circulation, here $\dot{m}_{\text{freshair}}$ is the mass flow rate of fresh air flowing through ventilation of the bus, e_{amb} and e_{cab} are the enthalpies of the outside and inside air. The third term represents the momentary heat exchange due to opening of doors at the bus stops, here $\dot{m}_{\text{doorair}}$ is the mass flow rate of air through the open doors and n_{do} is the number of doors that open. Finally, the forth term represents the metabolic heat gain from the people inside the bus, here n_{p} is the number of people on the bus and finally $\dot{Q}_{\text{p}}$ is the heat generated per person.

Although the heat balance across the bus is continuously changing, the climate control does not follow the same dynamic behaviour. Therefore, the assumption was made to assume average values for the inputs of the formula with exception of the ambient temperature.

The values that have been assumed are stated in table 3.2.

Table 3.2: Input variables for equation 3.1

U	40	W/(m2*k)	Convective heat transfer assumed
A	72	m2	Only for sides, roof and bottom of bus
$\dot{m}_{freshair}$	2	kg/s	Mass flow of fresh air - ventilation (6120m3/h for 100% of the time, air density of 1.225 kg/m3)
T_{cab}	294	K	Inside temperature (21°)
e_{cab}	294000	J/kg	Enthalpy of inside air
$\dot{m}_{doorair} \cdot n_{do}$	0.6	kg/s	Mass flow of fresh air - doors (25% of the time doors are open at a volume flow of 10000 m3/s)
n_p	20	[-]	Number of people on the bus
Q_p	100	W	Metabolic heat generation per person

For U 40 w/(m^2*k) was assumed because this is close to the convective heat transfer coefficient for unforced convection at 10m/s, which is assumed to be the average bus velocity. This is in accordance with the measured data. For the area of the bus only the side, bottom and roof of the bus have been assumed as areas that transfer heat, because these areas experience the 10m/s air flowing by. The heat transfer across the other areas is negligible compared to these areas. Furthermore, the $\dot{m}_{\text{freshair}}$ has been assumed to be 2.0 kg/s. This is equivalent to 6120 m^3/hr at an air density of 1.225kg/m^3 which is the air flow rate for 12m long buses in Turkey at around 30 degrees Celsius [43]. Due to a lack of a specification sheet this value is also taken for the Arnhem trolleybuses. The higher temperature in Turkey could be compensated by the longer bus length of 18m. Furthermore, $\dot{m}_{\text{doorair}} \cdot n_{\text{do}}$ is taken as one value of 0.6 kg/s. This is was based on the assumption that the doors are open 25% of the time with an air flow of 10000 m^3/s which is equivalent to a tiny breeze. Finally, it is assumed that there are on average 20 people on the bus with each a metabolic heat generation of 100 watts. The 100 watts is based on the assumption that a person eats approximately 2000 calories per day.

The final step in relating the HVAC power to ambient temperature is the *coefficient of performance* (COP) of the climate control. The COP is calculated with the following formula:

$$\text{COP} = \frac{\text{P}_{\text{effective\_climate\_control}}}{\text{P}_{\text{consumed\_climate\_control}}} \tag{3.2}$$

Since the climate control is removing or adding energy to the bus, the COP can be higher than unity. For the heating operation of climate control a COP value of 4 is assumed and for the cooling process a COP of 5 is assumed. The average HVAC power can then be calculated by equation

$$\bar{P_{\text{cc}}} = \frac{\dot{Q_{\text{net}}}}{\text{COP}} \tag{3.3}$$

Admittedly, due to a lack of information, some of the inputs for the energy balance are educated guesses. However, in the temperature range, the data fits nicely. Therefore, it was assumed that the climate control power could be estimated with this approach within the range of -10°to 40°. The results of this approach together with the measured values from Kiepe GmbH are plotted in figure 3.7.

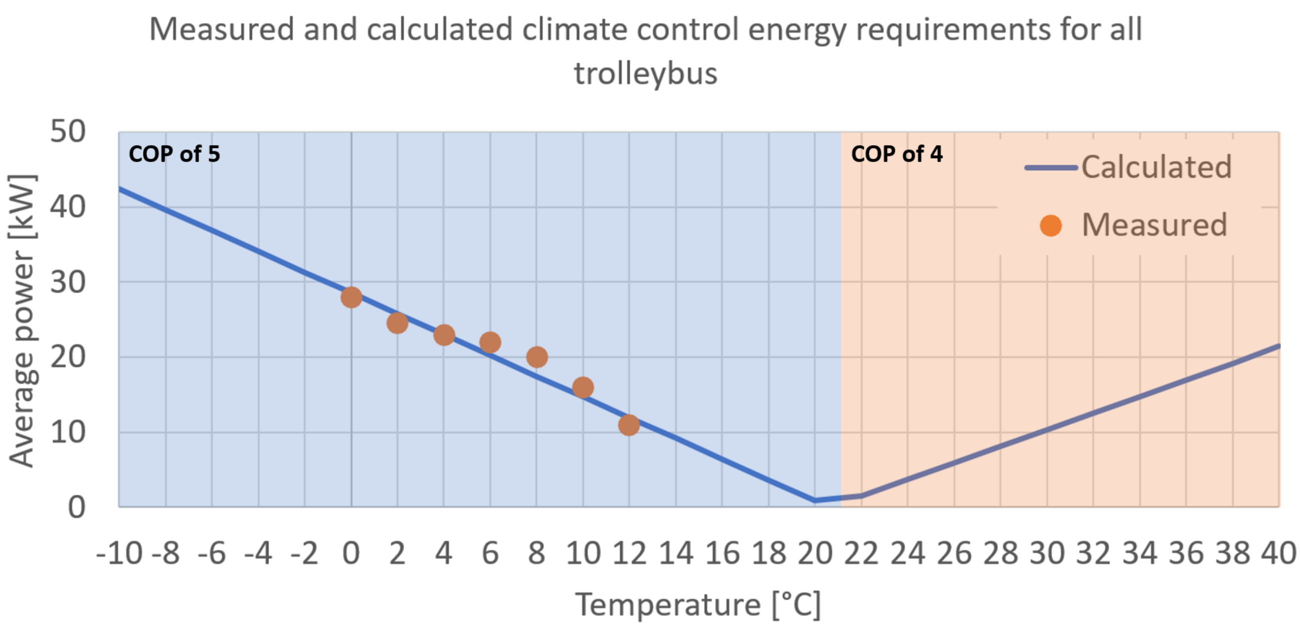

Figure 3.7: Comparison between the calculated and measured climate control average power demands

Since the results are similar to the measured data and because the approach is practical, this method was selected for the work in this thesis. However, the method has some major assumptions which could give significant errors in the approximation of the overall bus load. First of all, the buses are assumed to be at at a temperature of 21 °C. At the start of the day and during breaks this is not the case and the climate control temporarily needs to do more work to reach the desired set point. Furthermore, it could be that the climate control was just operational for a bus arriving at the final bus stop, but is now used for a new bus in the reverse direction. The climate control will then be operational for a longer duration than necessary.

It is clear that modeling the HVAC in this method results in the errors listed above, but how much this affects the actual HVAC output is not known and can be found by comparing the model with more measured data. However, the errors are assumed to be small since the extra HVAC power to reach the steady-state temperature can be reached within a fraction of the time of a workday. Moreover, the error of using the HVAC for longer than necessary on the ends of the lines can be in the worst case result in 5 minutes of additional HVAC power per line, which is not a lot considering the trip durations.

To get more accurate results a thermodynamic model could be constructed, but for this model to be working properly a lot of trip specific inputs are required. In addition, this model would - without a doubt - increase the computational burden. It is therefore only recommended to construct such a model if a very detailed HVAC power profile is required.

Now that we have a method for relating the HVAC loads to the ambient temperature, the logic in figure 3.5 can continue at the top right. Next, the ambient temperature for the Arnhem needs to be used to compute the actual HVAC loads. The per-minute ambient temperature data from nearby weather stations has been used. For the temperature data, the following locations have been used: Deelen (7km, NL), Kalkar (39km, DE), Soesterberg (45km, NL), Volkel (41km, NL), De Bilt and Hupsel (53km, NL). The selection of stations and the interpolation has been automatically carried out by Meteonorm. Furthermore, the data ha a resolution of one minute and is based on a data set from 2000 to 2009 for temperature variables and 1991 to 2010 for the irradiance data. Meteonorm generates realistic data by applying a stochastic model to the data.

By holding each fifth weather data point for 300 seconds - and removing the other points- the data was made into per-second data. Then a matrix was constructed that relates the ambient temperature for each second with the average HVAC power. Next,the on-time of the HVAC for each 5 minute interval was calculated using equation 3.4.

$$t_{\text{on}} = t_{\text{cycle}} \cdot \frac{\bar{P}_{\text{actual}}}{P_{\text{rated}}} \tag{3.4}$$

Here t_{on} is the on time of the HVAC and t_{cycle} is the cycle time of the HVAC which was found to be 5 minutes from empirical measurements. $\bar{P}_{\text{actual}}$ is the average load of the HVAC based on the heat balance over the bus (equation 3.1 and the COP. Finally, the P_{rated} is the rated HVAC power of 38.4 KW. In the third column of the matrix the rated power of 38.4 kW was placed in the first cells up-to the value of t_{on}. The remaining cells are zero. In this way, a matrix with HVAC powers based on the ambient temperature was constructed for the year.

The final step was bringing it all together, the year HVAC signal matrices were multiplied with the HVAC power matrix. In this way the HVAC powers for all the bus lines for the whole year were computed.

The first drawback of this approach is the computational burden later on in the model since clean bus power is already constructed for the year, this yields a lot of data.

Moreover, since the lines are not exactly multiples of five minutes long, the average HVAC power is not equal to what it should be based on the ambient temperature. To find how significant the error could be three parameters are accounted for; the relative error for each power, the absolute error for each power and the probability of occurrence for each power.

The first thing that can be concluded is that the duration of the line correlates with the error of the HVAC power. The smaller the duration, the larger the error because the final five minute block is a larger part of the line. Moreover, if the duration of traveling the line is just a little bit longer than a multiple of five minutes, the relative error is large for low HVAC powers. This is because the duration of the final block is short. However, since this is for low HVAC powers, the absolute error could still be low. The opposite is true for lines that are almost a new multiple of five minutes. Here the relative overall error is low, but stays constant at higher HVAC powers. It was found that the largest absolute error for each line occurs where the duration of traveling the line is the closest to $n + 0.5$ times the duration. Where n is the number of five minute blocks.

In figure 3.8, for each line the relative and absolute error for each line has been plotted for the measurement that was the closest to $n + 0.5$ the line duration. The largest error occurs for line two, in the direction of Zuid-Laren to Arnhem Central which is the shortest line.

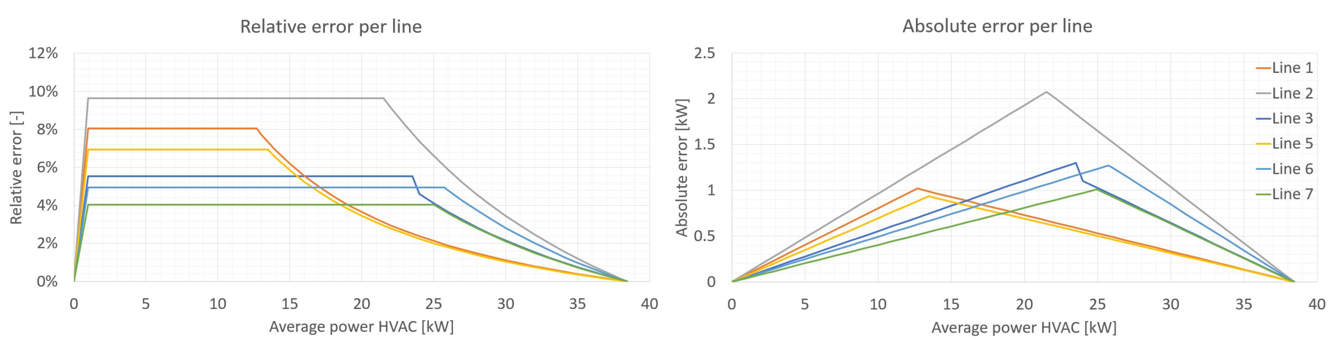

(a) Relative error for each line *(b) Absolute error for each line*

Figure 3.8: Error per line

The maximum error in the HVAC power is 2.1kW at 21.5kW of heating, which occurs at 5-6 °C (according to figure 3.7). At these temperatures, HVAC power is around 40% of total power. This makes the maximum error around 4%. In practice the error is a lot lower, because this only occurs for the shortest line in the winter. An error of between 1.5 % and 2.5% is more realistic. Considering the error that already exists due to the method of correlating the HVAC power to the ambient temperature, errors within these ranges are acceptable for the purpose of this model. Now that it is established that the HVAC model is sufficiently accurate, the HVAC for the whole year was added to the clean bus profiles for the year, resulting in the *realistic bus power profiles*.

3.3.4 Stage 6: Divide the line into sections

Now that we have constructed the realistic bus profiles for the lines, it is important to group the values under the different sections. If we know what buses are under the same substation simultaneously, power sharing between the buses can be accounted for. For each section a matrix was erected. Values from the matrices of the lines were put into the section matrices on the basis of the location columns next to the power columns. First the lengths of all sections had to be measured. This was accomplished by measuring the lines in both directions with the measurement tool of Google Maps. The results can be found in appendix C. The bus data is organized similarly to how it was done initially for the lines. Alternating location and power columns are placed in the matrix. The power values can still not be added together, because then the buses would share power without transmission losses. The logic for power sharing between buses is explained in the next stage. Figure 3.9, gives us the first inside into the traffic on the sections. Here - for illustration purposes- the traffic on each of the sections has been shown in a heatmap. The darker the color, the more buses are present at the section on the same time. The time is plotted for 25 hours because the bus schedule for a workday for this line operates till 1 AM. For the days with a different bus schedule, the results are shown in Appendix D.

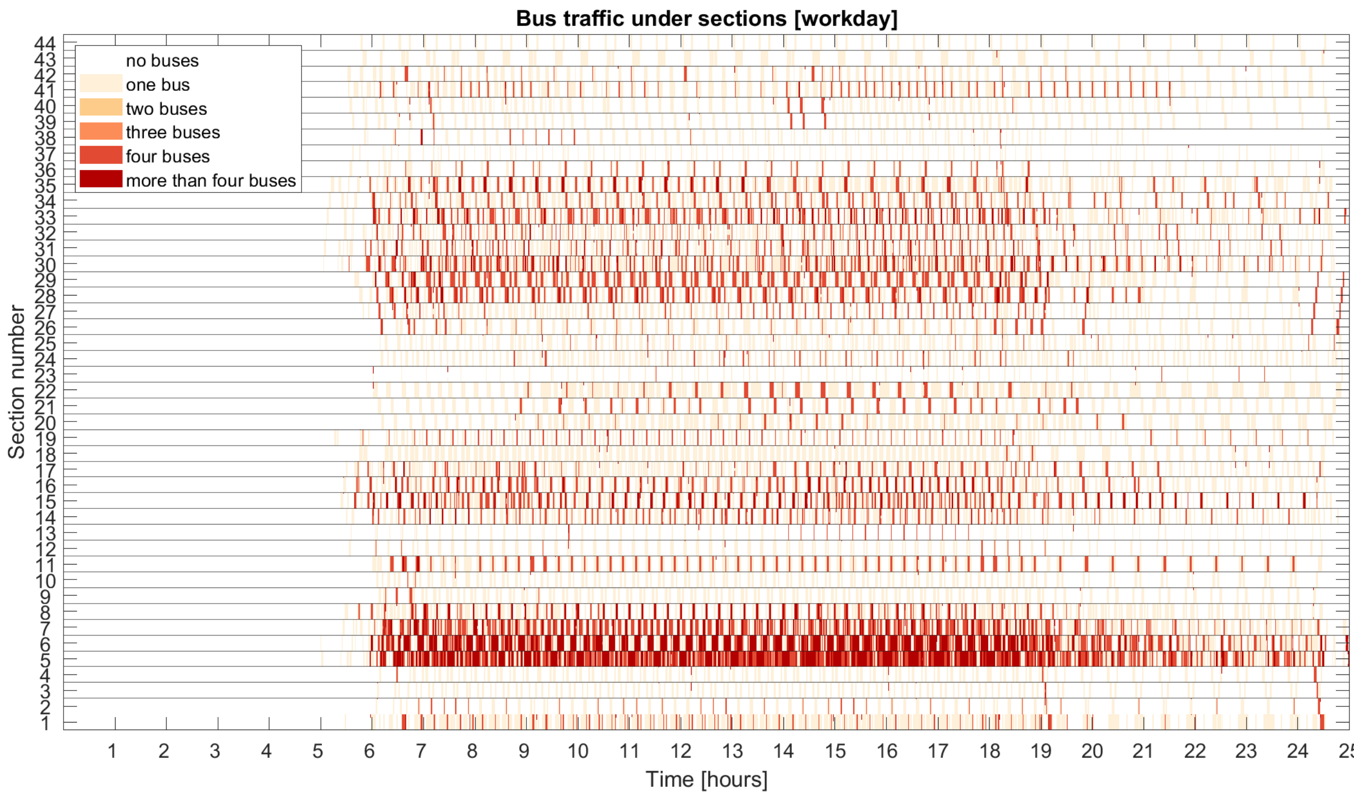

Figure 3.9: Traffic at each section for a workday

The first thing that is apparent from the figure is the large variation in traffic between the sections. This is logical, sections at the out skirts are expected to have less traffic than sections in the center. It is also clear that traffic simulations for trolleybuses that have been reported in literature do not capture the traffic that a real trolley grid experiences. Substations may have to power lots of buses simultaneously, considering that the substations power multiple sections.

Next, the columns of the sections under the same substations were put next to each other in *substation power matrices*. The implicit assumption here is that the substations cannot share power with each other. We know that this is not everywhere the case in the Arnhem grid, however due to a lack of information, we still decided to make this assumption. Parts of the Arnhem grid are likely to operate with unilateral connections and so are (parts of) other trolley grids.

3.3.5 Stage 7: Power sharing between buses

Buses that are under the same substation are able to share power with each other via the overhead lines. In this section, the logic of how this was incorporated in the model is discussed. In figure 3.10, the logic for power sharing between buses is illustrated.

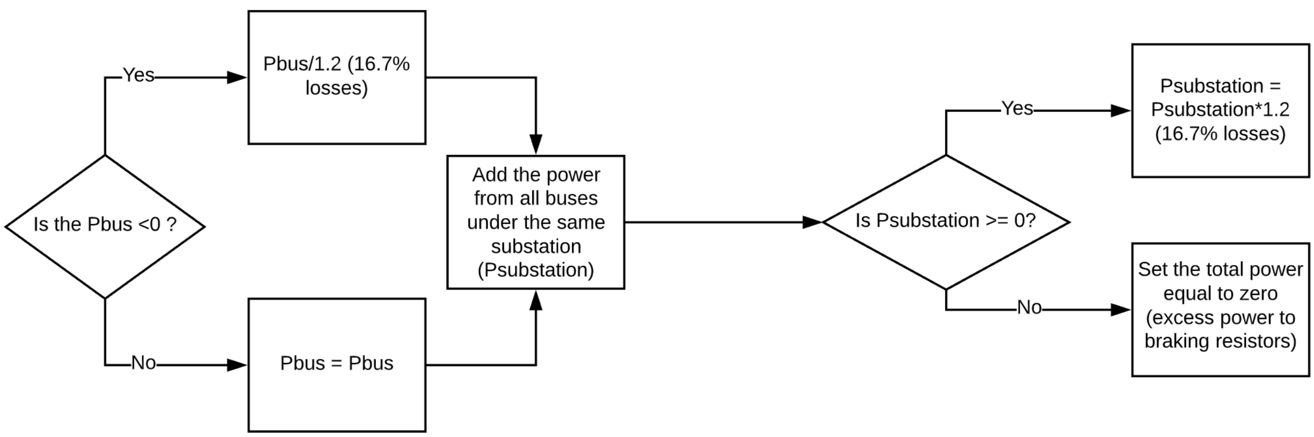

Figure 3.10: Logic for power sharing among buses

First, we must know for all the buses under the substation if they are operating in motor or generator mode. If they are operating in generator mode, the buses try to send power back into the trolley grid. In the model, this power was divided by 1.2 to account for 16.7% transmission losses. A constant line loss of 16.7% was assumed because at this stage the grid topology is unknown, therefore no reliable input can be used for power flow calculations. It could - for instance - be that there are a lot of parallel overhead lines in the city centre. The current would then be divided among the overhead lines to feed to the buses, thereby reducing the power losses. The 16.7% losses was established as a conservative estimate. In the Gdynia, Poland network the average transmission losses are 8.5%. However, transmission losses of 15% and higher have been found [44].

If the buses are using power, the power remains unchanged. Next, the powers from all the buses under the substation are summed. If the overall power is negative, the power must be set to zero. This is because the substations cannot feed power back to the AC grid due to the rectifiers. Hence, the power is fed to braking resistors on the buses. If the power is equal to or higher than zero, this power must be multiplied by 1.2. It is important to note that for the simulation it was assumed that the buses cannot recuperate their own braking energy. Some newer buses have batteries and or supercapacitors on board. However, older trolleybuses have backup diesel generators. Since the Arnhem grid operates a variety of buses, it was assumed that no buses have on-board storage yet. It is recommended to investigate the option of buses using their own power though, as this can save up to 20% of the total bus energy [29].

3.3.6 Stage 8: Verification

Now that the model has been constructed, it is important to validate the results from the model. In figure 3.11, the overall grid energy that was measured by Connexxion is compared with the grid energy that has been computed by adding the annual energy from the substations. As said before, HAN has shared the bus measurements with the highest energy and the lowest energy. For the model, initially the plan was to use both data sets to see which one matched the sum of the substation powers provided by Connexxion best. However, after using the minimal energy bus trips, it was found that the results matched the measurements reasonably well. Due to time constraints, it was decided to use this data set before analysing the maximum energy data set. In figure 3.12, the annual measured energy output under each substation is compared with the computed output.

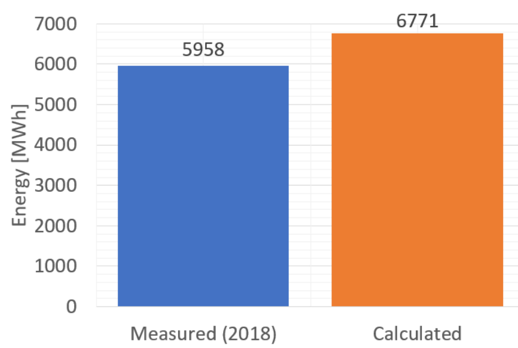

Figure 3.11: Arnhem trolley grid energy consumption

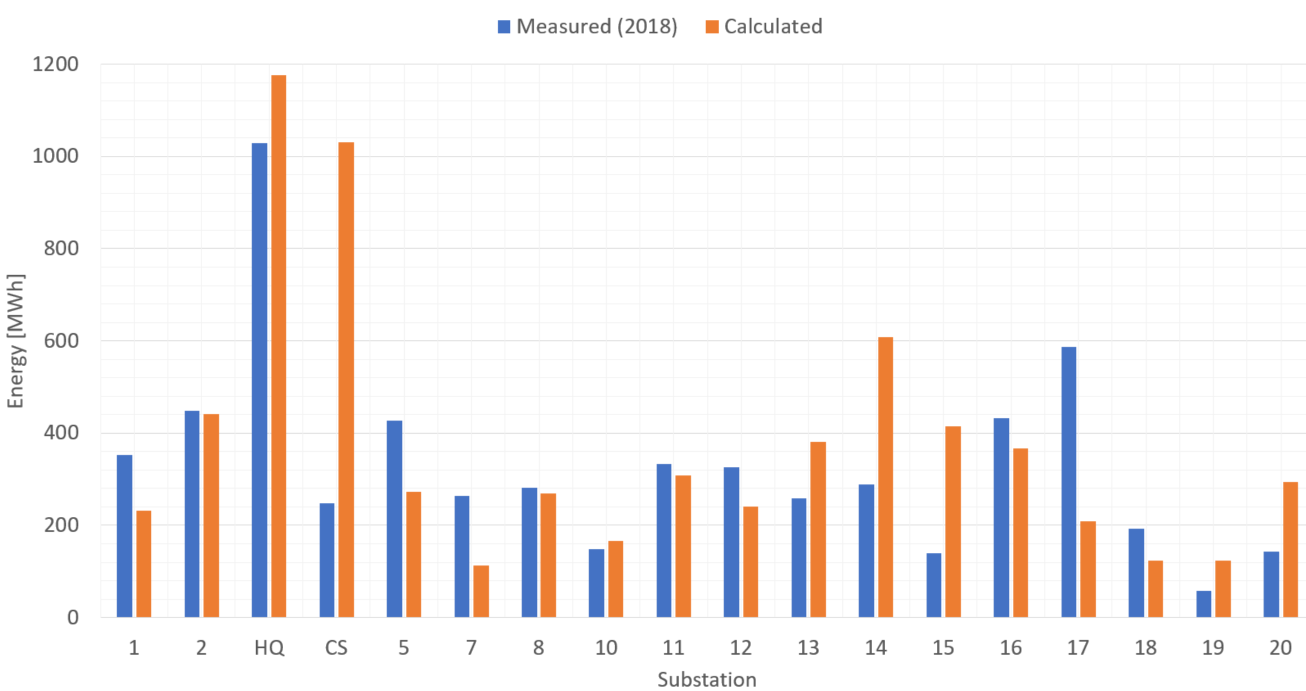

Figure 3.12: Substation energy consumption

Overall, the difference between the measured grid load and the computed grid load is 14%. The main reason for this may be that the losses in the overhead lines are assumed to be 16.7%. This assumption is likely to high as this number for a similar grid in Gdynia is 8.5% [44]. Later, it was found that 10% transmission losses in overhead lines is a common assumption [45].

However, at the substation level, the profiles match reasonably well. Substations 3 & 6 and 4,9 & 21 are grouped together as HQ and CS. These substations together provide power to their sections, but it is not clear how much each substation contributes. A general trend that was observed is that substations in the centre of the grid consume less energy than was calculated with the model. The opposite is true for substations in the outskirts. This observation shows that there are bilateral connections between the substations and that outside substations aid the inside substations in their power demands. Placing the PV in the city centre has two benefits: the first benefit is that the power does not need to travel all the way from the outside substations, which will result in lower energy losses. The second benefit has to do with the observation that the city centre is busier than the outskirts. More power from the PV will therefore flow directly into the trolley grid as oppose to the MVAC grid. This will therefore raise the renewable energy share of the grid further. It can also be seen that the energy for the CS substation is massively off. Part of the reason could be because the stand still time of the buses at the CS is larger than normal in the measured data. It was found that the calculations are precise enough for this work. If the overhead line topology becomes available, it may be interesting to repeat the simulations with power flow calculations.

Next, the monthly loads for the PV are analyzed to see if there are no abnormalities on a monthly scale. In figure 3.13, the monthly variation in bus load is illustrated.

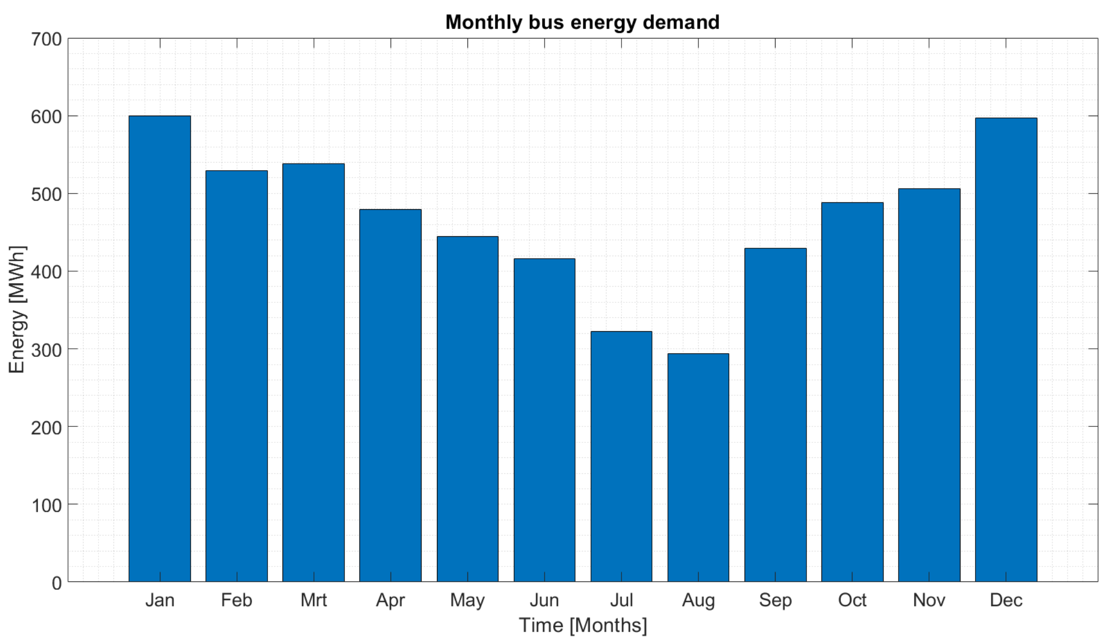

Figure 3.13: Grid monthly energy

In July and August there is a drop in power, due to a reduced number of buses on the lines because of the summer schedules. In the winter months, the bus load is higher due to higher HVAC loads. The months look as expected.

The next step is to investigate the power profile of the grid. This profile is plotted in figure 3.14.

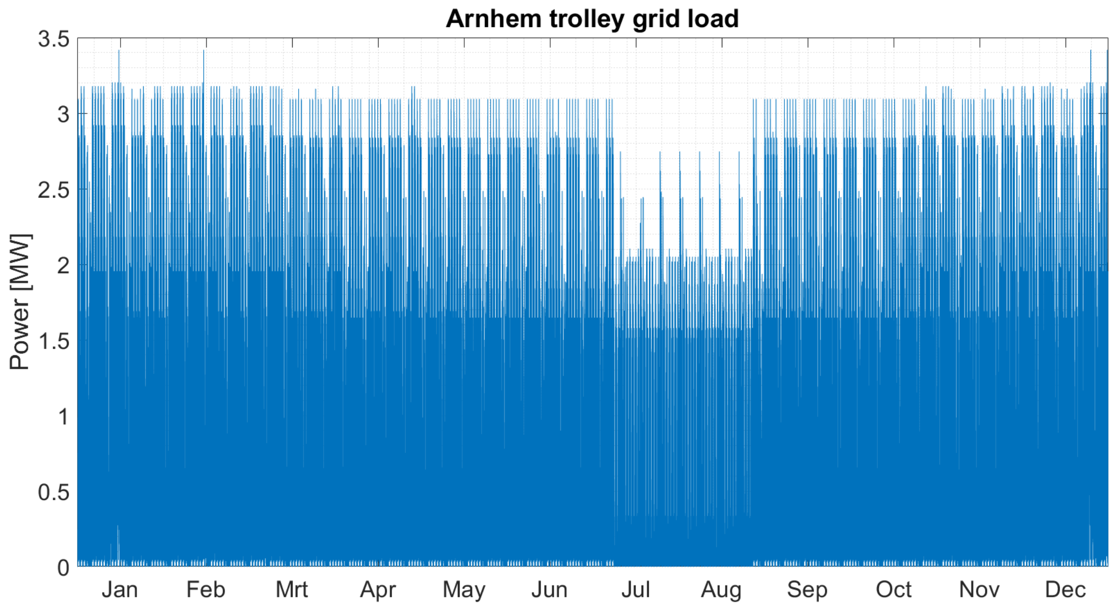

Figure 3.14: Grid power consumption

Here, the workday load peaks are visible, followed by the lower peaks in the weekend. However, in this plot the effect of varying climate control power is not visible. This is because even when the climate control is not used as much (eg. the spring), there are still moments when it is active at rated power while the buses are accelerating. Therefore, the power peaks are of constant magnitude throughout the year.

To see the variations in the grid load on all time scales, figures 3.15 and 3.16 show the long-term and short-term load variations. In figure 3.15, the year is plotted with the average powers for the days, weeks and months. In figure 3.16, the average powers for the hours, minutes and seconds is shown.

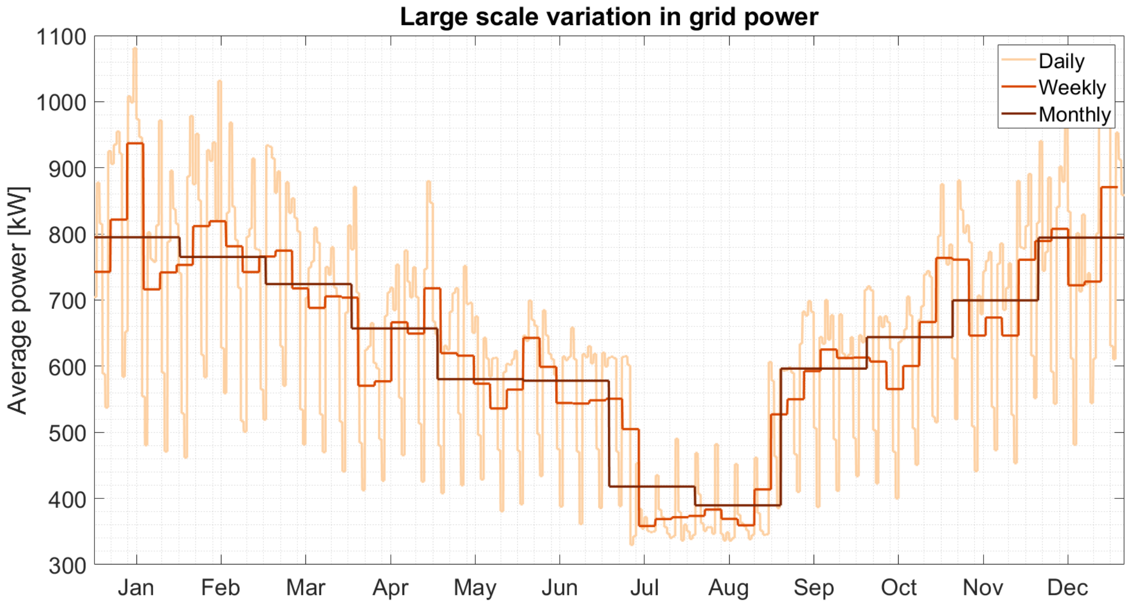

Figure 3.15: Annual grid load profile

The effects of varying HVAC load is clearly visible throughout the year. A 25% difference between June and December is found. Both months use the non-summer bus schedules, therefore it can be concluded that the HVAC demands vary a lot throughout the year. The daily fluctuations are mainly the result of buses not driving in the night. To further investigate the load behaviour of the grid, two days were analyzed for short term load variations. In figure 3.16a, the second, minute and hourly power averages are shown for the 21st of June. In figure 3.16b, this is done for the 22nd of December, since the winter solstice of 2019 fell on a Sunday (which operates with a different bus schedule). Both days use the same bus schedule for a workday that is not in the summer. In both plots, the day starts with a load, this is due to the buses driving till 1 AM.

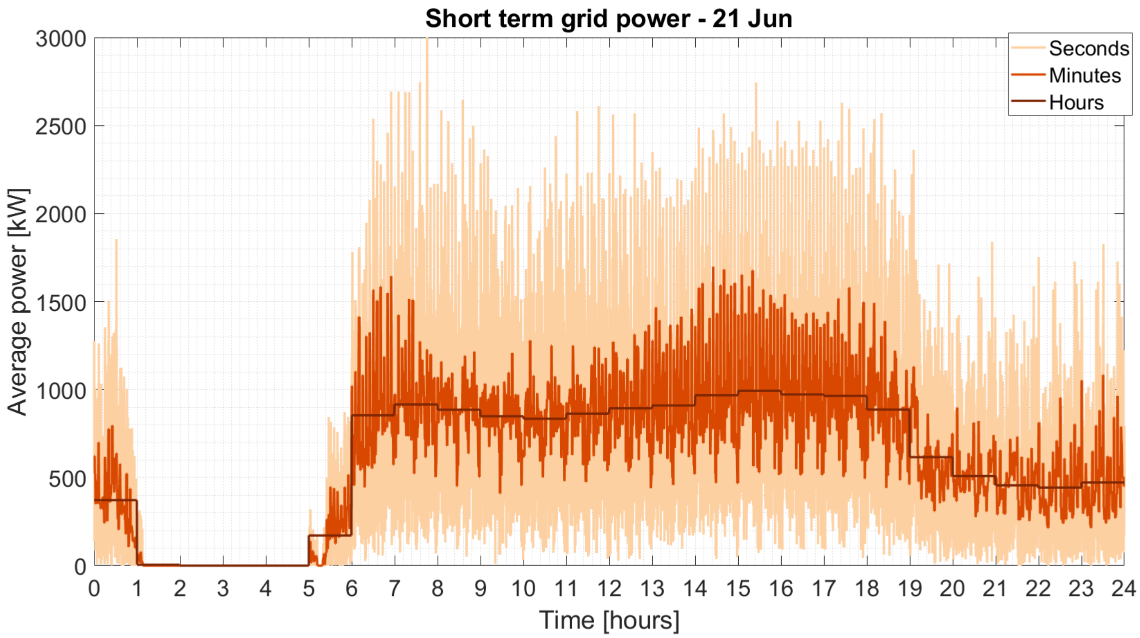

(a) Grid load profile 21st of June (summer solstice)

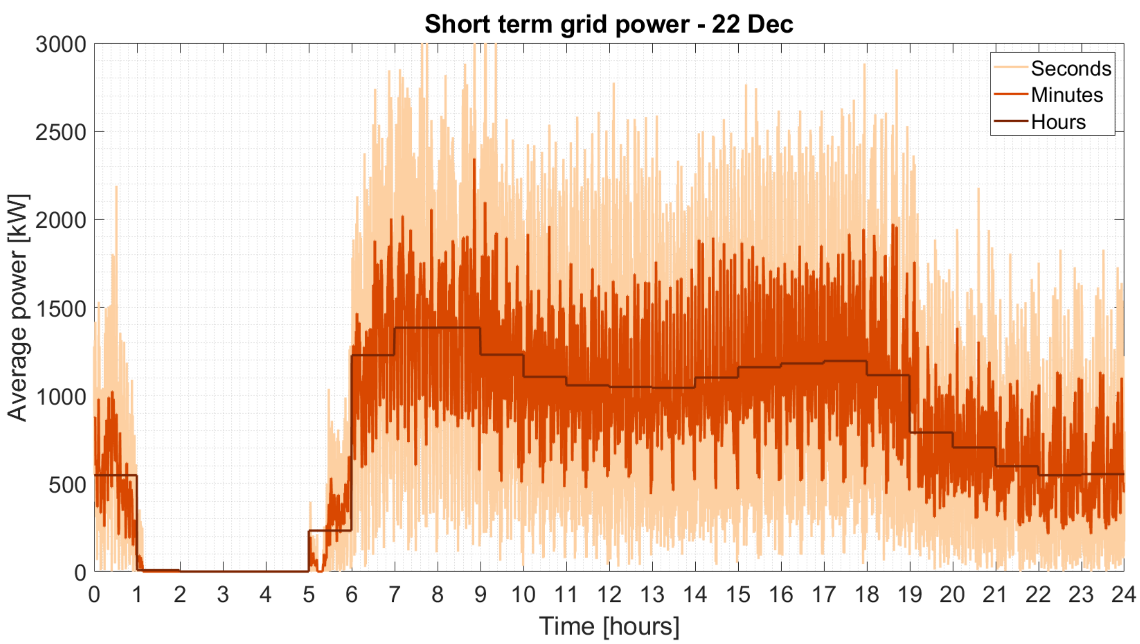

(b) Grid load profile 22nd of December

Figure 3.16: Grid power consumption

It is clear that in both cases the load in the morning and evening increases, this is because there are more buses driving at these times. Furthermore, in both cases the hourly variation in the afternoon is low. This is because the ambient temperature and the bus schedules in this time frame are not varying much. In the evening the load in both plots drops, this is due a reduced number of buses driving.

Furthermore, on the minute and second time scales, the variation may be large due to accelerating and decelerating buses. Another reason for the minute scale variation may be that buses are beginning or ending their trips. Now that we have looked at the grid load, it is important to study the individual sections and substations to see if there are no abnormalities in the load profiles. These load profiles are shown in appendix E and confirm that there are no abnormalities present.

In conclusion, in this section the steps to make the substation load profiles from the bus load profiles have been outlined and the model has been validated on the based of an energy comparison with measured data sets. Finally, it was observed that the load profiles contain no abnormalities. It was therefore assumed that the results yield a usable representation of a the Arnhem trolley grid. In the next section, the PV model is explained.

3.4 Modelling the solar PV

In this section the input data for the solar PV model is analyzed first. Afterwards, the model is explained and validated.

3.4.1 Input data

As stated before, Arnhem does not have a KNMI station, the data used for the model is a mix from other stations. For the radiation data, the locations that were used are; Wageningen(16km, NL), De Bilt(49km, NL), Bocholt (48km, DE), Cabauw(65km, NL), Bochum(113km, DE) and Osnabrueck (151km, DE). For the temperature data, the following locations have been used: Deelen (7km, NL), Kalkar (39km, DE), Soesterberg (45km, NL), Volkel (41km, NL), De Bilt and Hupsel (53km, NL). The selection of stations and the interpolation has been automatically carried out by Meteonorm [41]. Furthermore, the data ha a resolution of one minute and is based on a data set from 2000 to 2009 for temperature variables and 1991 to 2010 for the irradiance data. Meteonorm generates realistic data by applying a stochastic model to the data.

Since the Netherlands is located in the Northern Hemisphere, the optimum model azimuth is 0°(south facing). The optimum inclination is less straightforward and was iteratively determined by changing the inclination and analyzing the global horizontal irradiance for a tilted plane. This value can be calculated by hand using the Direct Nominal Irradiance (DNI), Diffuse Horizontal Irradiance (DHI) and the Global Horizontal Irradiance (GHI) for a non-tilted plane. However, Meteonorm has an option to automatically compute the GHI for any tilt angle, so this option was chosen instead.

In table 3.3 the annual solar energy per m^2 for varying inclination angles is illustrated.

Module tilt angle (θ_{M})	GHI potential (kWh/(m2 ·yr)
0	990
10	1092
20	1122
30	1152
36	1159
37	1161
38	1160

Table 3.3: Energy yield as a function of module tilt

The optimum module tilt is **37°**. It is therefore assumed that the modules will be facing to the south under the optimum inclination. Considering these design choices, we can now scrutinize the weather input data for the model. In this section first the GHI and ambient temperature are discussed as they are the most important input parameters. Then the assumptions that had to be made about the ground temperature and the cloud coverage are talked about. The other input parameters for the model can be found in appendix F. In figure 3.17 the GHI and the ambient temperature are plotted.

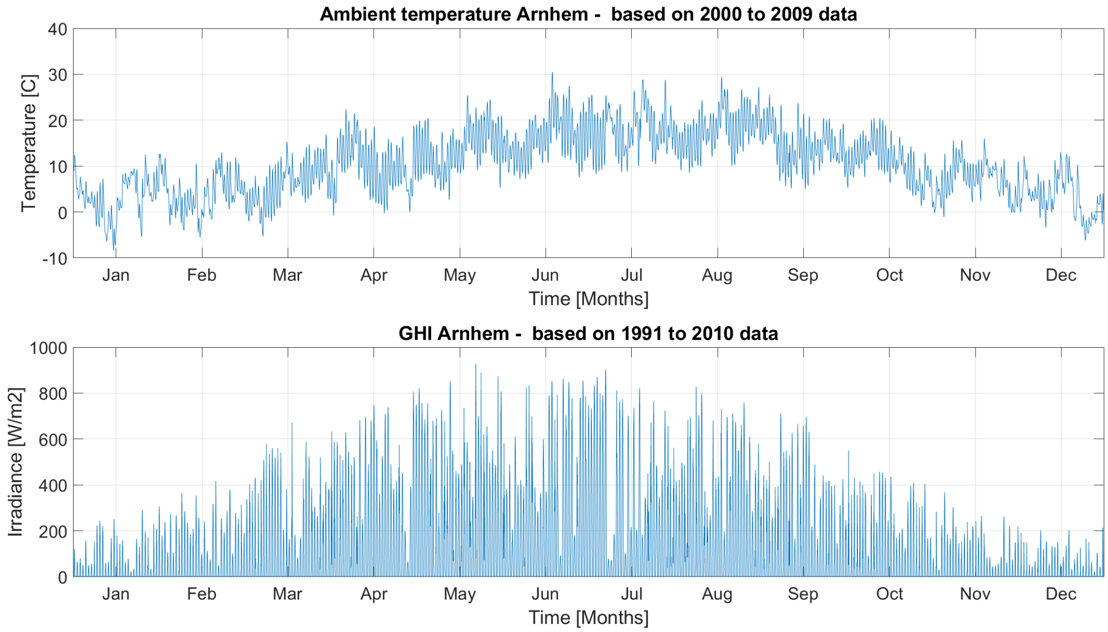

Figure 3.17: Ambient temperature and GHI data [41]

As expected the ambient temperature and irradiance are higher in the summer than in the winter and the profiles look realistic. However, the ambient temperature may be a slight underestimate in comparison with today's measurements due to global warming. Small variations in ambient temperatures only have small effect on the module performance, and therefore this small underestimate is accepted for this work.

As stated before, some assumptions had to be made about the ground temperature and the cloud coverage. For both the ground temperature and cloud coverage, the same dataset has been used as the other parameters but with hourly resolution. The cloud coverage is quantified in the Octa scale, where zero means no clouds at all and eight means complete overcast. Since no information was available on how much cloud coverage and ground temperature change per minute, it was therefore decided to replicate each hour datapoint for 60 times without introducing randomization. The cloud coverage and ground temperature can be found in appendix F. Now that we have discussed the meteorological data. It is time to discuss the PV model.

3.4.2 PV model

In this section, the PV model is explained and its outputs are used to validate its use in this work. The goal of the PV model is to convert the input irradiance (GHI) into usable power in a realistic way. For this work we assume that this is realised when the solar power is converted to AC power. Cable losses and interconnection losses between the panels are not within the scope of this thesis and are assumed to be neglible (and compensated for by the overhead line transmission losses of 16.7%). In the model the efficiency of the modules depend on the module temperature and the irradiation on the modules. There are several methods for calculating the module temperature. The module temperature has effect on the module efficiency and consequently the energy output of the modules. It is therefore important that the module temperature is calculated in a precise manner. Three models for calculating the module temperature have been compared. These models are the *Nominal Operating Cell*

Temperature (NOCT) Duffie-Beckman (DB) and a *Fluid Dynamic (FD)* model. The NOCT model is the simplest of the three and computes the module temperature on a linear correlation with the ambient temperature and the irradiance. Due to its simplicity, the model gives large errors with changes in wind speed. The DB model is an extention of the NOCT model using an additional empirical term to take the wind speed into account. Although this model is more accurate than the NOCT model it still fails to accurately capture the effect changing meteorological parameters on the module temperature. The output for the module temperature at varying wind speeds is shown in figure 3.18. In this work, a FD model has been used. The model is recreated from the Solar Energy book and applied to the setting of Arnhem [42].

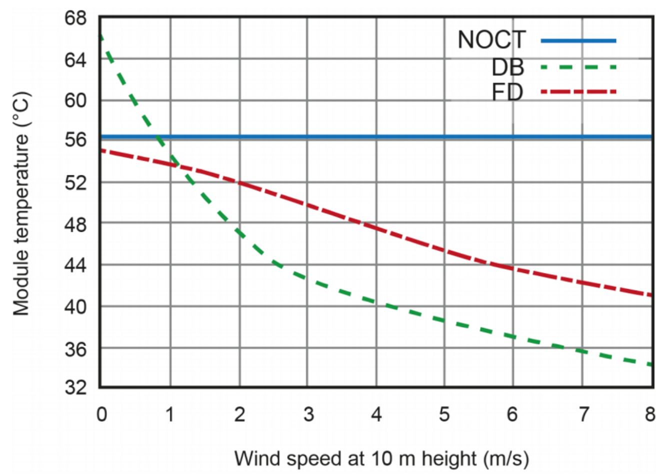

Figure 3.18: Module temperature as a function of wind speed [42].

3.4.3 The Fluid-Dynamic model

The module temperature is calculated with equation 3.5.

$$T_M = \frac{\alpha G + h_c T_{\mathrm{a}} + h_{r,\mathrm{sky}} T_{\mathrm{sky}} + h_{r,\mathrm{gr}} T_{\mathrm{gr}}}{h_c + h_{r,\mathrm{sky}} + h_{r,\mathrm{gr}}} \tag{3.5}$$

Here α is the absortivity of the module, G is the irradiance on the module, T_{a}, T_{gr} and T_{sky} are the ambient temperature, ground temperature and the sky temperature, respectively. Finally, h_c is the overall convective heat transfer coefficient of the module, $h_{r,\mathrm{gr}}$ and $h_{r,\mathrm{sky}}$ are the heat transfer coefficients with the ground and the sky and can be estimated with equations 3.6 and 3.12.

$$h_{r,\mathrm{sky}} = \epsilon_{\mathrm{top}} \sigma (T_{\mathrm{M}}^2 + T_{\mathrm{sky}}^2)(T_{\mathrm{M}} + T_{\mathrm{sky}}) \tag{3.6}$$

$$h_{r,\mathrm{gr.}} = \epsilon_{\mathrm{back}} \sigma (T_{\mathrm{M}}^2 + T_{\mathrm{gr.}}^2)(T_{\mathrm{M}} + T_{\mathrm{gr.}}) \tag{3.7}$$

It is clear that $h_{r,\mathrm{gr}}$ and $h_{r,\mathrm{sky}}$ depend on T_{M} and thus need to be solved iteratively. According to Smets. et al, nearly exact solutions are obtained after five iterations [42]. The overall convection transfer is made up of forced and free convection and can be calculated by taking the cubic root of the cubes of forced and convective coefficients [46].

$$h_{\mathrm{mixed}}^3 = h_{\mathrm{forced}}^3 + h_{\mathrm{free}}^3 \tag{3.8}$$

Convective heat transfer has to do with the movement of fluids. This movement can either be *free* or *forced*. *Free convection* occurs when the fluid moves due to temperature differences in the fluid. On the other hand, *forced convection* happens when a fluid is moved by external forces. Furthermore, forced convection may induce turbulent or laminar flow while free convection only induces laminar flow. Turbulent flow has a greater heat transfer than laminar flow and both scenarios should therefore be studied separately [47].

The laminar and turbulent heat transfer coefficients of the forced flow can be calculated with the following equations [42]:

$$h_{\text{forced}}^{lam.} = \frac{0.86 Re^{-0.5}}{Pr^{0.4}} \rho c_{\text{air}} w \tag{3.9}$$

$$h_{\text{forced}}^{turb.} = \frac{0.028 Re^{-0.2}}{Pr^{0.4}} \rho c_{\text{air}} w \tag{3.10}$$

Where Re is the *Reynolds number* that expresses the ratio of inertial to viscous forces,

$$Re = \frac{w D_h}{v} \tag{3.11}$$

Where w is the wind speed at the height of the PV array, D_h is the hydraulic diameter of the module, which is used as a relevant length scale, and v is the kinematic viscosity of the air. Pr is the Prandtl number which is the ratio between the momentum diffusivity and the thermal diffusivity. It is considered to be 0.71 for air [48]. ρ and c_{air} are the density and the heat capacity of air. The hydraulic diameter of a rectangle - and thus a solar panel - is given as

$$D_h = \frac{2LW}{L+W} \tag{3.12}$$

To calculate the free heat transfer coefficient we must look at the Nusselt number Nu, which expresses the ratio between the convective and conductive heat transfer [49].

$$Nu = \frac{h_{\text{free}} Dh}{k} = 0.21(\text{Gr} \cdot \text{Pr})^{0.32} \tag{3.13}$$

Here k is the heat conductivity of air and Gr is the *Grashof number*, which is the ratio between buoyancy and viscous forces,

$$Gr = \frac{g\beta(T - T_{\text{a}})D_h^3}{v^2} \tag{3.14}$$

Here, g is the acceleration due to gravity on Earth and β is the volumetric thermal expansion coefficient of air, which can be approximated to be $\beta = \frac{1}{T}$. Equation 3.13 can be rearranged to find the free convective heat coefficient. Now that we have found both the free and forced convective heat transfer coefficients we can calculate the mixed convective coefficient with equation 3.8.

This mixed convective coefficient is valid for the top surface of the module, the heat transfer coefficient for the rear surface was scaled from the top surface by using the Installed Nominal Operating Cell Temperature (INOCT) conditions that are provided by the manufacturer [49].

First an energy balance across the module is constructed,

$$\alpha G_M - h_c^T(T_{\text{INOCT}} - T_{\text{a}}) - h_{r,\text{sky}}(T_{\text{INOCT}} - T_{\text{sky}}) = h_c^B(T_{\text{INOCT}} - T_{\text{a}}) - h_{r,\text{gr.}}(T_{\text{INOCT}} - T_{\text{gr.}}) \tag{3.15}$$

Next, we define R as the ratio of the actual to the ideal heat loss from the back side,

$$R = \frac{h_c^B(T_{\text{INOCT}} - T_{\text{a}}) + \epsilon_{\text{back}}\sigma(T_{\text{INOCT}}^4 - T_{\text{gr.}}^4)}{h_c^T(T_{\text{INOCT}} - T_{\text{a}}) + \epsilon_{\text{top}}\sigma(T_{\text{INOCT}}^4 - T_{\text{sky}}^4)} \tag{3.16}$$

If we then substitute equation 3.15 into equation 3.16 we get equation 3.17 which we can solve with the INOCT specifications from the manufacturer. R can then be multiplied with h_c^T to get H_c^B. Finally, h_c can be computed by adding both heat transfer coefficients.

$$R = \frac{\alpha \mathrm{G_M} - h_c^T(T_{\mathrm{INOCT}} - T_{\mathrm{a}}) + \epsilon_{\mathrm{back}}\sigma(T_{\mathrm{INOCT}}^4 - T_{\mathrm{gr.}}^4)}{h_c^T(T_{\mathrm{INOCT}} - T_{\mathrm{a}}) + \epsilon_{\mathrm{top}}\sigma(T_{\mathrm{INOCT}}^4 - T_{\mathrm{sky}}^4)} \tag{3.17}$$

Some other input parameters for the temperature model are still lacking; the sky temperature, the wind speed at module height, the absortivity of the module and the front and rear side emissivity of the module. I will quickly explain the assumptions that were made for these parameters.

First the sky temperature is computed based on the cloud coverage [49]. If the cloud coverage is six octa or higher, the sky is seen as cloudy. If the cloud coverage is below six octa, the sky is presumed clear. A cloudy sky temperature can be calculated with equation 3.18 and a clear sky temperature with equation 3.19 [50] .

$$T_{\mathrm{sky}} = T_{\mathrm{Ambient}} \tag{3.18}$$

$$T_{\mathrm{sky}} = 0.0052 \cdot T_{\mathrm{Ambient}^{3/2}} \tag{3.19}$$

Wind speed in the atmosphere is different at different heights. Therefore, the wind speeds needs to be scaled to the module height.

$$w = w_r(\frac{y_{\mathrm{M}}}{y_r})^{\frac{1}{5}} \tag{3.20}$$

In equation 3.20, y_{M} and y_r are the module and anemometer heights, respectively [49]. Furthermore, the factor 1/5 is based on the surroundings, which are assumed to be open country [42]. However, this parameter should be changed based on the location where the PV would installed.

The absortivity of the module depends on the reflectivity and the efficiency of the module.

$$\alpha = (1 - R)(1 - \eta) \tag{3.21}$$

As is typical for solar modules, the reflectivity is assumed to be 0.1 [49]. Furthermore, the emissivity of the glass front and rear surfaces are 0.84 and 0.89, respectively [51].

Now that we have looked at the meteorological data and the temperature model, it is time to select the solar panels. I have selected the 'AstroSemi 365W' mono-crystalline panels from Astronergy. Mono-crystalline panels are premium solar panels which have a higher efficiency than poly-crystalline solar panels. These panels are also used in the largest solar park in the Netherlands [52]. The panels have a rated output of 365Wp at STC and a module efficiency of 19.7% at STC. Further specifications can be found in appendix G.

Now that all the inputs for the model are discussed, it is time to look at the model performance. In figure 3.19, the module temperature is plotted for the summer months.

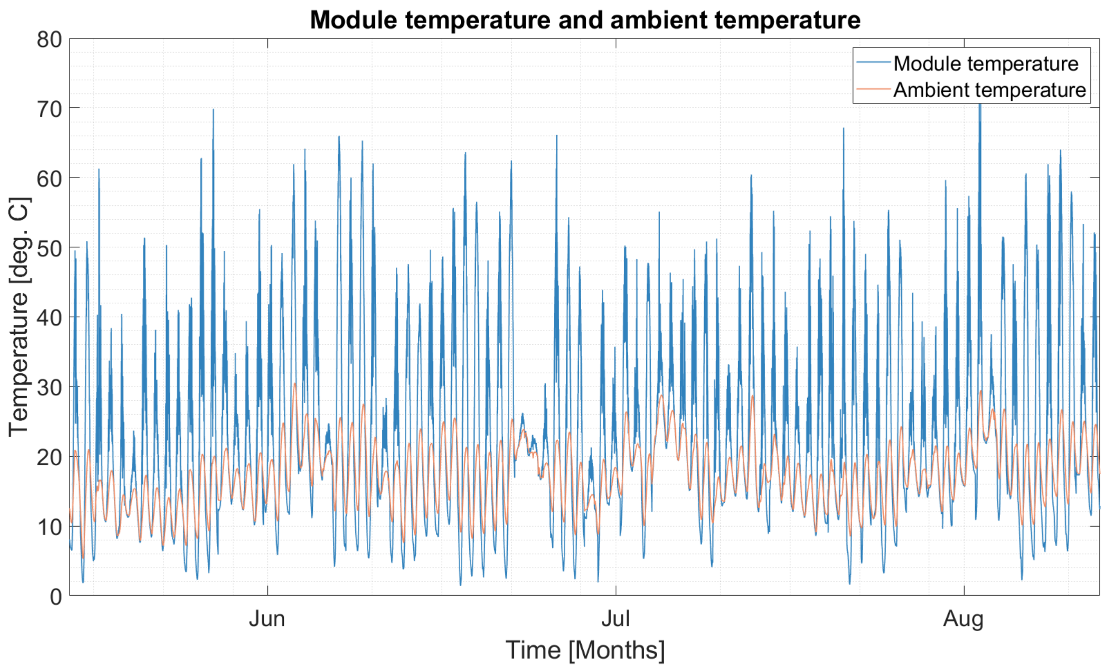

Figure 3.19: Module and ambient temperature for the summer months

It is clearly visible that the module temperature has the same trend as the ambient temperature, which makes sense since $h_c T_a$ contributes a lot to the module temperature. Furthermore, there are two days at the beginning of June when the module temperature is almost equal to the ambient temperature. This can be explained by the lack of irradiance on these days, which can be seen in figure 3.17. In the night the module temperature may drop below the ambient temperature. The lowest module temperature are found when the sky is clear. This is in line with the expectations, and therefore the model found to be operating properly.

The next step in sizing the PV is to achieve the *dynamic efficiency*. The manufacturer of the solar modules have expressed the nominal efficiency. However, the actual efficiency of the modules are affected by a lot of parameters. In this work, I have considered the module temperature and the radiation on the models to have affect on the module efficiency, as is recommended by Smets et al. [42].

The module efficiency can be calculated with equation 3.22.

$$\eta(T_{\mathrm{M}}, G_{\mathrm{M}}) = \eta(25°C, G_{\mathrm{M}})[1 + \kappa(T_{\mathrm{M}} - 25°C)] \tag{3.22}$$

Here the overall module efficiency depends on the module efficiency based on the module irradiance that is corrected for the module temperature. κ correlates the module temperature with the module efficiency.

$$\kappa = \frac{1}{\eta(\mathrm{STC})}\frac{\partial \eta}{\partial T} \tag{3.23}$$

For c-Si cells, the typical value for κ is -0.0035/°C. However, κ can be calculated precisely if the partial derivative of efficiency as a function of module temperature is known.

For this purpose we need to look at the temperature coefficients that are provided by the manufacturer. AstroEnergy states that the modules have a power temperature coefficient of -0.34%/°C. This coefficient can be used to calculate the power output at the maximum power point by scaling the power output at STC.

$$P_{\mathrm{MPP}}(T_{\mathrm{M}}, G_{\mathrm{STC}}) = P_{\mathrm{MPP}} + \frac{\partial P_{\mathrm{MPP}}}{\partial T}(\mathrm{STC})(T_{\mathrm{M}} - T_{\mathrm{STC}}) \tag{3.24}$$

The module efficiency based on the varying module temperature can be calculated with

$$\eta(T_{\mathrm{M}}, G_{\mathrm{STC}}) = \frac{P_{\mathrm{mpp}}(T_{\mathrm{M}}, G_{\mathrm{STC}})}{G_{\mathrm{STC}}\mathrm{A}_{\mathrm{M}}} \tag{3.25}$$

Here A_{M} is the module area. Finally, the partial derivate of efficiency as a function of module temperature can be calculated by rearanging equation 3.26.

$$\eta(T_{\mathrm{M}}, G_{\mathrm{STC}}) = \eta(\mathrm{STC}) + \frac{\partial \eta}{\partial T}(\mathrm{STC})(T_{\mathrm{M}} - 25°C) \tag{3.26}$$

Next we need to calculate the efficiency for the actual irradiance. Here we must first calculate the power output at the maximum power point at this irradiance level.

$$P_{\mathrm{mpp}}(25°C, G_{\mathrm{M}}) = FF \cdot V_{\mathrm{OC}}(25°C, G_{\mathrm{M}}) I_{\mathrm{SC}}(25°C, G_{\mathrm{M}}) \tag{3.27}$$

In figure 3.20, the dynamic efficiency for the summer months is plotted.

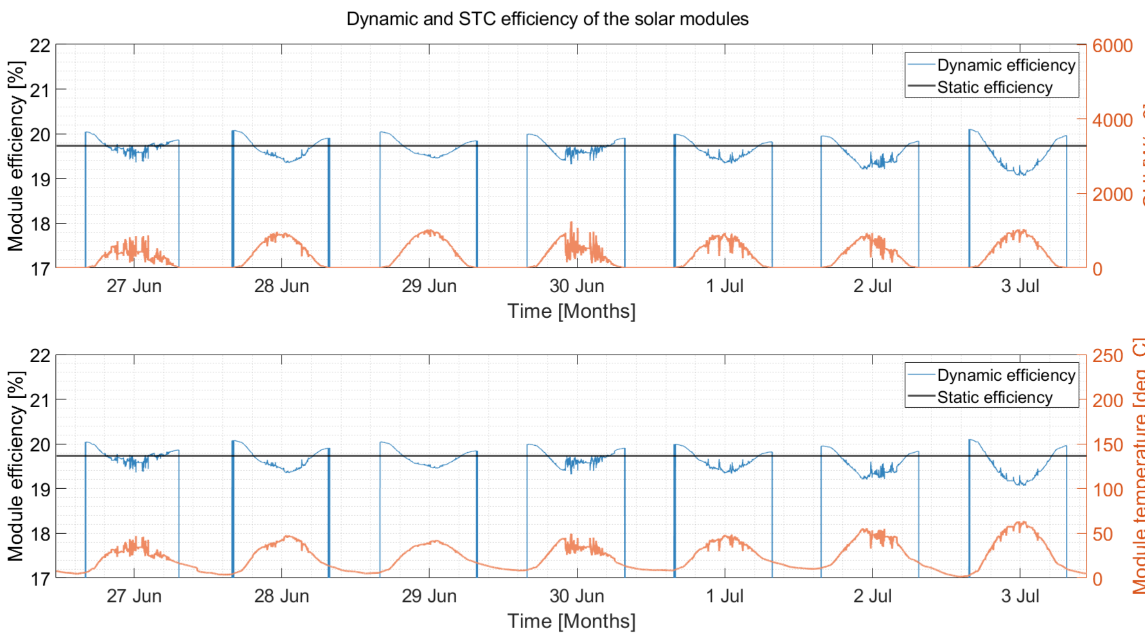

Figure 3.20: Module efficiency as a function of GHI and module temperature

It can be seen that the dynamic efficiency is on average lower than the static efficiency. This is because the static efficiency is determined at 1000 w/m^2 and 25 °C. From the second subplot it can be seen that the module temperature is much higher than 25 °C. This is in part the result of heating due to the high irradiance levels. The efficiency profile looks as expected and is therefore deemed valid for this work.

The final part of the PV model is to generate the power output of the modules. This is done by multiplying the dynamic efficiency by the GHI. Since data with a minute-resolution is used as an input, the values need to be made into values with a resolution of seconds. This is done by interpolating between the two data points and adding a small randomization of 2% to maintain the dynamic nature of the data.

The final validation of the PV model is illustrated in figures 3.21, 3.22 and 3.23. Here the monthly PV generation is showed, followed by the yearly power profile and the short time PV fluctuations for the 21ŝt of June and December are presented.

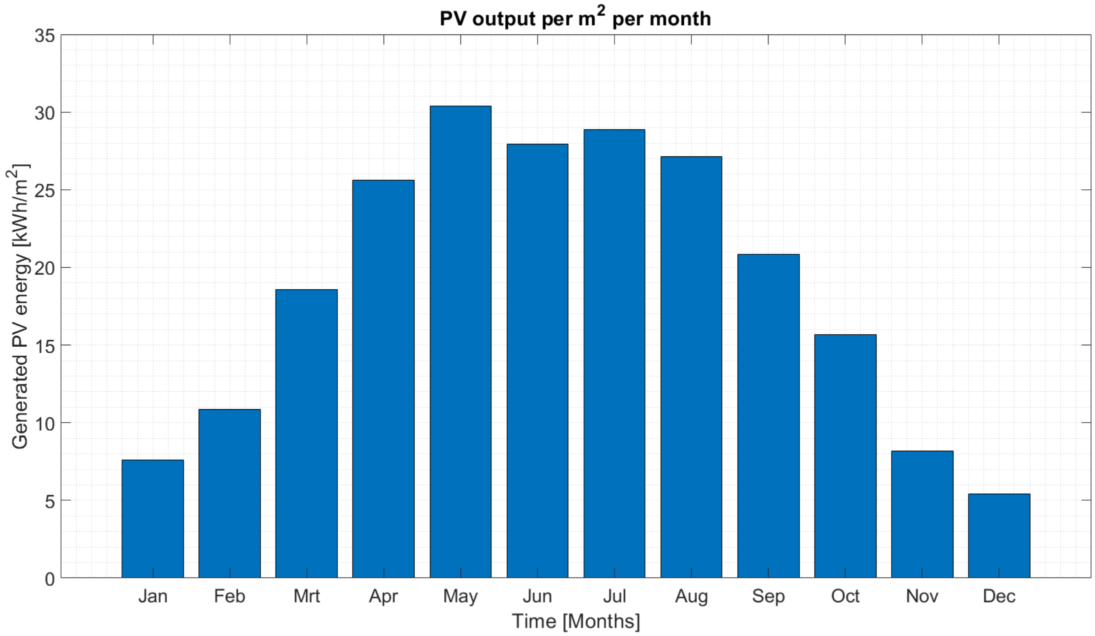

Figure 3.21: Monthly PV energy yield

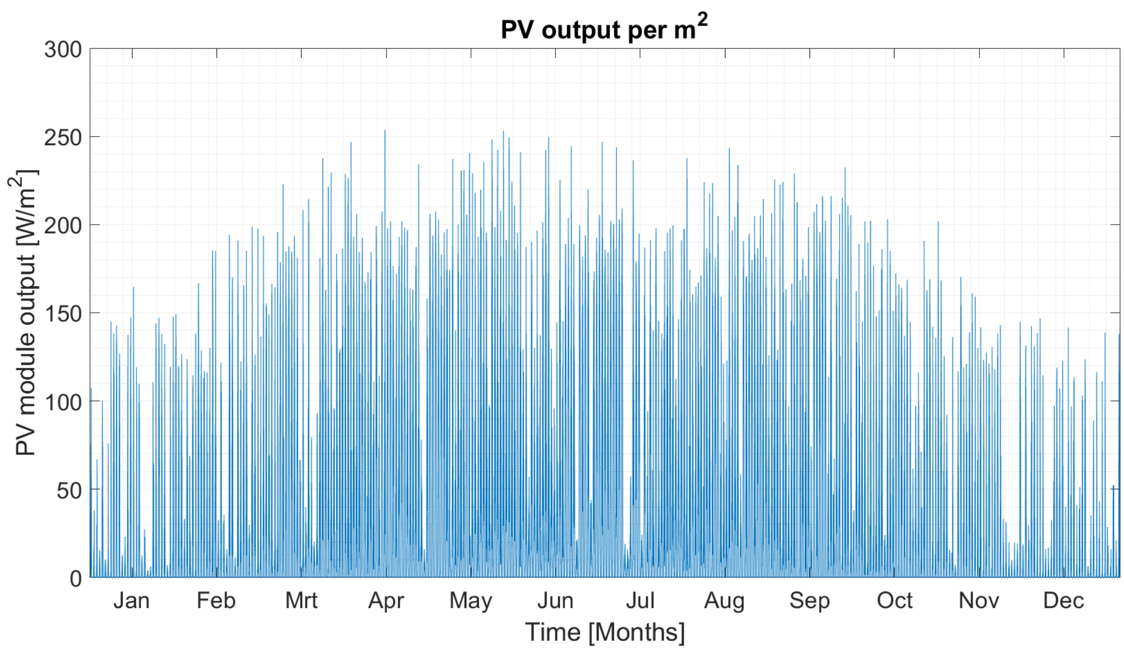

Figure 3.22: PV generation

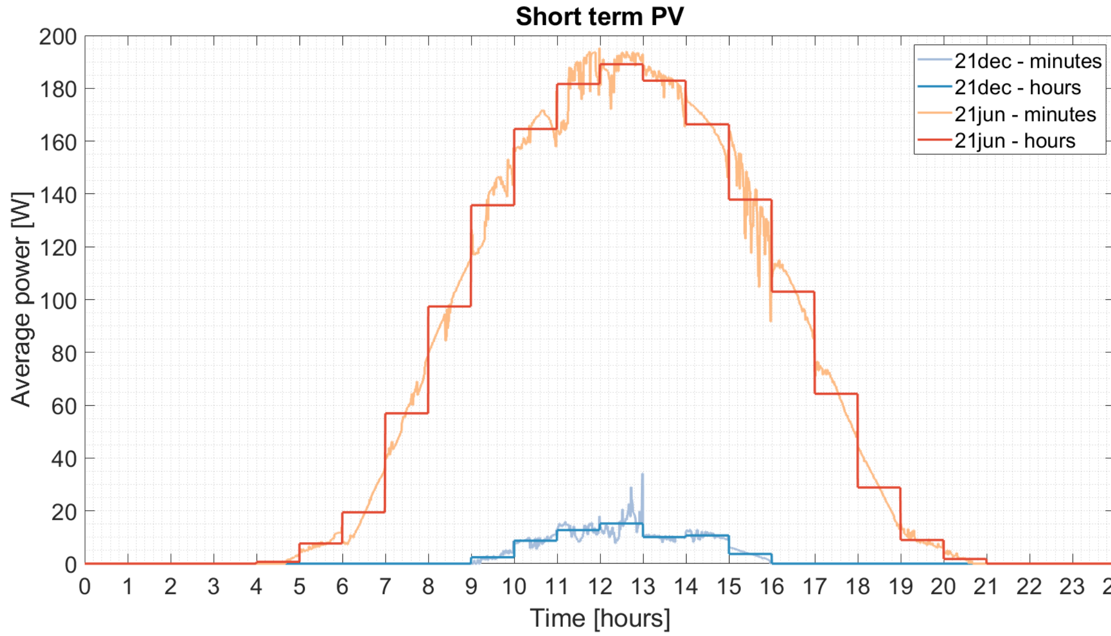

Figure 3.23: $PV_generationforshortscale$

The results look realistic under the assumptions of the model. However, it is important to remember that the assumptions of no cable losses, no (mutual) shading and static converter losses are not realistic. It should be kept in mind however, that this is not the aim of the PV model. The model should yield results for a general PV system, where the location specific conditions can be included in a later stage. In this section we have looked at the input data of the PV model, the underlying assumptions of the model, the model itself and validated its performance.

To summarize, in this chapter the methods have been described in detail. First the grid power model was introduced. This model consists of 8 stages that are used to model the trolley grid. Furthermore, a PV model is explained. In this model a dynamic efficiency of the modules is calculated with a fluid dynamic model. The module yield is calculated based on the irradiance and the module temperature. In the next section, the models are used to size PV systems for the grid.

Chapter 4: PV results

In this chapter, it is investigated what parameters have effect on the PV system size. Furthermore, PV systems without storage are sized for each substation and the performance is analyzed.

4.1 Sizing a PV system for a trolley grid - theory

From an energy perspective two parameters are important for evaluating the performance of a PV system. What fraction of the PV energy power goes to the buses (PV utilization) and what fraction of bus load is powered by the PV. The PV utilization and the PV powered bus demand are calculated with equations 4.1 and 4.2 respectively.

$$U_{\mathrm{PV}} = \frac{E_{\mathrm{DC}}}{E_{\mathrm{DC}} + E_{\mathrm{AC}}} \tag{4.1}$$

$$U_{\mathrm{Bus}} = \frac{E_{\mathrm{DC}}}{E_{\mathrm{load}}} \tag{4.2}$$

In both equations E_{DC} is the PV energy powering to the DC-grid (trolleybuses). Moreover, in equation 4.1 E_{AC} is the energy powering the AC-grid. Finally, E_{load} is the load of the trolleybuses.

A system with a high PV utilization but little bus load that is PV powered uses its PV effectively, but has little impact on making the buses greener. This system is likely undersized. On the other hand, a system with low PV utilization and with much bus load powered by PV dumps most of its power to the MVAC grid but is still able to have a large impact on the making the bus power more sustainable. This system is oversized. The optimal PV system therefore has a high PV utilization and provides much of the bus load.

There are many parameters that affect the PV performance, in this work the parameters are grouped in three clusters; bus parameters, grid parameters and city parameters.

The bus parameters have to do with the load of the buses, these include the mass of bus and whether a bus has an on-board battery for In-Motion-Charging (IMC). A heavier bus or a bus that charges an on-board battery requires more power.

The second group of parameters are *the grid parameters.* These parameters have to do with the length of the sections, the number of sections under a substation, the consistency of traffic under the substations. In this group also the size of the PV systems included.

The final group of parameters are *the city parameters.* The hours of sun light and the average ambient temperature are important city parameters, because they affect the PV output and the climate control power requirements of the buses. Further city parameters are a long list of section specific conditions like; the number of bus stops under a substation, the number of stop lights, the inclination of the road, other traffic on the section, etc.

In this thesis the bus parameters and the city parameters are not considered. It is assumed that bus loads are as measured by the HAN university with the exception of the HVAC. Buses with IMC are not considered in this work. The city parameters are also not varied in this work, because this thesis is concentrated on a case study of the Arnhem trolley grid only. However, two grid parameters are considered. These are *the consistency of traffic under the substations* and *the size of the PV systems.* In this work, the consistency of traffic is defined as *the fraction of time buses are under a substation* . A substation with a large fraction of time with buses is said to have a constant stream of traffic, and a substation with a low fraction of time of buses is has an inconsistent stream of traffic. Why both parameters are important is discussed next.

The first parameter on the list is bus traffic. Whether a bus is driving under a substation affects the PV utilization. The larger the percentage of time a bus is under the substation, the more time the PV could send its power to the bus and the higher the PV utilization becomes. Only in case of a very oversized PV system this may not be true. A similar relation holds true for the bus load. The longer the sun is up, the larger the fraction of the bus load could be supplied by PV. The maximum attainable bus load that could be met with the PV is therefore a lot higher in the summer than in the winter. The reason for this is because the buses are driving a larger fraction of the time when the sun is up. Substations that contain sections that are subject to constant stream of traffic during the day time are therefore promising candidates for PV. There are two more traffic related parameters that effect the PV system performance: The number of sections under a substations and if substations are bilaterally connected with each other. Both these parameters affect the possibility that the PV system could use its energy to power buses. In the case of bilaterally connected sections, the domain that the PV could feed power to increases. This makes the base load on the substations more consistent and increases the time that the PV can power the buses. However, the substations with larger loads may lose some of the load to other substations. The recommended size of the PV systems for these substations may consequently be lower, while the PV utilization rises.

The second parameter is the size of the PV system. The larger the PV system, the greater the effect on the bus load. Unfortunately, the trade-off is that the system will dump more of its power into the Arnhem grid and therefore the PV utilization drops.

4.2 Effects of traffic on the PV system

First the traffic under each substation is investigated. This is done with equations 4.3 and 4.4.

$$F_{\mathrm{PV}\to\mathrm{Bus}} = \frac{t_{\mathrm{GHI}} \cap t_{\mathrm{bus}}}{t_{\mathrm{GHI}}} \tag{4.3}$$

$$F_{\mathrm{Bus}\leftarrow\mathrm{PV}} = \frac{t_{\mathrm{GHI}} \cap t_{\mathrm{bus}}}{t_{\mathrm{bus}}} \tag{4.4}$$

$F_{\mathrm{PV}\to\mathrm{Bus}}$ is the time in the year that PV and buses are both available divided by the time that the sun is available. $F_{\mathrm{Bus}\leftarrow\mathrm{PV}}$ is the time in the year that PV and buses are available divided by the time that the buses are driving. The first term gives the fraction of time that the PV could ideally feed the buses. The second term gives the fraction of time that the bus load could ideally be met with PV. In both equations, t_{GHI} and t_{bus} denote the seconds per year of active sun power and at least one bus under the substation. For the whole year, two vectors are constructed with a second resolution, that have 0 when there is no bus or no GHI and a 1 when there are buses and GHI. The results are shown in figures 4.1 and 4.2. Note that CS stands for Central Substations and are substations 4,9 & 21 combined. HQ stands for head quarters and denotes the location of Connexxion's head quarters, this is the combined effort of substations 3 & 6.

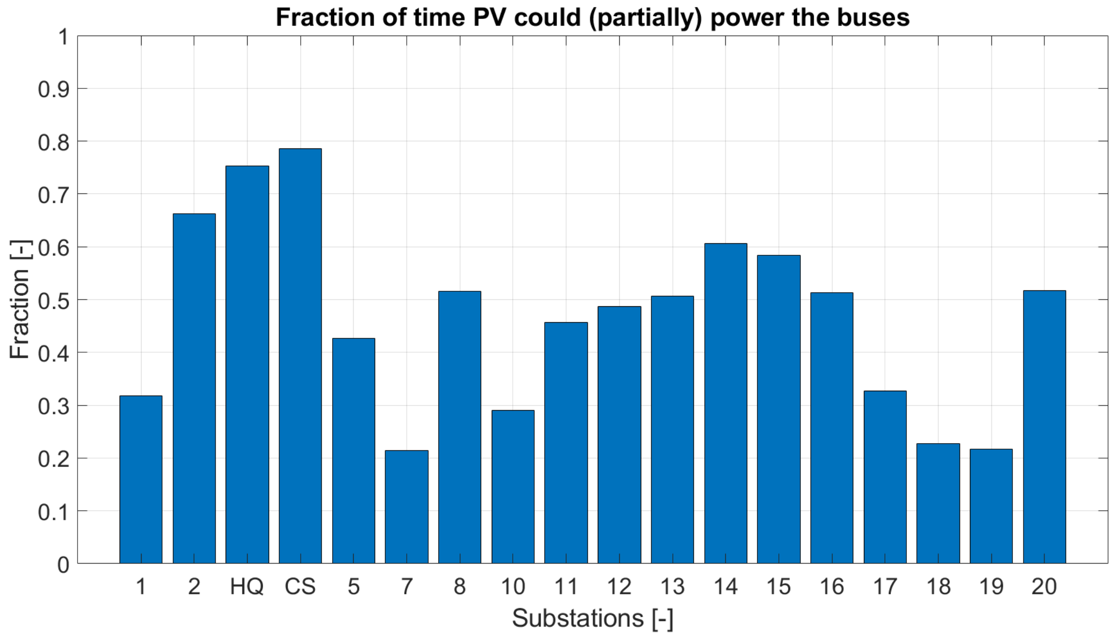

Figure 4.1: Fraction of time PV could (partially) power the buses

In figure 4.1, on the y-axis the fraction of time the PV could *ideally* power the buses. The actual PV utilization will be lower, because the magnitude of PV and bus load will not be equal at the times that they are both available. It can be concluded that placing PV on all substations may not be desired. The ideal PV utilization for sections with low traffic, like substations 7, 18 and 19 is only slightly higher than 20%. Placing PV on these substations only makes sense if these substations have a storage medium installed. Even if these substations are bilaterally connected to neighboring sections, placing PV there would be sub-optimal. This is because the PV would then be exported from the section to the other substation(s) resulting in increased transmission losses. Fortunately, the figure also shows that substations with a lot of traffic (constant traffic), like CS could have an ideal PV utilization of almost 80%. PV on these substations may be installed without bilateral connections or energy storage.

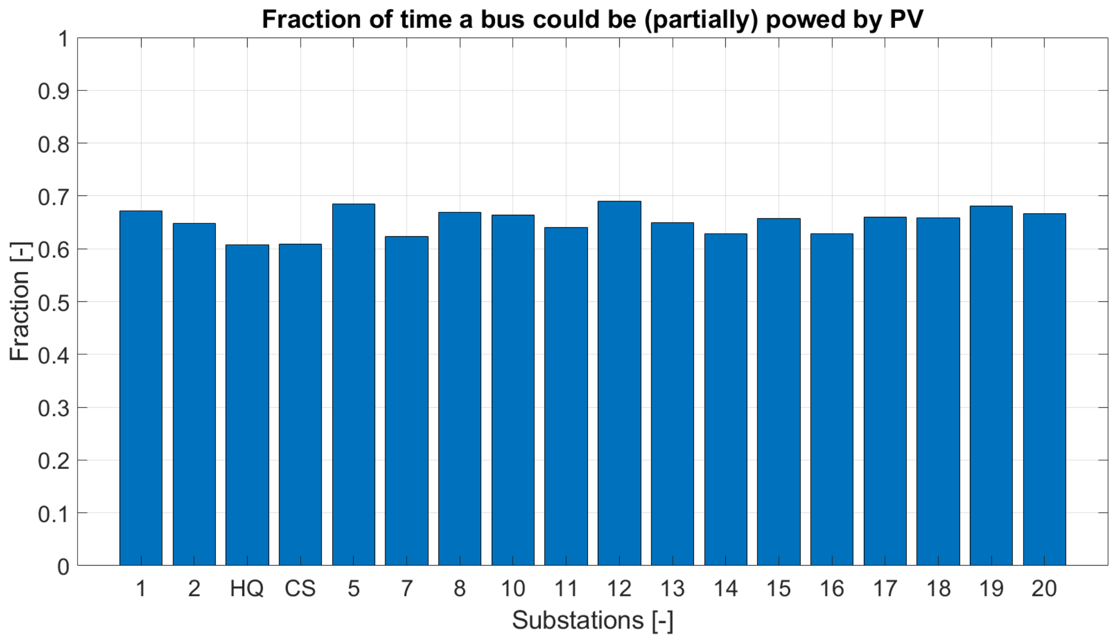

Figure 4.2: Fraction of time a bus is driving when there is sun light

Figure 4.2 shows the fraction of bus demand that can be met with the PV. From the figure it can be concluded that the variation between substations is small and that the bus load varies between 60 and 70%. The values cannot go above 70%, because 30% percent of the time buses are driving when the sun has yet to rise or is already set. The variation between substations has to do the with bus schedule. It is also important to note that reaching these values requires a large PV system, because all power spikes of the buses need to be provided by PV. A system of this size would have a low PV utilization, hence a trade-off has to be made. Finally, the values likely have a high variation throughout the year. Low in the winter and high in the summer.

4.3 Sizing PV systems for the substations

In this work, the PV size was varied between 10% energy neutral up to 150% energy neutral (EN) in steps of 10% for all substations. An energy neutral PV system produces as much energy as the load of the substation for the year. For illustration, the results for the HQ substation (high traffic) and substation 7 (low traffic) have been shown in figure 4.4. These substations have been considered, because the measured annual energy corresponds nicely to the computed energy (see figure 3.12)

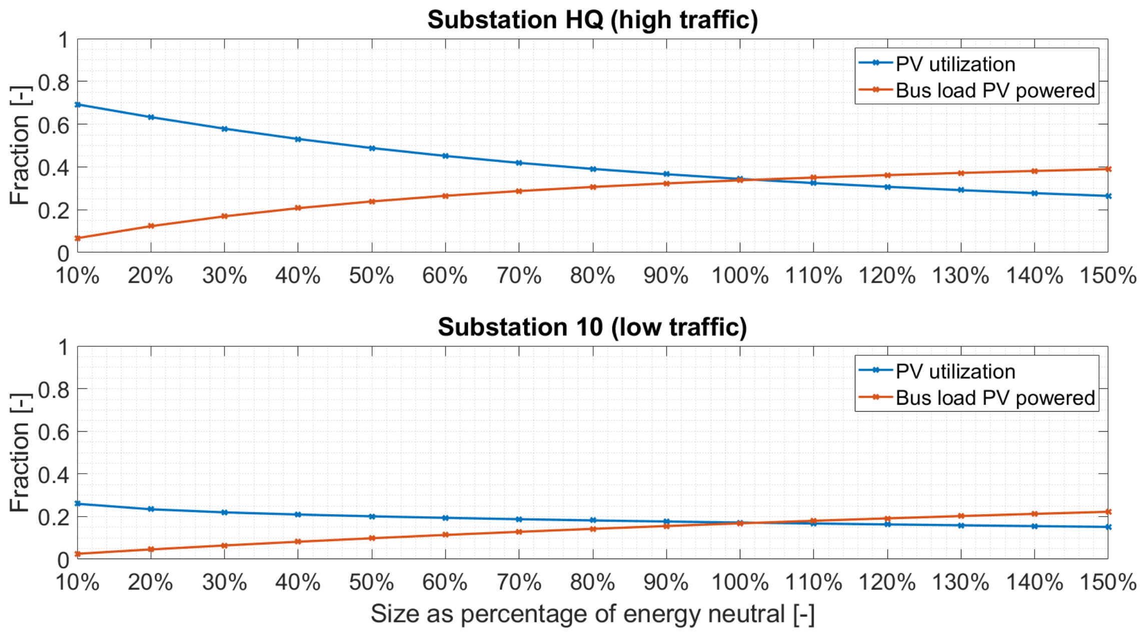

Figure 4.3: Performance of PV systems with varying sizes for high traffic (CS) and low traffic substation (10)

From these plots it is clear that the higher traffic substation has a better PV utilization than the low traffic substation for all system sizes. Unfortunately, for both systems the sizing of PV does come with large compromises. For the PV on CS a 70% PV utilization can be achieved, sadly this would only yield an increase of 7% in the renewable energy share. In contrast, if a large PV system is installed 40% of the bus load can be PV powered, however this would be accompanied by large power dumps in the AC grid. The prospect for the PV system on substation 10 are even worse. For (very) small PV systems, the PV utilization approaches the ideal PV utilization of figure 4.1, for (very) large PV systems the fraction of bus load powered by PV approaches figure 4.2. These findings show that PV potential for increasing the renewable energy share while minimizing the use of the AC-grid for seasonal storage is low. Moreover, increasing the PV system size and curtailing is also not a promising solution because of the diminishing returns for large PV systems. Especially for low traffic substations storage is therefore essential.

In case a sole PV system is to be installed, an optimum system size can be estimated. If we consider that the power from the PV to the substation is a *benefit* and the power from the PV to the Arnhem grid is a *cost*, we can find the highest *net social benefit* by finding the maximum for benefit minus cost. In this work, the weights of the costs and benefits are equal. In reality, they could be set to specific criteria.

In figure 4.4, the optimal PV sizes for all substations are shown on the y-axis and on the x-axis the $F_{\text{PV}\rightarrow\text{Bus}}$ is shown. In the figure, the size of the markers are proportional to the PV system size.

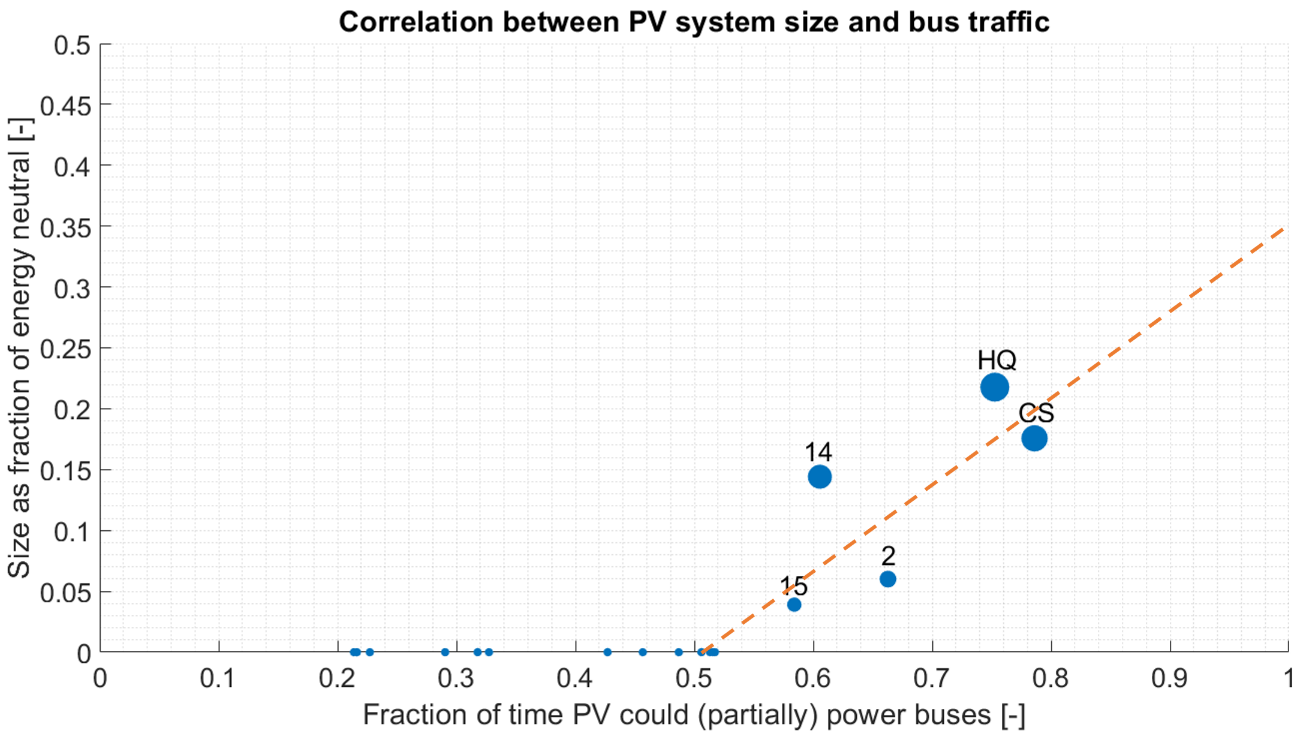

Figure 4.4: Correlation between optimal PV system size and $F_{\mathrm{PV}\rightarrow\mathrm{Bus}}$

The graph shows that there is a correlation between bus traffic and PV size. It is also clear that ideal PV utilization is not the only contributing factor to the PV size. Moreover, for most sections the costs are always higher than the benefits, which means that the marginal costs are always higher than the marginal benefits. Which by definition means that no matter the size of the PV system, the system will always send more power to the Arnhem grid than the buses. The optimal system size is therefore, no PV system. It is also apparent that the substations that should have PV installed, only need a maximum of 23% of the EN size. If the orange line is extrapolated to x is one, the maximum recommended PV system size can be approximated for a system with a consistent base load. In the Arnhem grid this is about 45%. To increase the recommended PV size further, a storage system is required. In the next chapter the performance of the PV systems is investigated.

4.4 PV system performance

In this section, first the PV utilization and the bus demand powered by PV is investigated to examine the energy performance of the PV. Next, the research focuses on a high traffic and low traffic substation to illustrate the short-term and long-term energy and power mismatch between the bus load and the PV generation.

In figure 4.5, the bus demand met by PV is plotted against the PV utilization.

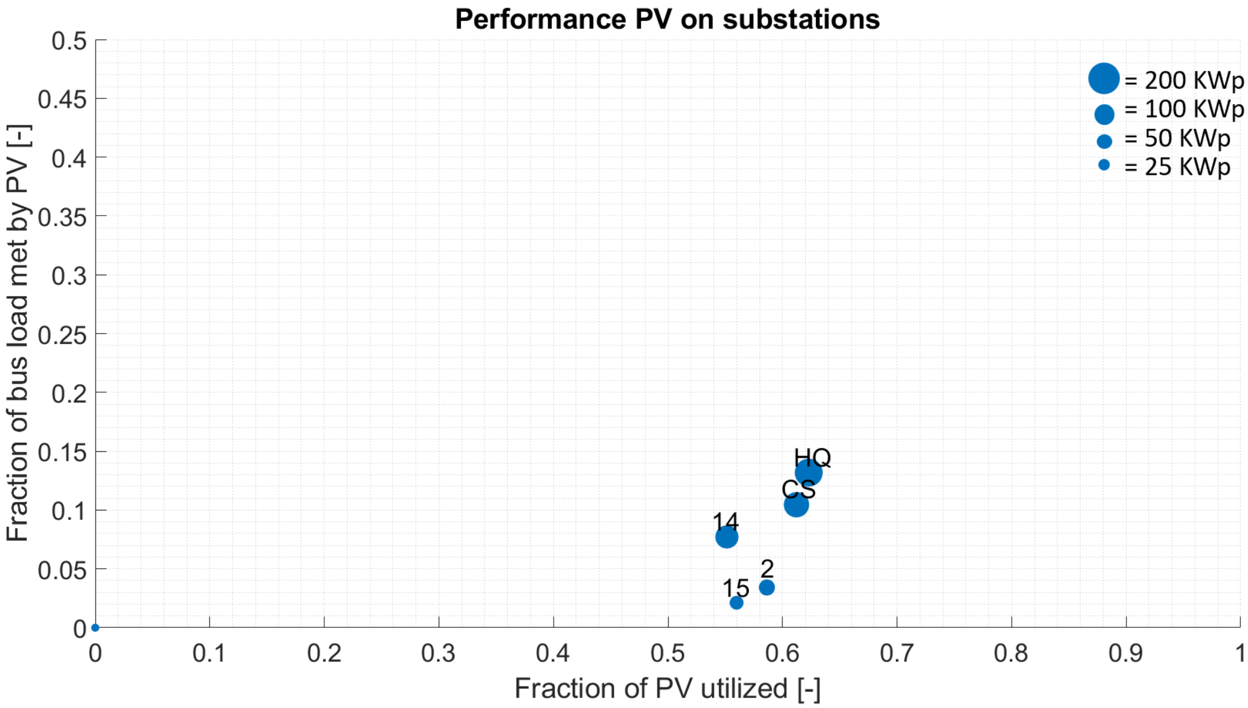

Figure 4.5: PV performance for all substations

From this plot it can be concluded that the PV on the best performing substation can only provide 13% of the bus demand and still sends 38% of its energy to the MVAC grid. Overall, a PV system of this size could increase the renewable energy share of the grid by 8.2%. In table 4.1, the PV size and the annual energy to the buses and the MVAC grid are displayed.

Table 4.1: PV system specifications

Substation	PV size (kWp)	To buses (MWh/yr)	Dump (MWh/yr)
2	19	13	9
HQ	158	113	69
CS	145	102	65
14	61	39	32
15	11	7	6

While computing the yearly PV utilization and the fraction of bus load that is PV powered is certainly useful, it does not tell the whole story. The PV power can vary a factor six between summer and winter and the bus power demands vary with a factor 2 between summer and winter as well (except winter is higher). Therefore, the mismatch between power supply and demand will be high. For substation HQ (high traffic) and substation 15 (low traffic), the monthly energy shares to the buses are shown in figures 4.6a and 4.6b.

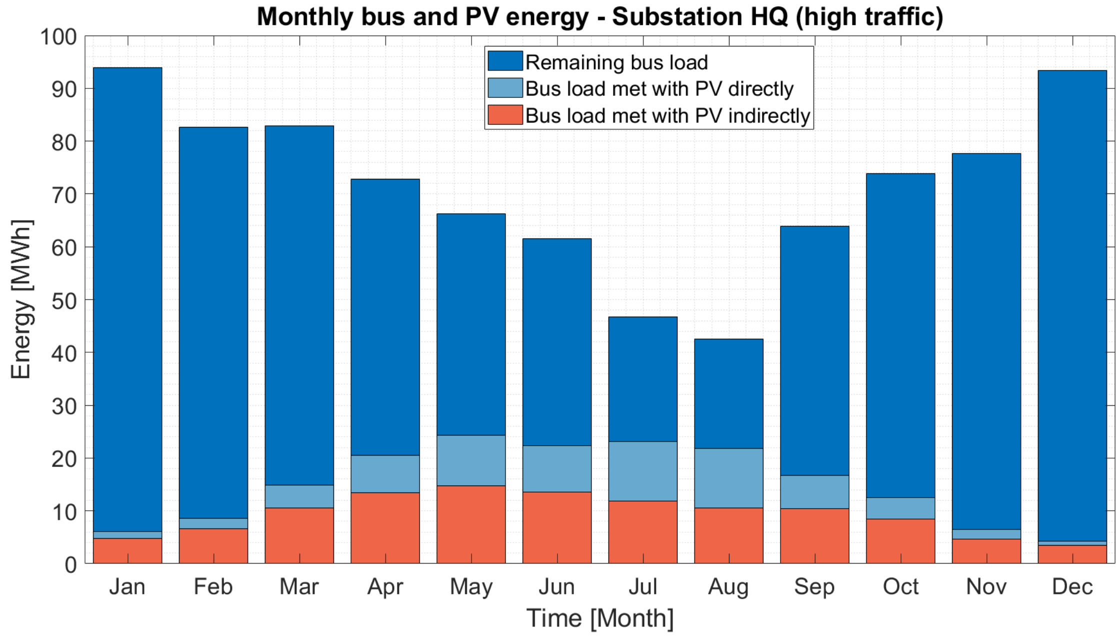

(a) Monthly bus energy demand and PV - Substation HQ

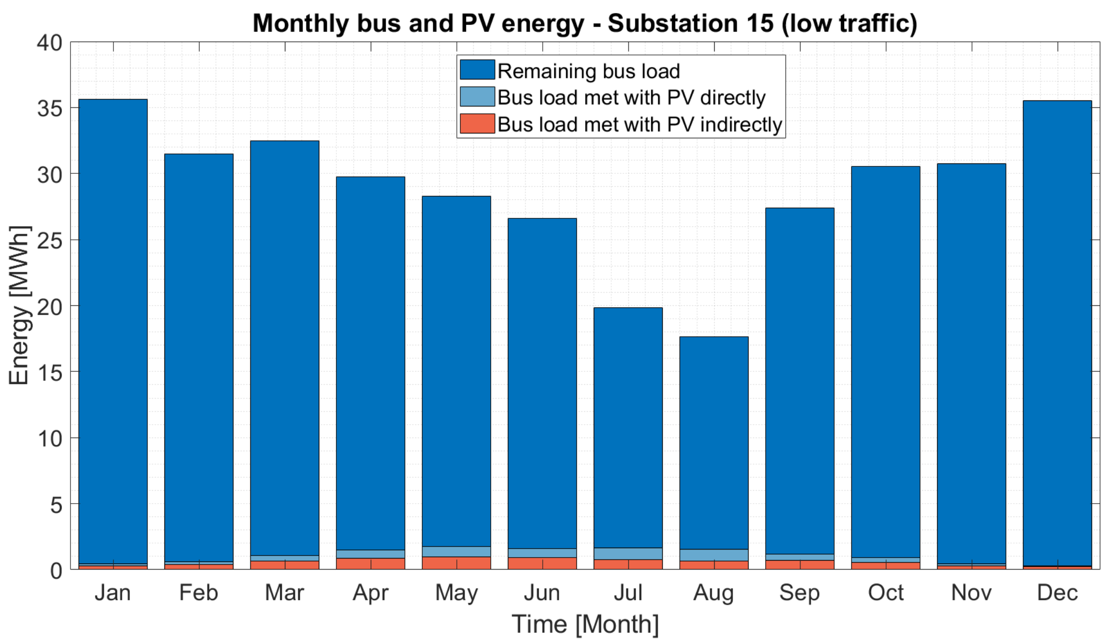

(b) Monthly bus energy demand and PV - Substation 15

In both figures the orange bar represents the energy from the PV that is directly utilized by the buses. The light blue bar represents the energy that is generated by PV but dumped in the AC-grid and the dark blue bar represents the remaining energy demands of the buses. In figure 4.6a, it is clear that the fraction of the energy from PV powering the buses is a lot higher in the summer than in the winter. In like manner, the dump in the Arnhem grid is a lot higher in the summer as well. In figure 4.6b, it is hardly visible that the PV system has an impact on increasing the renewable energy share at all. Two things are evident from the figures; to reach high levels of renewable energy share in the trolley grid, both PV systems need seasonal energy storage. In addition, the storage must be large because it needs to supply the large energy demands of the winter. It is also clear that the low traffic substation benefits more from small scale storage, since this storage would be similar to increasing the consistency of traffic for that substation.

Finally, the PV systems should be evaluated on a power level. This is important because the power level tells us what power is exchanged with the AC-grid and what the peak power intake and export are. The connections from the substations to the AC-grid are designed for a specific rated power. If the import or export of power is higher than this limit, the power exchange is physically limited. Moreover, it is common that the trolley grid operator is a contractual agreement with the Distribution System Operator (DSO) about the maximum power exchange between grids. This may also limit the maximum power exchange. Finally, the peak power intake or export are critical criteria for designing an energy storage system. It should be noted that the next chapter does not actually use the peak power exchange as part of its design. Parallel/series configuration and type of storage are not in the scope of this work.

Figure 4.7 show the power exchange for substation HQ (high traffic). The power exchange is positive when PV provides more power than the buses and vice versa.

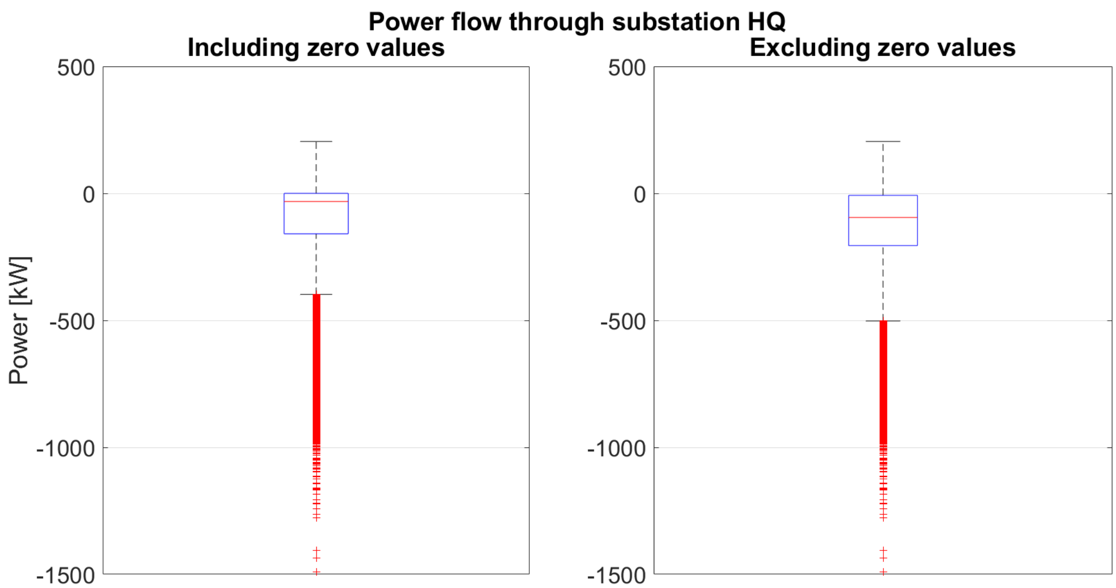

Figure 4.7: Power flow for high traffic substation (HQ)

On the left side a boxplot is shown of the power flow through the HQ substation for the whole year. The right boxplot also shows the power flow through the HQ substation, but here the times when the mismatch is zero are excluded. The left plot gives an accurate representation of the power flow, while the right gives more inside in the power profile.

The line in the boxplot show that the median power exchange is negative, this makes sense since the PV is only sized for 23% EN. The limits of the box show the 25$^{\text{th}}$ and 75$^{\text{th}}$ percentile of power exchange. The end of the whiskers show the final statistically significant limits. Finally, the red values are the individual outliers and show the peak powers that are expected only a few times in the year. The maximum power dump of the PV is around 250 kW while the maximum import is 1.5 MW.

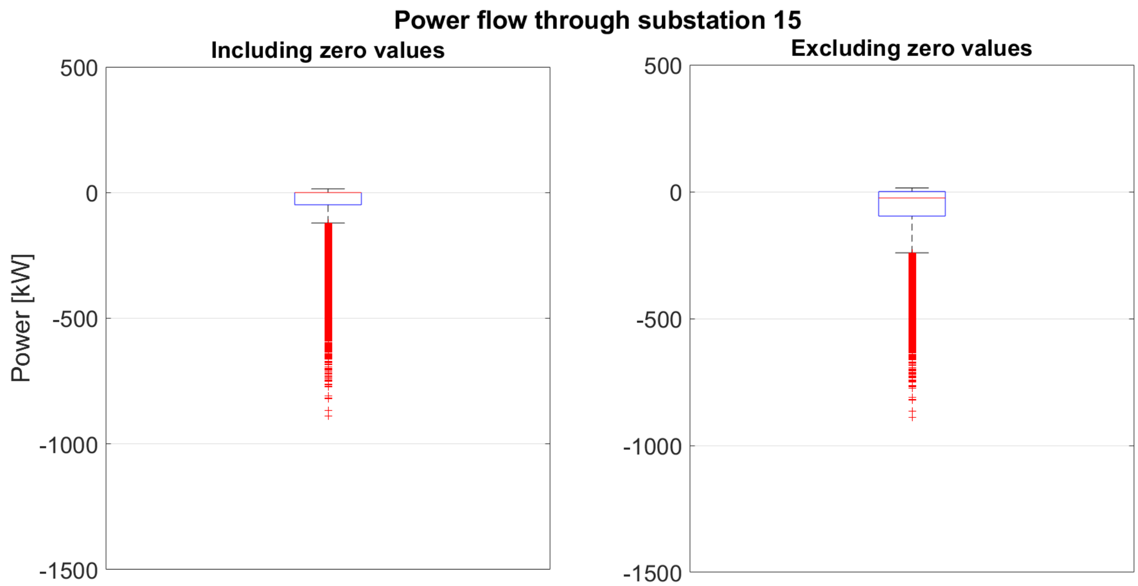

Figure 4.8: Power flow for low traffic substation (15)

In figure 4.8 the power level for substation 15 (low traffic) is plotted. Here, the median is closer to zero. This means that the average import of the substation is lower. Also the peak import is a lot lower than for the HQ substation. Moreover, it seems like there are no instances when the substation is exporting power. This is not the case because the power utilization is only 52% but because the PV system is so small in comparison to the bus load the export is not visible.

To recap, in this chapter we have discussed what parameters have effect on the PV performance in trolley grids. Furthermore, the effects of bus traffic and PV system size on the PV utilization and the PV powered bus load have been investigated in detail. A correlation was found between the consistency of bus traffic and the PV system size. In addition, PV systems were sized for each substation on the basis of a net social benefit criterion. It was found that 13 of the 18 substations were not eligible for PV. The substations that should receive PV, should only have a few percent of the energy neutral size installed with a maximum of 23% for substation HQ. Finally the performance of the PV systems was analyzed. The PV utilization of all substations is in the range of 55 to 62%, while the fraction of PV powered bus load is only 8.2%. For substation HQ (high traffic) and substation 15 (low traffic) the monthly variation between generation and load and the power exchange on the substations were displayed. These plots showed that the mismatch between PV and load on the short-term and the long-term is significant for both substations and that energy storage should be installed to increase the renewable energy share further. This option is investigated in the next chapter.

Chapter 5: Results for PV and storage

In this chapter, a storage model is introduced and applied to the PV systems. Finally, the performance of the new systems are analyzed.

5.1 Energy storage

In figure 5.1 the storage system is shown.

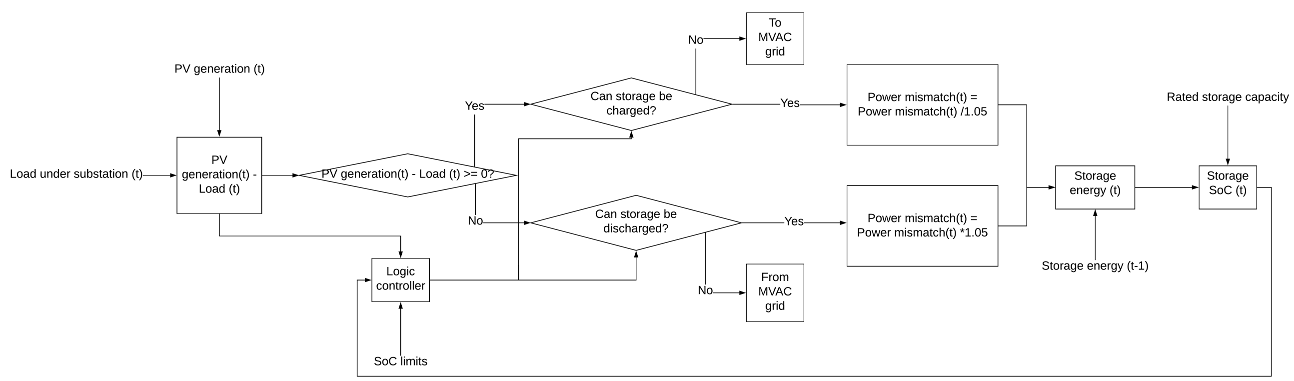

Figure 5.1: Overview of the storage system

Starting from the left, the bus load is subtracted from the power generation for each substation leading to the power mismatch. The logic controller checks if it is possible to charge or discharge the storage system based on its *state of charge* (SoC). The SoC is the fraction of total storage that is filled at that instant in time. It is only possible to charge a storage medium if the SoC remains within the upper and lower charge limits. These charge limits depend on the storage medium, but for the model the charge limits of lithium-ion battery storage were assumed. At the end of the section, the choice for lithium-ion batteries is explained. Figure 5.2 shows the logic controller.

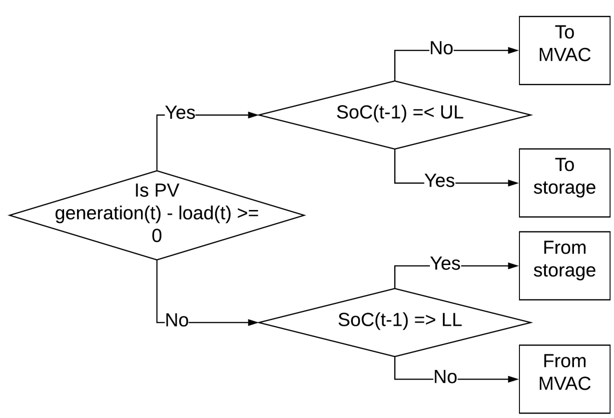

Figure 5.2: Logic controller of the storage system

The 1 is the mismatch between the generation and load. The controller first checks if this mismatch is higher or lower than zero. The 2 is the state of charge of the previous moment. The controller checks if the state of charge is within the upper limit (UL) and the lower limit (LL) of the storage. If the output to the switch is 0, the storage medium is charged or discharged. If the output to the switch is 1, the power is imported or exported to the MVAC grid instead.

The price of lithium-ion batteries has come down a lot the last decade and is competing with lead-acid batteries over the lifetime of the system [53, 54]. Although the price is steadily declining, lithium-ion batteries are much too expensive for seasonal storage and seasonal storage is a requirement to make the system energy neutral. For this purpose chemical storage could be used in the form of hydrogen or ammonia, but chemical storage suffers from large conversion efficiency losses. Two issues with lithium-ion batteries are the degradation and self-discharge of the batteries over time. However, for batteries to self-discharge, they have to not be used for some time and a real feasible storage size can only store energy in the range of days to weeks. Therefore, these storage systems are continuously charged and discharged. The degradation of the batteries remains an issue, but this issue is worse for lead acid batteries [55]. Therefore, it was decided to use the characteristics of lithium-ion batteries. The lower limit, upper limit and initial SoC are 0.2 ,0.95 and 0.5, respectively. An efficiency of 95% has been assumed for charging and discharging of the batteries. In this simple model, no ramping constraints for the battery power are assumed. Moreover, how the storage cells are connected with each other is not within the scope of this work. In figure 5.3, the SoC of the storage is shown for an 90% EN PV system for substation HQ to validate the working of the storage medium.

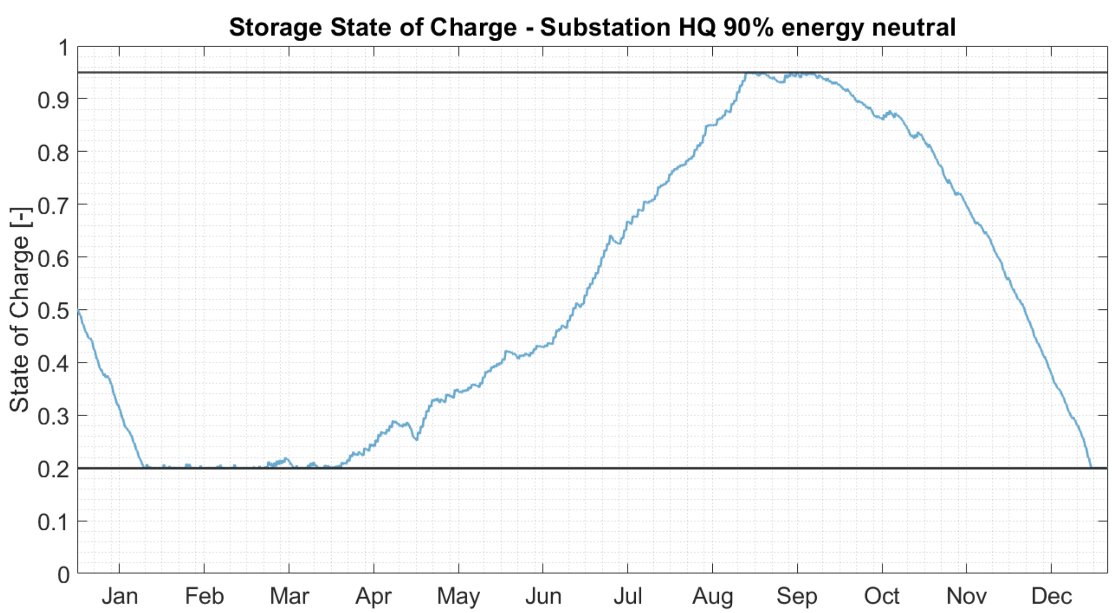

Figure 5.3: State of Charge of storage for an 90% energy neutral PV system on substation HQ

The black lines indicate the lower and upper charge limits of the storage. In this example, the system has a PV utilization close to one, because the upper limit of the storage is only reached for a short amount of time. However, the fraction of PV powered bus load is lower, because from February to April power has to be imported from the AC-grid. Furthermore, the storage is empty at the end of the year. In this work, it is assumed that the storage is charged to the initial SoC by importing energy from the AC-grid. Next, the storage medium is sized for the PV on the substations

5.2 Sizing the energy storage

In this section the storage is sized the PV system proposed in the previous chapter. Later, the PV and storage are resized to improve the system performance.

In figure 5.4, the effects of storage on the power utilization and PV powered bus load are shown. The storage was in this scenario sized to allow no grid dumping.

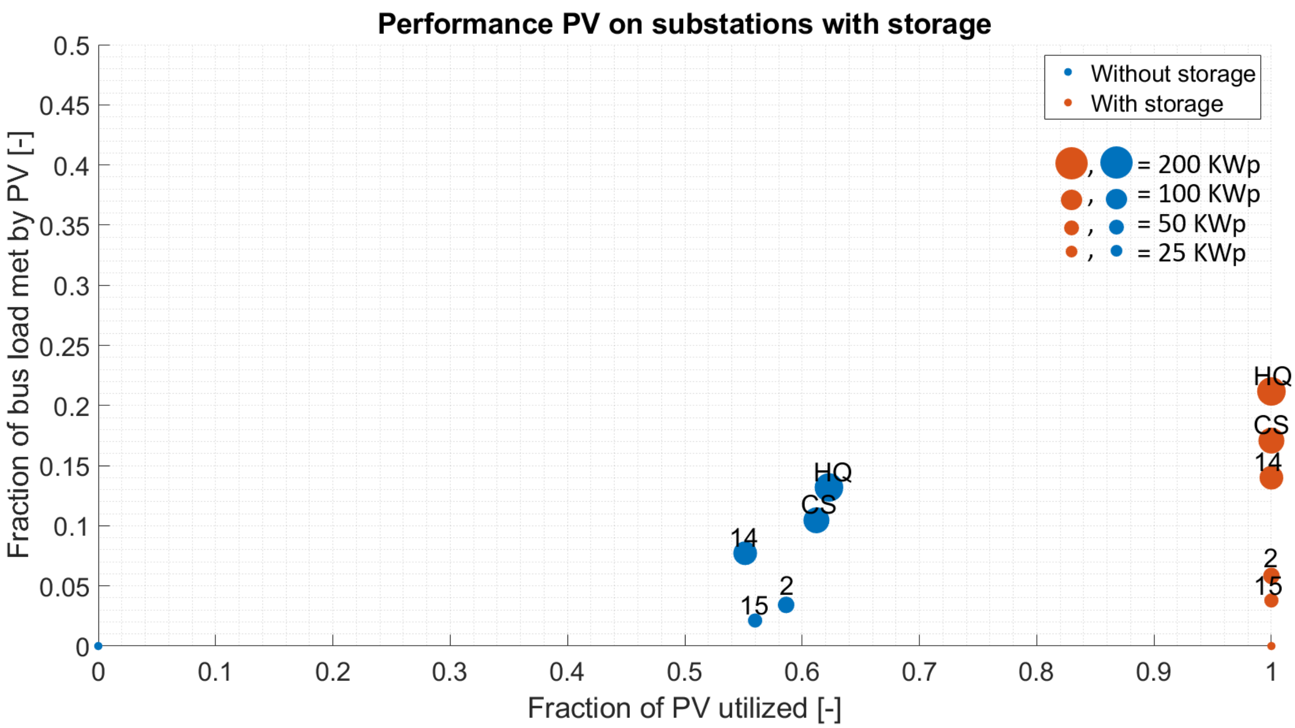

Figure 5.4: Effect of storage on PV system

The storage sizes are shown in table 5.1.

Table 5.1: Storage sizes for PV system

Substation	Storage size (kWh)
2	2
HQ	480
CS	375
14	30
15	2

Since the PV systems are much smaller than the bus load, the majority of the energy shall be imported. Energy storage is not going to change that. Although it is technically possible to place storage on the substations it is not recommended, this is because the storage will not be used outside the summer. If lithium-ion batteries are used for storage, then the storage is expensive if you account for the investment costs and compare it with the few operational hours. In addition, lithium-ion batteries discharge over time, which would make the case even worse. One could of course make the storage smaller, so that is used more throughout the year. However, this would reduce the effect on bus demand. Overall, placing storage is not recommended for these PV systems. The overall bus load that is provided by PV is 13.5%.

This is not to say that PV and storage do not have potential for increasing the renewable energy share. However, the PV and the storage should be sized together instead of sizing storage for a PV system that is optimized for operation without storage.

To find an optimum PV and storage combination for each substation, one could attempt to define a cost function to minimize. However, this approach would be rested on a lot of assumptions. Rather, in this thesis, an appropriate PV and storage range is derived by analysing a variety of PV and storage systems. In figure H.1 and 5.6 this is shown for substation HQ (high traffic) and substation 10 (low traffic), respectively. The system sizes are shown in table H.1.

Table 5.2: PV system sizes for substation HQ (high traffic) and substation 10 (low traffic)

Size	Substation HQ (kWp)	Substation 10 (kWp)
1.0 EN	746	120
0.9 EN	671	108
0.8 EN	596	96
0.7 EN	522	84
0.6 EN	448	72
0.5 EN	373	60

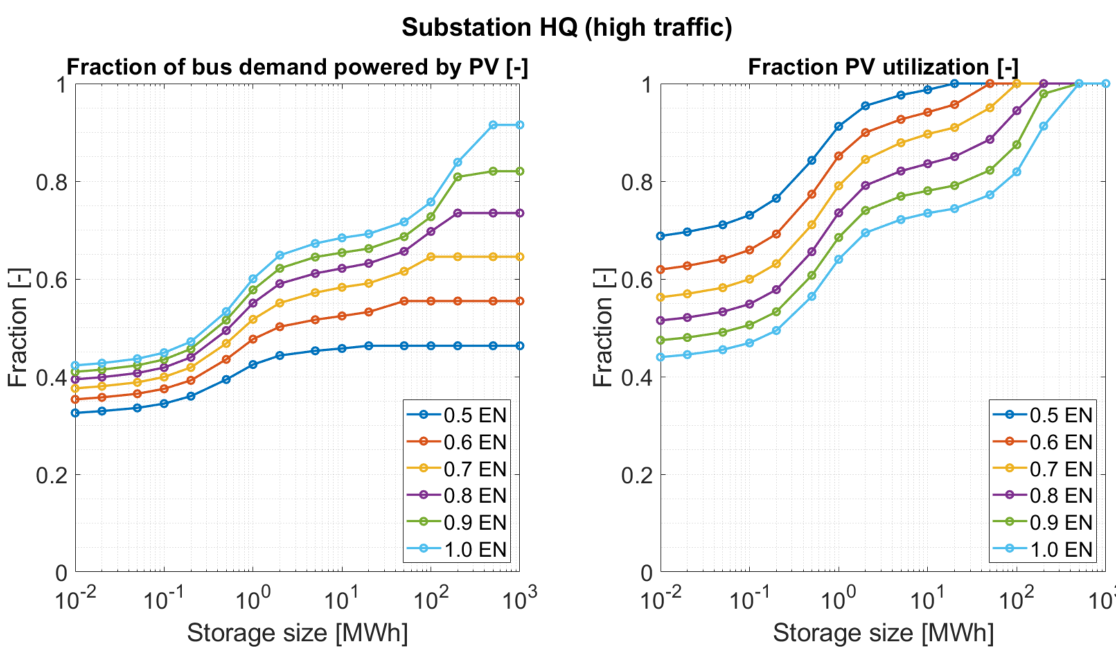

Figure 5.5: PV impact as a function of PV size and storage size - substation HQ

In figure H.1, the performance of a variety of PV and storage sizes are shown for substation HQ. In the left plot the effects of the different PV and storage sizes on the fraction of PV powered bus load are displayed, the right plot shows the effect on utilization of the PV power. The fraction of the bus load powered by PV does not converge to the energy neutral size of the PV system for large storage systems as one may suspect. The reason for this are the losses for charging and discharging the energy storage system. The plot shows that there are two combinations of PV and storage that may perform best. The first combination is a small PV system (0.5 EN) with small storage (10 kWh). With this combination 35% of the bus load is powered by PV and 30% of the PV is dumped in the AC-grid. Increasing the PV size for this storage does not yield much increase in the PV powered bus load, but it does increase the dump in the AC-grid. Another promising option is to install a larger PV system (0.8 EN) with 0.5 to 2 MWh of storage. These systems provide 55-60% of the bus load, with 25-30% dump in the AC-grid. Installing an energy neutral PV system with 200 to 500 MWh of storage to achieve no dump in the AC-grid is in practice to expensive.

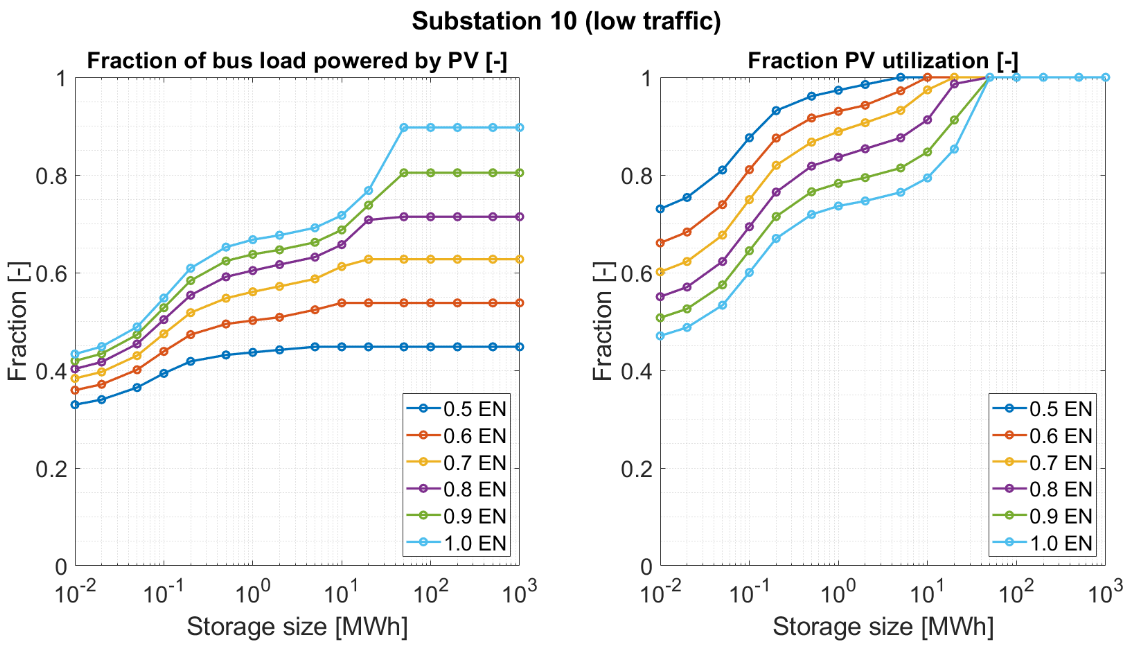

Figure 5.6: PV impact as a function of PV size and storage size - substation 10

For a poor traffic substation, small storage sizes can make a big improvement in the PV utilization and the PV powered bus load. This is because the second and minute matching of PV and load are worse for these sections. For the 0.5EN PV system it is recommended to invest in a small storage size (up to 10 kWh or smaller). These systems are cheap and have a limited dump of only 30% (which may be manageable because of the small PV system) and still increase the renewable energy share with 32%. To increase this share the other option is to install larger PV (0.8EN) with large storage (200-400 KWh). These systems supply 55-60% of the bus load, with a dump of 18-24%. Again, the energy neutral PV with 50 MWh of storage is economically not feasible. The minimal storage size was set on 10 kWh. Since, it was found that the logic for the storage system does not work for smaller sizes. The logic controller checks if the storage medium is between lower and upper limit, and then subtracts or adds power. However, if the storage medium is approaching one of the limits, the addition or subtraction of power could push the storage medium over its physical limitations. This could be avoided by adding an additional logic step that limits the amount of power that could be drawn or stored based on the left-over energy in the storage. However, the problem was identified late and could therefore not be changed due to time constraints.

Figures H.1 and 5.6 showed that powering over 60% of the bus load with PV is not feasible, since the storage medium cost becomes to high. In the next section a different approach for sizing the PV is suggested to reduce the storage costs. In this approach, a PV system is sized to power the aggregated grid load instead of the load from all individual substations. This will reduce the peak powers and create a more stable base load. Therefore, a higher PV utilization could be achieved with the same storage size. The mismatch for an aggregated energy neutral PV system and the trolleybus load is shown in figure 5.7.

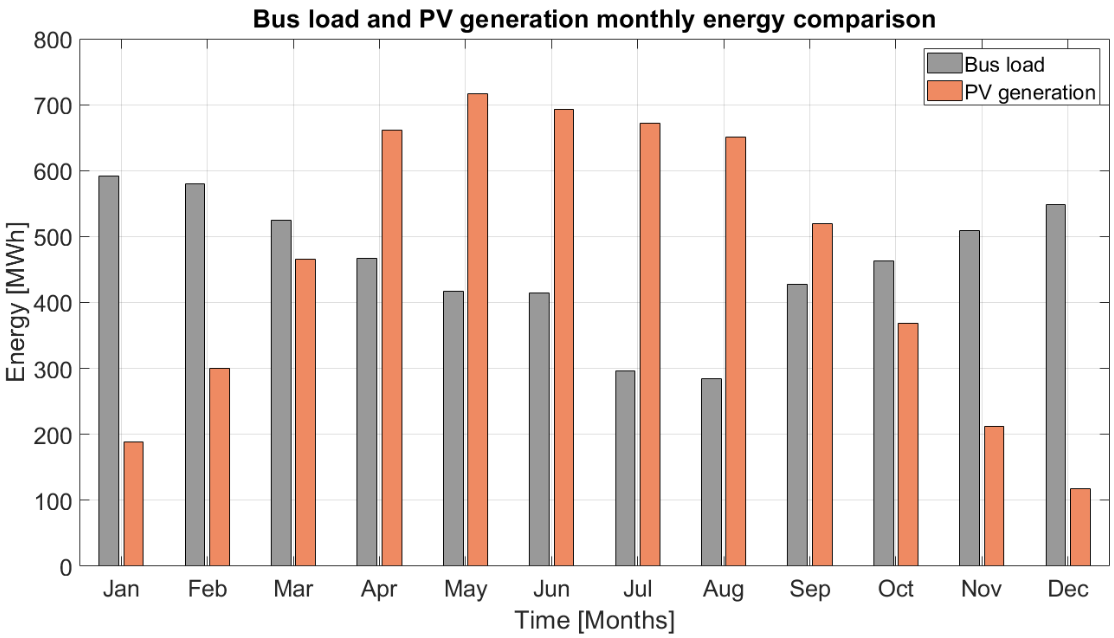

Figure 5.7: Monthly bus load and PV generation

Since the mismatch is large on a seasonal scale, the PV system is expanded with a wind system to improve the seasonal matching between generation and load.

To recap, in this chapter energy storage mediums are sized for PV systems. First this was done for the PV systems according to the net benefit optimization of the previous chapter. However, it was found that these PV and storage systems have little impact on supplying the bus loads. Next, for high traffic (HQ) and low traffic (10) substations, the PV and storage have been resized for a large range. For both substations, two promising PV and storage combinations were found. The first option is to install small PV (0.5EN) with small storage (10kWh or lower), this option is relatively cheap but only supplies 35% of the bus loads. The other option is to go for a larger PV system (0.8 EN) with larger storage (0.5 to 2 MWh for substation HQ, 200 to 400 kWh for substation 10). These systems supply 55-60% of the bus loads. It can be concluded that the inclusion of storage systems yield a large improvement. However, to increase the renewable energy share above 60%, a different approach needs to be adapted. This approach is outlined in the next chapter.

Chapter 6: Increasing the renewable energy share; the aggregated approach

In previous chapter it was found that PV and storage systems could increase the renewable energy share to around 60% for low and high traffic substations. In this chapter, an aggregated approach is suggested to further increase the renewable energy share. In this chapter, the PV and storage are not sized for individual substations, but rather for the grid as a whole. Furthermore, to improve the matching of the power generation with the bus loads, the PV system is combined with a wind system.

6.1 A simple wind power model

For this work a simple wind model is constructed. The hub height, rotor radius, cut-in, cut-out and rated wind speed are copied from a reference 5 MW turbine from NREL and are provided in table 6.1 [56].

Table 6.1: Parameters for the wind model [56].

Hub height (m)	90
Rotor radius (m)	63
Cut-in wind speed (m/s)	3
Cut-out wind speed (m/s)	25
Rated wind speed (m/s)	11.4

The same wind data that was used for the PV model is used again for the wind model. This may not be optimal, since the wind speeds are higher near the sea. However, since the power is used in Arnhem it makes sense that the turbine is placed there as well. Moreover, the data had to be scaled to the hub height of the turbine. The data was originally measured at ten meters above ground. Since the wind speed varies a lot in the lower part of the atmosphere, the wind speed data had to be scaled to the hub height. This scaling is done in two steps, first to 60 meters and then to 90 meters. Scaling from ten to 60 meters is done using the *log wind profile* this is a semi-empirical fit that applicable for scaling wind speed in the atmospheric boundary layer. The fit is appropriate until a height of 60 meters, because until that height the surface roughness may affect the wind speed. Above 60 meters, the *power profile* is used. The log wind profile and the power wind profile can be calculated with equations 6.1 and 6.2, respectively.

$$u(z_2) = u(z_1)\frac{\ln((z_2 - d)/z_0)}{\ln((z_1 - d)/z_0)} \tag{6.1}$$

$$u(z_3) = u(z_2)\left(\frac{z_3}{z_2}\right)^{\alpha} \tag{6.2}$$

Here z_1, z_2 and z_3 are the heights at which wind speeds u_1, u_2 and u_3 occur. u_1, u_2 and u_3, are the wind speeds at 10,60 and 90 meters, respectively.

z_0 is the surface roughness in meters. The rougher the surface, more it reduces wind speed at lower altitudes. For wind turbines on land, a surface roughness of 0.3 meters is commonly assumed. For the model I therefore also decided to use 0.3 meters [57].

α is the power factor and it depends on the atmospheric conditions. It is common practice to assume that the atmosphere has on average a neutral stability. This means that the atmosphere neither assists nor resists vertical movement. For these conditions a power factor of $\frac{1}{7}$ is empirically derived. The measured and computed wind speed at 60 and 90 meters are shown in Appendix F.

Now that we have the established input data and the parameters of the wind turbine we can calculate the power output of the turbine. A wind turbine converts the kinetic energy of the wind into rotational energy, which is finally converted to electrical energy in the generator. The kinetic energy of the wind can be calculated with equation 6.6.

$$E = \frac{1}{2}mv^2 \tag{6.3}$$

Here m is the mass of the wind and v^2 is the wind speed squared. Mass is equal to the volume of the wind (Q) and the density of the wind (ρ).

$$E = \frac{1}{2}\rho Q v^2 \tag{6.4}$$

Next, the volume of the wind can be expressed as the cross-sectional area of the wind reaching the blades times the length of the wind column. The length of the wind column depends on how long we measure the incoming wind. To calculate the power of the wind, the volume flow of wind can be expressed as the cross-sectional area times the wind velocity instead.

$$P = \frac{1}{2}\rho A v^3 \tag{6.5}$$

Moreover, the area of the blades can be expressed as pi times the radius squared.

$$P = \frac{1}{2}\rho \pi r^2 v^3 \tag{6.6}$$

Now we have reached the formula for kinetic power in the wind with parameters that we can fill in. However, the turbine is not able to extract all the power from the wind. The limit for power extraction is the *Betz-limit*, derived by German physicist Albert Betz. He derived that the maximum theoretical limit of power extraction is 59.3%. [58] In practice this limit is lower.

To calculate the actual fraction of power that is harnessed by the turbine we can use the power at rated wind speed. From the cut-in wind speed up to the rated wind speed the wind turbine aims to extract the maximum power from the wind. From the rated wind speed to the cut-out wind speed the turbine aims to extract the rated power for which the turbine was designed, in this case 5 MW. It does this by lowering the fraction of power it extracts from the wind. To get the fraction of power extracted from the wind - referred to as the capacity factor - we can rewrite equation 6.7 to 6.8.

$$P = \frac{1}{2}\rho \pi r^2 v^3 c_p \tag{6.7}$$

$$c_{\mathrm{p}} = \frac{P}{\frac{1}{2}\rho \pi r^2 v^3} \tag{6.8}$$

We evaluate 6.8 at the rated wind speed and find a power factor of 45%.

Now we can use the wind speed data and equation 6.7 to calculate the power for the whole year. However, if the wind speed is below the cut-in or above the cut-out wind speed the power is set to zero. Furthermore, if the power is above the rated wind speed and below the cut-out wind speed the power is set to 5 MW.

Now we need to see if the 5MW turbine has the right size for the trolleybuses. In this work, the turbine is sized to make the trolley grid energy neutral. We can do this by comparing the yearly energy yield of the turbine with the energy demand of the grid. It was found that the turbine was oversized and the rated power that was required is 3.4MW instead. For this crude model a wind turbine of 3.5MW with small losses is therefore assumed. For this turbine the radius was scaled to 53m. The other parameters are kept the same. The power output of the turbine for the winter and summer months is shown in figure 6.1.

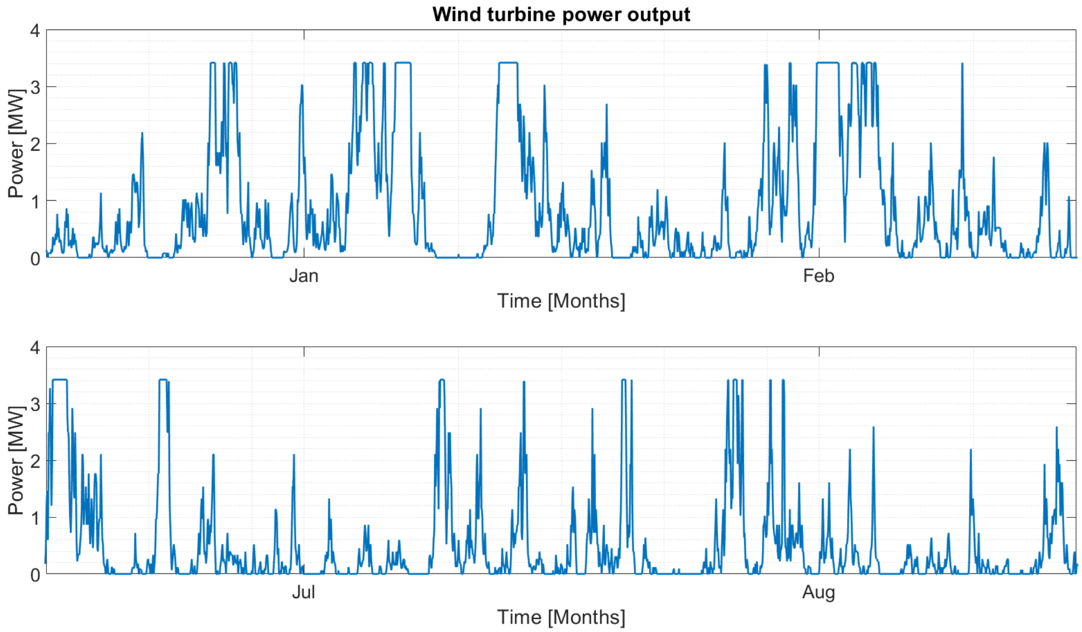

Figure 6.1: Power output of wind turbine in winter and summer

As expected, the winter the average wind speed is higher than in the summer, the profiles look realistic.

6.2 Sizing a hybrid (PV and wind) power system

In figure 6.2 the monthly grid load and PV and wind generation are shown. From the figure it is evident that wind has a better seasonal match with the grid load than PV. However, wind has the downside of having a worse short-term match with the grid load. This is illustrated in figure 6.3. In this figure, the grid load is compared with the PV and wind generation for the second week of March to show the short-term matching of the profiles. The month March was selected, because in this month the grid load and wind and PV generation fit best.

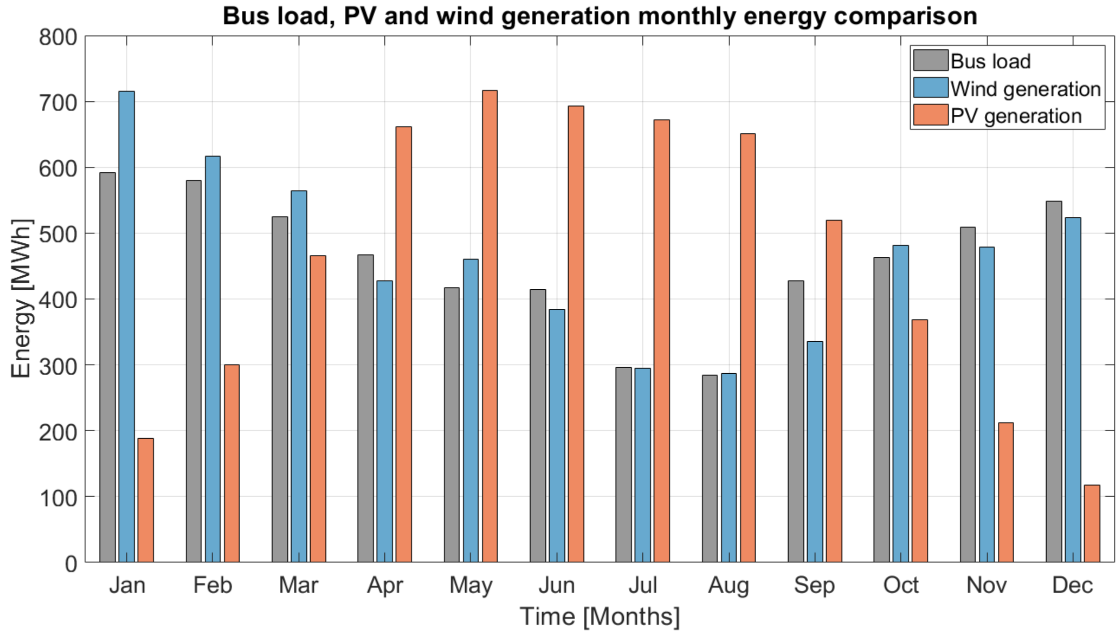

Figure 6.2: Monthly bus load and PV and wind generation

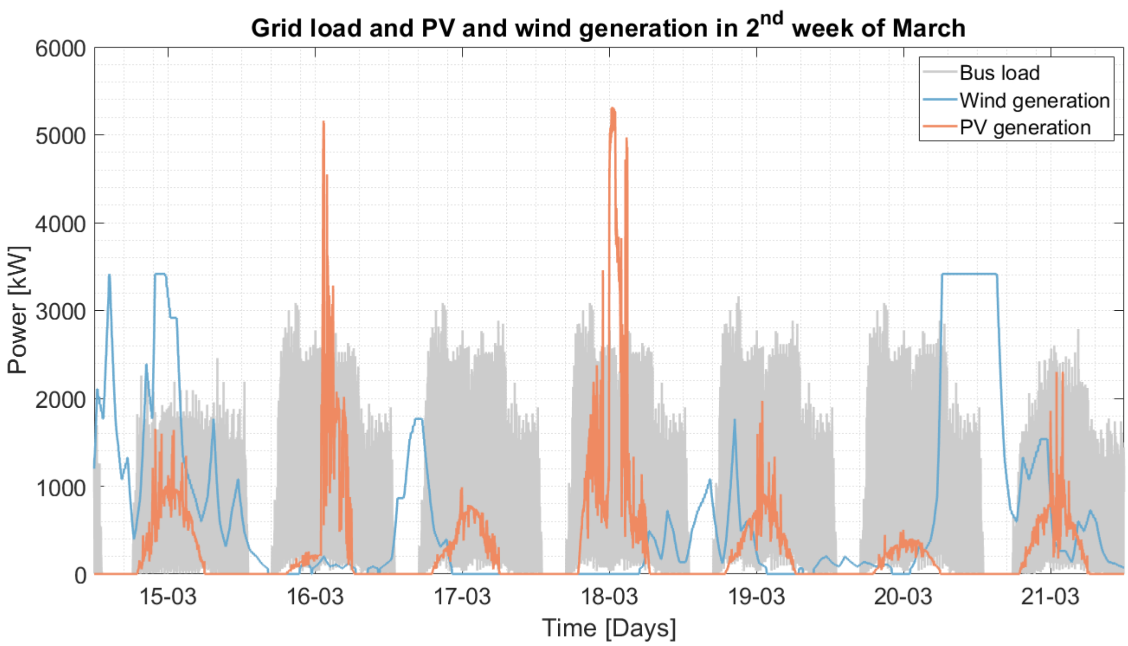

Figure 6.3: Bus load and PV and wind generation for 2nd week of March

A system that consists of PV and wind could give a good trade-off between short-term and long-term generation and load matching. In figure 6.4, the ratio PV and wind has been varied between 100% PV and 100% wind in steps of 5%. Near the optimum of 50% wind and 50% power, the ratio was varied for every percent.

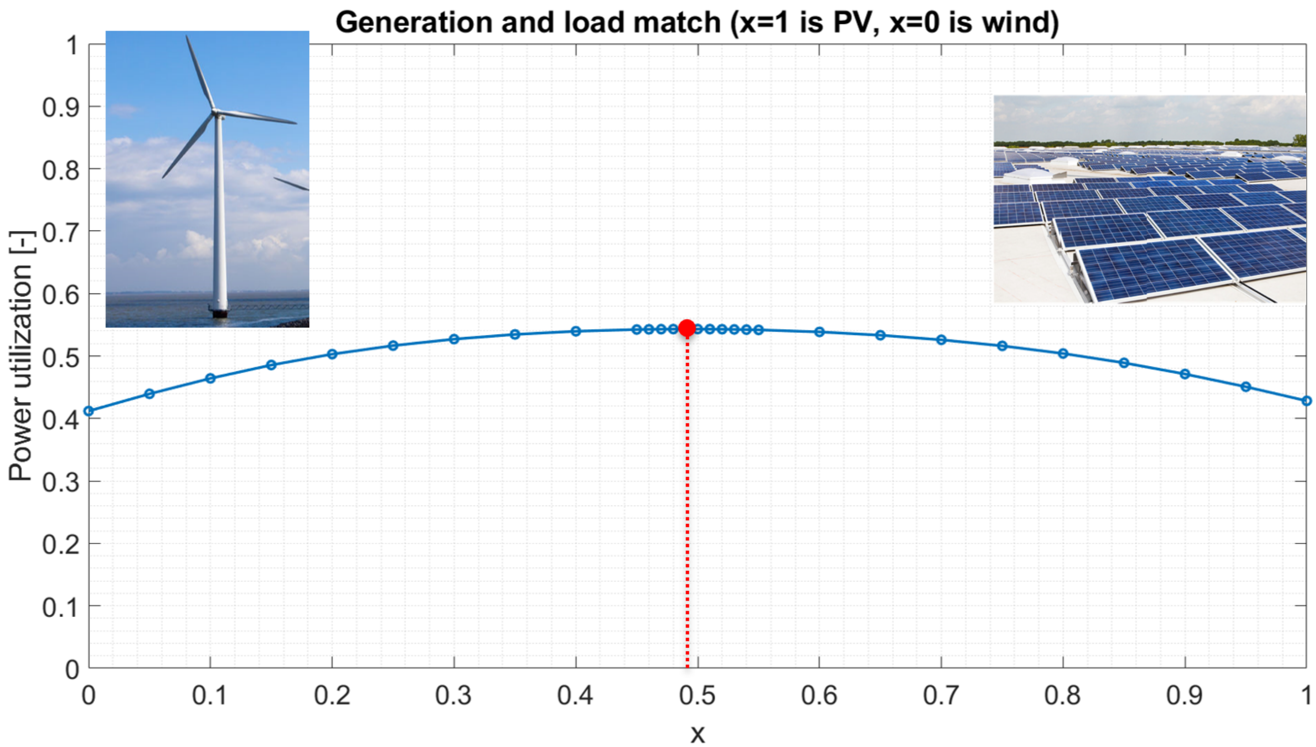

Figure 6.4: Combination of wind and solar energy

It was found that the optimum ratio for Arnhem is 51% PV and 49% wind. The power utilization for a 100% wind system is 41% with the load, while a PV system has a utilization of 43%. The hybrid system has a power utilization of 55%. Because the hybrid system consists of roughly equal PV and wind it is interesting to see how it performs with support of storage. In the final section, the storage is varied for the PV, wind and hybrid systems to investigate how the system performance improves.

6.3 Sizing storage system for the PV, wind and hybrid power systems

In table 6.2, the sizes for the power systems are shown.

Table 6.2: Sizes of aggregated systems

	PV (MWp)	**Wind (MW)**
PV	8.6 (1.0 EN)	0
Wind	0	3.5 (1.0 EN)
Hybrid	4.3 (0.51 EN)	1.75 (0.49 EN)

In figure 6.5 the power utilization for the PV, wind and hybrid systems are shown for varying storage sizes. In figure 6.6 the same data is plotted till a maximum storage size of 100 MWh. The power utilization for each system is calculated with equation 4.1.

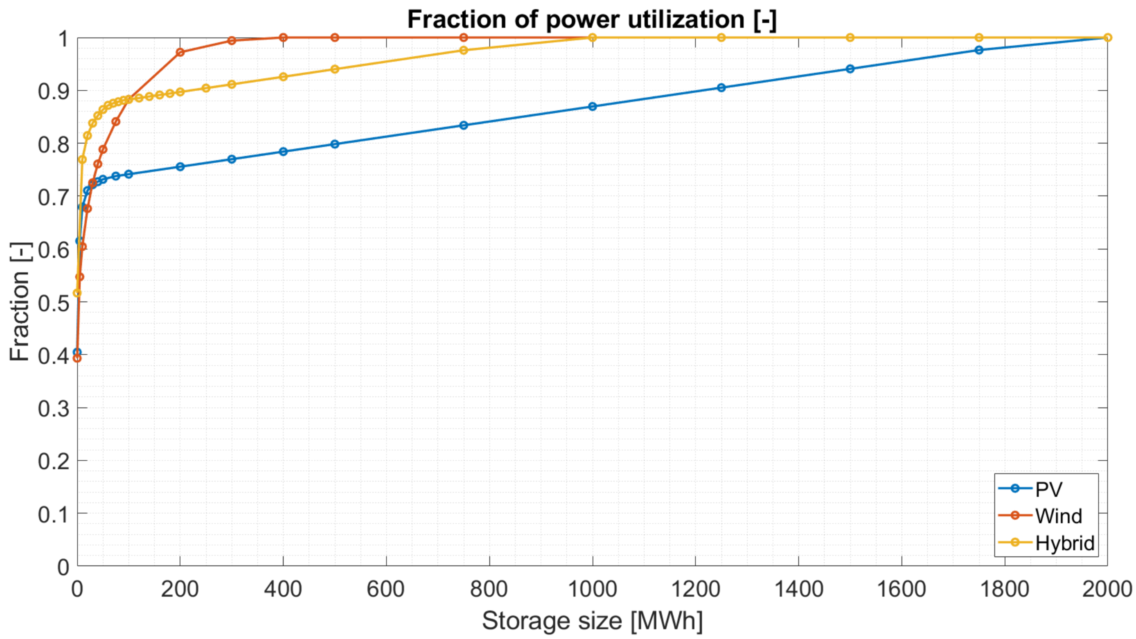

Figure 6.5: Power system performance with varying storage sizes

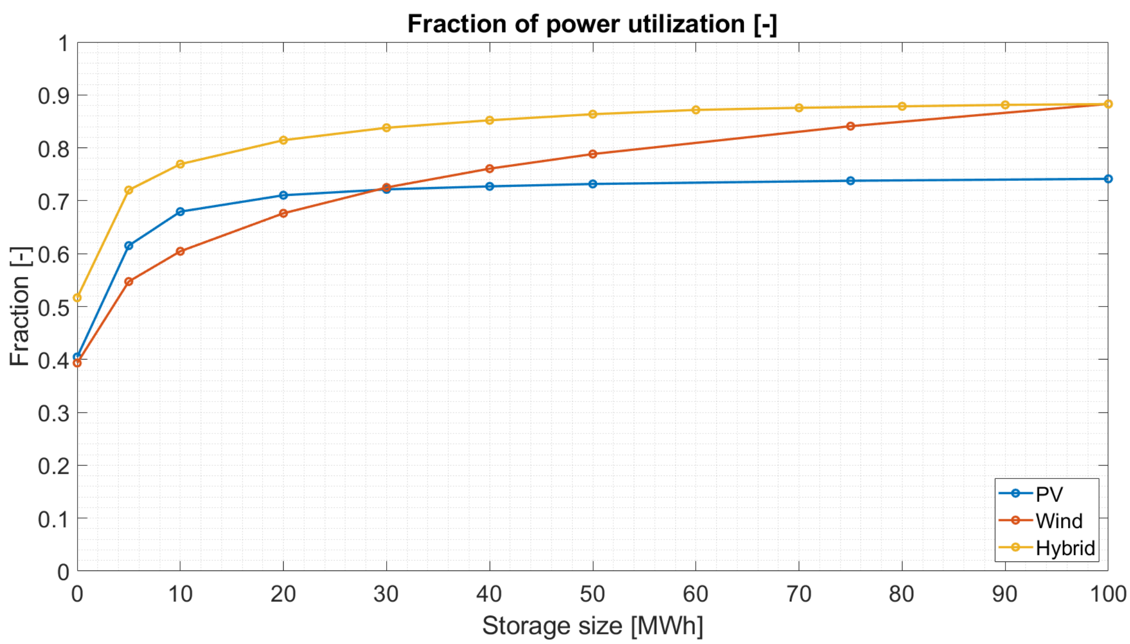

Figure 6.6: Power system performance with varying storage sizes - up to 100 MWh

It is evident that no system can eliminate AC-grid dump completely in a economically feasible manner. Which system performs best depends on the storage size that is installed. The hybrid system is the preferred system up to 100 MWh of storage, after that the wind system performs better. The PV system performs better than the wind system until 30 MWh of storage.

Since PV and storage have a higher power utilization than wind for small storage sizes, the PV system is recommended over a wind system. However, the hybrid system outperforms both systems and should be installed to attain the maximum renewable energy share in the Arnhem trolley grid. An EN hybrid system with 5-10 MWh of storage could make the energy supply of the whole Arnhem grid renewable, while using the AC-grid for 23-28% of the energy storage. As a first estimation, this system looks most promising because the storage may still be affordable.

6.4 CO_2 assessment of the hybrid system

In this section the equivalent CO_2 emissions (eq.CO_2 emissions) of the hybrid system are compared with the current grid emissions. The comparison in this chapter is simple and should give an impression of the emission savings that could be obtained.

First some basic assumptions for this analysis should be explained. It is assumed that the analysis is performed for 30 years, which is the lifespan of the PV and wind systems. Furthermore, it is assumed that there are no changes to the load of the grid and the composition of the energy mix (see figure 1.6). In reality, the load of the trolley grid will likely increase and the energy mix will become more renewable. Furthermore, it is assumed that the emissions in table 1.1 incorporate the total emissions for the energy sources, are applicable for the Netherlands and do not change in 30 years.

If we assume that the power generated by the hybrid system are for 51% generated by PV and 49% generated by wind and that the system has 7.5 MW of lithium-ion batteries installed (very large), the eq.CO_2 emissions can be computed.

Wind has an eq.CO_2 emissions of 11g per kWh and the total emissions are therefore 30 Mton per year. PV has an eq.CO_2 emissions of 48g per kWh and the total annual emissions are 137 Mton. Furthermore, lithium-ion batteries have a eq.CO_2 emissions of approximately 1 Mton per kWh [59]. The eq.CO_2 emissions of the battery system is 5000 Mton. Tesla PowerWalls are large lithium-ion batteries that are commercially available (in the US), these batteries have a 10-year warranty on performance [60]. Therefore, for this simple comparison it is assumed that the battery system will last for 10 years. The result is an 80% decrease in the overall eq.CO_2 emissions in the 30-year lifetime of the system. The results are summarized in table 6.3.

Table 6.3: Equivalent CO_2 emission comparison between business as usual and hybrid system.

	Business as usual	**Hybrid system + storage**	
Energy per year (GWh/yr)	6	Wind	3
		PV	3
Emissions per energy (g eq.CO_2/kWh)	552	Wind	11
		PV	48
Extra emissions (Mton eq. CO_2)	0	Battery system	15000
Total emissions in 30-years (Mton eq. CO_2)	9.9E+04	2.0 E+04	
Emission reduction with hybrid system	**80%**		

To summarize, in this chapter PV and wind have been combined to power the aggregated load of the trolley system. It was found that a hybrid system with 51% PV and 49% wind has the highest power utilization of 55%. For this system and for 100% PV and 100% systems, the storage system size was varied. The hybrid system with 5 to 10 MWh of storage seems the most promising system. This system can achieve 72% to 78% power utilization while exchanging the left-over power with the AC-grid. Finally, a CO_2 assessment of the system showed that the system can reduce the equivalent CO_2 emissions by 80% when compared to the business as usual scenario over the lifetime of the system.

Chapter 7: Conclusions and Recommendations

In this final chapter first the conclusions of the work are listed. Then limitations of the work are discussed, followed by the recommendations. Finally there are suggestions for future work.

7.1 Conclusions

The whole thesis project started with one objective in mind:

Investigating the attainable renewable energy share of the Arnhem trolleybus grid while minimizing the need for seasonal storage.

RQ1: What renewable energy source has the most potential for increasing the renewable energy share?

In this work, PV and wind are both considered as possible renewable energy sources for increasing the renewable energy share in trolley grids.

From a practical point of view, PV has advantages over wind. These advantages are; the modules are more urban-friendly and are modular. It has the added benefit that it produces DC power which could be added to the sections directly at a higher energy efficiency and could make the voltage profile more robust and reduce transmission losses. The cost for onshore wind and PV are comparable.

From an energy point of view the choice between PV and wind is less obvious. An aggregated PV system without storage, size to make the trolley grid energy neutral has a PV utilization of 43%. For a wind system this wind utilization is 41%. Aggregated means that power systems are sized for the grid load as a whole and energy neutral means that the annual energy generation of the power systems is equal to the grid load. The key Wind has a better seasonal fit with the grid load, since the trolleybus load increases in the winter due to Heating, Ventilation and AC. The wind generation also increases in the winter. In addition, in the summer different bus schedules are active. Therefore, the total number of buses decreases in the summer. It was found that a system with 49% wind and 51% PV has the highest direct power utilization of 55%. difference between PV and wind is that PV has a better daily fit with the grid load and wind has a better seasonal fit. This is because the trolleybus load increases in the winter due to Heating, Ventilation and AC. The wind generation also increases in the winter. In addition, in the summer different bus schedules are active. Therefore, the total number of buses decreases in the summer. It was found that a system with 49% wind and 51% PV has the highest direct power utilization of 55%.

In practice, the PV system is preferred over the wind system because of the practical reasons and because the PV power utilization can improve a lot with small storage. Wind works better with large storage, but in practice this is too expensive.

Nonetheless, it is recommended to install a hybrid system (51% PV and 49% wind) instead. This system gives the best trade-off between the short-term and long-term matching of the PV and wind and can reach a power utilization of 55%.

RQ2: Where should this renewable energy source be connected to the trolley grid system?

In this work, the PV is placed on the AC-side at the substations (between the transformer and the rectifier). Here the excess PV can be send to the AC-grid. This wouldn't be possible at the DC-side because of the rectifier in the substation and the PV has to either be stored or wasted.

However, the bus load at the substations is inconsistent and therefore the PV was powering the AC-grid most of the time. Therefore the recommended system is an aggregated power system. This system can power the combined load of the trolley grid and thereby have a more consistent base load and reduced power peaks. It can be connected to the medium-voltage AC grid.

RQ3 & RQ4: What size should the PV system be and how much power is directly utilized by the buses (without storage)?

For each substation a PV size has been established that maximizes the net social benefit of PV energy to the buses (benefit) and PV energy to the AC-grid (cost). Many substations have an inconsistent stream of traffic; therefore, the PV cannot send its power to the buses most of the time and consequently for thirteen of the eighteen substations the recommended PV size is no PV. The substations that should receive PV according to the optimization should only have a few percent of an energy neutral PV system installed. Since only 8.2% of the bus load is directly supplied by PV, the PV system should be supported by energy storage. Simply increasing the PV size and curtailing the excess PV to limit grid dump is not a successful strategy to improve the renewable energy share of the trolleybuses due to the inconsistent stream of bus traffic under the substations. The extra installed PV will send a larger share of its power to the AC-grid.

RQ5: How does the renewable energy utilization improve with energy storage?

To improve the PV system, storage was added to the PV that was sized to maximize the net social benefit. However, since the PV generation is much smaller than the bus load, the storage has limited effect on improve the PV utilization. The storage is primarily used to store energy in the summer (when the PV is overproducing), but its use drops throughout the year. A better approach is to size the PV and storage at the same time. In this work this was done for a low and high traffic substation. The PV system size was varied between 50% energy neutral and 100% energy neutral and the storage was varied between 10 KWh and 1 GWh for both substations. Two combinations have potential. A 50% energy neutral system with 10 KWh of storage can be an affordable option that can increase the renewable energy share to 35% while using the Arnhem grid for 25% of the PV storage (for both substations). To increase the renewable energy share further, an 80% energy neutral PV system could be installed with 0.5 to 1 MWh of storage for the high traffic substation and between 200 and 400 kWh for the low traffic substation. In both cases, the PV utilization increases to 55-60% while the grid dump is 25-30% for the high traffic substation and 18-24% for the low traffic substation. It makes sense that the high traffic substation needs more storage, since the PV system is six times larger (due to the larger bus load). Increasing the PV system with 20% increases the renewable energy share by 5-10% while the grid dump increases by 10-15%. Increasing the storage size would make the systems too expensive.

To maximize the renewable energy, share the Arnhem grid, a third approach was suggested. Instead of sizing the PV systems for the individual substations, an energy system is sized for the aggregated grid load. In this way the base load is higher, and the peaks are reduced. For the hybrid system – and a 100% PV and 100% wind system – the power utilization with varying storage sizes was investigated. It was found that a PV system has a higher power utilization up to 30 MWh of storage. Furthermore, the hybrid system outperforms both the wind and the PV systems up to 100 MWh of storage, if more storage is installed the wind system is the better option. The most promising option is to install the hybrid system with 5-10 MWh of storage. This system could power 72% to 78% of the Arnhem grid directly, while using the AC grid as storage for the remaining power. A simple CO_2 balance showed that this system could reduce the equivalent CO_2 emissions by 80% over a 30-year span.

7.2 Limitations

The conclusions from this work come with some limitations. The most important limitation is that the case-study is carried out in only one grid. The result of this is that performance of the systems is only evaluated under one set of city parameters (like meteorological parameters), the potential for PV and storage in warmer climates is a lot different than it is in the Netherlands. Two important reasons for this hypothesis are because the ambient temperature is higher, therefore the buses need less or no heating in the winter. Heating can constitute up to 43% of the total bus load in the winter for the Arnhem trolleybuses [14]. Moreover, the warmer climate have more equivalent sun hours per day. Therefore, the energy output of the PV is higher than it is in Arnhem. Consequently, the PV output in the summer is also higher and the demand for storage increases again. Finally, if the trolley grid is located closer to the equator, the variation in sun hours per day is smaller and the seasonal variation between PV and bus load is smaller as a result.

Other limitations of this work have to do with a limited knowledge about the trolley system. The topology of the overhead lines and an overview of which sections are bilaterally connected was not shared during the this work.

Bilateral connections allow substations to power each others bus load through the section separations. This has a large effect on the short time scale matching between PV and bus load and may improve the potential for PV on substation with a low consistency of traffic by a lot. However, since the grid operates to minimize power losses, the PV on busier substations may lose some load to neighboring substations. Therefore, the PV utilization for busier substations may drop. In this work, it was found that substations are bilaterally connected in the Arnhem grid but which substations in specific is not known.Furthermore, the lack of the topology of the overhead lines means that the power flow on the overhead lines cannot be computed accurately. It could be, for instance, that sections near the city centre have many parallel lines to power the buses. The current in each line would be lower and the transmission losses would be lower. In this work, therefore a constant restive loss of 16.7% was assumed instead. Due to this limitation, not only can the losses for power flow on the overhead lines not accurately be assessed, also placement of PV directly on the section is not possible. Placing PV on the sections could - on top of increasing the renewable energy share - increase the voltage where the voltage drops the most. This would reduce transmission losses and better equip the PV for developments in the trolley system (e.q. In-motion-Charging of buses and grid multi-functionality). Moreover, the Heating, Ventilation and AC (HVAC) of the buses demands a large fraction of the total bus load. It is therefore important that the HVAC load is simulated accurately. For this work, only a correlation between ambient temperature and average HVAC power in the range of 1 to 12 degrees was available. To increase the range for the whole year a simple heat balance across the bus was constructed. However, a specification of the buses was lacking. Finally, only two sets of measurements for each bus trip in both directions was made available. These data sets are from trips with the highest and lowest overall energy. By using a dataset that represents the average energy per trip or by combining multiple data sets, the power profiles may become more representative. In this work only the data sets with the lowest overall energy have been used. For line 1, the difference between the mean average energy per trip and the minimal energy per trip is 15%.

The final limitation of this work is time. The location specific characteristics (mutual shading, cable losses etc.) of the solar panels was were not considered. Furthermore, the only storage constraint that is accounted for is that the storage medium remains within the lower and upper states of charge, the ramping constraints and design of the storage medium was also not accounted for. The assumptions for the wind model are more rough still. It was assumed that the turbine has the same design as a 5 MW turbine with a scaled down radius. In practice, the forces, moments, and losses for the turbine have to be calculated carefully. In this work, only an small loss was arbitrarily assumed. Furthermore, the location for the turbine was not optimized. Finally, the CO_2 impact of the various systems has not been quantified.

7.3 Recommendations

In this section the recommendations on how to improve the work are shared. These recommendations are grouped in three categories below

- Grid model
  - Improve the HVAC power estimation. Preferably, this is done by using more measured data in a wider ambient temperature range. Otherwise, a specification sheet for the trolley bus could improve the accuracy of the input parameters for the heat balance.
  - Repeat the HVAC power estimation but turn of the climate control when the bus is using 300 kW or more. In practice, above this limit the climate control is turned off. This is not included in this work.
  - Compute the power flow over the overhead lines instead of assuming a constant power loss of 16.7%
  - Include bilateral connections to investigate the effects on power sharing and renewable energy potential.
  - Use multiple sets of measured velocity and power data of the buses to see how much the data sets vary and to get a more representative bus power profile.
- Results

  - For the aggregated approach the power system does not need to be close to the trolley grid. Therefore, the PV and wind could be located at more suitable locations. Furthermore, the location specific conditions and their affects on the location and performance of the renewable energy systems must be established.
  - Change the ratio between PV and wind for the hybrid system and investigate the power utilization within the 5-10 MW storage range. The fact that a 51% PV and 49% wind system has the best power utilization without storage does not mean that it has the best utilization with storage.
  - In figures H.1 and 5.6 (the plots with PV and storage sweeps for the high and low traffic substations) shows that there are two storage ranges where the PV utilization jumps up. In appendix H, a first approach is suggested to relate these storage ranges with storage times. It is recommended to investigate if there are storage time scales for which the storage should be sized to optimally support the PV.

- General
  - Repeat the work in this study for another trolley grid. This shows how well the results are generalize-able and how large the effects of city parameters are.
  - Investigate how the trolleybuses transition from one bus line to another at the central station and time how long the buses are there on average.
  - Model the bus traffic on line 9.

7.4 Future work

The first recommendation for future work is to investigate DC-side placement of PV. On top of increasing the renewable energy share, the PV could help improve the voltage profile of the overhead line. These challenges are listed in appendix B. Since the overhead lines are low voltage, they suffer from voltage drops, especially if there are multiple buses that are accelerating. By placing PV on the sections, not only does the voltage profile remain more robust, as a result the transmission losses in the overhead lines decrease. Moreover, the grid is better prepared for the load increase in the future due to In-Motion-Charging buses (buses that charge a battery while attached to the overhead lines) and grid multi-functionally (EV charging, LED street lights, etc.). In appendix H interesting insights for PV sizing and placement and storage sizing and placement are shared.

Finally, it is recommended to investigate which storage medium is best able to support the PV and to investigate where on the section the PV and storage may placed.

Bibliography

[1] W. R. Cline *et al.*, *The economics of global warming.* Institute for International Economics, 1992.

[2] Š. Hamacek, M. Bartłomiejczyk, R. Hrbáč, S. Mišák, and V. Stỳskala, "Energy recovery effectiveness in trolleybus transport," *Electric Power Systems Research*, vol. 112, pp. 1–11, 2014.

[3] M. Bartłomiejczyk, "Practical application of in motion charging: Trolleybuses service on bus lines," in *2017 18th International Scientific Conference on Electric Power Engineering (EPE).* IEEE, 2017, pp. 1–6.

[4] M. Bartłomiejczyk, R. Hrbáč, V. Stỳskala, and M. Połom, "Trolleybus with traction batteries for autonomous running," 2013.

[5] L. Brunton, "The trolleybus story," *IEE Review*, vol. 38, no. 2, pp. 57–61, 1992.

[6] L. Chapman, "Transport and climate change: a review," *Journal of transport geography*, vol. 15, no. 5, pp. 354–367, 2007.

[7] J.-Q. Li, "Battery-electric transit bus developments and operations: A review," *International Journal of Sustainable Transportation*, vol. 10, no. 3, pp. 157–169, 2016.

[8] "Trolley 2.0," https://www.trolleymotion.eu/trolley2-0/, accessed: 2020-01-30.

[9] M. Salih, D. Baumeister, M. Wazifehdust, P. Steinbusch, M. Zdrallek, S. Mour, P. Deskovic, T. Küll, and C. Troullier, "Impact assessment of integrating novel battery-trolleybuses, pv units and ev charging stations in a dc trolleybus network," in *2nd E-Mobility Power System Integration Symposium*, 2018.

[10] A. Dhabi, "Renewable capacity statistics 2018," *IRENA, Renewable Capacity Statistics*, p. 21, 2018.

[11] K. Smith, S. Galloway, A. Emhemed, and G. Burt, "Feasibility of direct current street lighting & integrated electric vehicle charging points," 2016.

[12] A. Whiteman, J. Esparrago, and S. Elsayed, "Renewable energy statistics 2018," *The International Renewable Energy Agency: Abu Dhabi, UAE*, 2018.

[13] S. Solomon, G.-K. Plattner, R. Knutti, and P. Friedlingstein, "Irreversible climate change due to carbon dioxide emissions," *Proceedings of the national academy of sciences*, vol. 106, no. 6, pp. 1704–1709, 2009.

[14] T. P. EU. (2020) Network based energy storage system for eberswalde. [Online]. Available: http://www.trolley-project.eu/

[15] Connexxion. (2018) Dienstregeling. [Online]. Available: https://www.connexxion.nl/getmedia/5760466e-13fc-4b45-a4a9-2818eb84a40a/LF_breng_600_Arnhem_Stad_dec_-2018.pdf

[16] IEA. (2020) Electricity information. [Online]. Available: https://www.iea.org/subscribe-to-data-services/electricity-statistics/

[17] T. Bruckner *et al.*, "Report of ipcc working group iii–mitigation of climate change, annex iii: Technology–specific cost and performance parameters 2014 [ ]," *: https://www. ipcc. ch/pdf/assessmentreport/ar5/wg3/ipcc_wg3_ar5_annexiii. pdf–(: 08.01. 2018).*

[18] S. Arrhenius, "Xxxi. on the influence of carbonic acid in the air upon the temperature of the ground," *The London, Edinburgh, and Dublin Philosophical Magazine and Journal of Science*, vol. 41, no. 251, pp. 237–276, 1896.

[19] U. Nations. (2000) Sustainable development goals. [Online]. Available: https://www.un.org/sustainabledevelopment/

[20] G. Stana and V. Brāzis, “Trolleybus with ess motion simulation considering common mass increase and transmission losses,” in *2017 IEEE 58th International Scientific Conference on Power and Electrical Engineering of Riga Technical University (RTUCON)*. IEEE, 2017, pp. 1–6.

[21] D. Baumeister, M. Salih, M. Wazifehdust, P. Steinbusch, M. Zdrallek, S. Mour, L. Lenuweit, P. Deskovic, and H. B. Zid, “Modelling and simulation of a public transport system with battery-trolleybuses for an efficient e-mobility integration,” in *1st E-Mobility Power System Integration Symposium*, 2017.

[22] M. Wazifehdust, D. Baumeister, M. Salih, P. Steinbusch, M. Zdrallek, S. Mour, and C. Troullier, “Potential analysis for the integration of renewables and ev charging stations within a novel lvdc smart-trolleybus grid,” 2019.

[23] D. Baumeister, M. Salih, M. Wazifehdust, M. Koch, P. Steinbusch, M. Zdrallek, S. Mour, and C. Troullier, “Scenario analyses of a dynamic lvdc smart-trolleybus-network with battery-assisted traction loads,” in *2019 IEEE PES Innovative Smart Grid Technologies Europe (ISGT-Europe)*. IEEE, pp. 1–6.

[24] M. Salih, D. Baumeister, M. Wazifehdust, M. Koch, P. Steinbusch, M. Zdrallek, S. Mour, and C. Troullier, “Optimized positioning for storage systems in an lvdc traction grid with non-receptive power sources and photovoltaic systems,” in *2nd E-Mobility Power System Integration Symposium*, 2020.

[25] P. Bernhardt, C. Sauer, and M. Hendrix, “Ermittlung des energiebedarfs zur bewegung von fahrzeugen in mikroskopischen verkehrssimulationen,” 2015.

[26] A. S. Tomar, B. P. Veenhuizen, L. Buning, and B. Pyman, “Viability of traction battery for battery-hybrid trolleybus.”

[27] D. Iannuzzi, D. Lauria, and P. Tricoli, “Optimal design of stationary supercapacitors storage devices for light electrical transportation systems,” *Optimization and Engineering*, vol. 13, no. 4, pp. 689–704, 2012.

[28] P.-H. Hsi and S.-L. Chen, “Electric load estimation techniques for high-speed railway (hsr) traction power systems,” *IEEE transactions on vehicular technology*, vol. 50, no. 5, pp. 1260–1266, 2001.

[29] A. Ritter, P. Elbert, and C. Onder, “Energy saving potential of a battery-assisted fleet of trolley buses,” *IFAC-PapersOnLine*, vol. 49, no. 11, pp. 377–384, 2016.

[30] IRENA. Power generation costs 2019.

[31] Statista. (2015) Estimated levelized cost of electricity generation netherlands. [Online]. Available: https://www.statista.com/statistics/974195/estimated-levelized-cost-of-electricity-generation-netherlands//

[32] K. Strunz, E. Abbasi, and D. N. Huu, “Dc microgrid for wind and solar power integration,” *IEEE Journal of emerging and selected topics in Power Electronics*, vol. 2, no. 1, pp. 115–126, 2013.

[33] A. Awasthi, A. Sinha, A. K. Singh, and R. Veeraganesan, “Solar pv fed grid integration with energy storage system for electric traction application,” in *2016 10th International Conference on Intelligent Systems and Control (ISCO)*. IEEE, 2016, pp. 1–5.

[34] S. M. Vasisht, C. Vishal, J. Srinivasan, and S. K. Ramasesha, “Solar photovoltaic assistance for lhb rail coaches,” *Current Science*, vol. 107, no. 2, pp. 255–259, 2014.

[35] M. Lencwe, S. Chowdhury, and H. ElGohary, “Solar photovoltaic integration on locomotive roof top for south african railway industry,” in *2016 51st International Universities Power Engineering Conference (UPEC)*. IEEE, 2016, pp. 1–5.

[36] J. Hernandez and F. Sutil, “Electric vehicle charging stations feeded by renewable: Pv and train regenerative braking,” *IEEE Latin America Transactions*, vol. 14, no. 7, pp. 3262–3269, 2016.

[37] F. Ciccarelli, L. P. Di Noia, and R. Rizzo, “Integration of photovoltaic plants and supercapacitors in tramway power systems,” *Energies*, vol. 11, no. 2, p. 410, 2018.

[38] B. Kilic and E. Dursun, “Integration of innovative photovoltaic technology to the railway trains: A case study for istanbul airport-m1 light metro line,” in *IEEE EUROCON 2017-17th International Conference on Smart Technologies*. IEEE, 2017, pp. 336–340.

[39] W. Weiying, W. Mingliang, L. Qi, and C. Weirong, “Method for improving power quality of metro traction power supply system with pv integration,” in *2017 Chinese Automation Congress (CAC)*. IEEE, 2017, pp. 1682–1685.

[40] M. Salih, M. Koch, D. Baumeister, M. Wazifehdust, P. Steinbusch, and M. Zdrallek, “Adapted newton-raphson power flow method for a dc traction network including non-receptive power sources and photovoltaic systems,” in *2019 IEEE PES Innovative Smart Grid Technologies Europe (ISGT-Europe)*. IEEE, pp. 1–5.

[41] KNMI. Meteorological data downloaded with meteonorm.

[42] A. H. Smets, K. Jäger, O. Isabella, R. van Swaaij, and M. Zeman, *Solar Energy: The physics and engineering of photovoltaic conversion technologies and systems*. UIT, 2016.

[43] Ş. Ünal, “An experimental study on a bus air conditioner to determine its conformty to design and comfort condition,” 2017.

[44] M. Bartłomiejczyk and M. Połom, “Spatial aspects of tram and trolleybus supply system,” in *8th International Scientific Symposium on Electrical Power Engineering (ELEKTROENERGETIKA)*, 2015, pp. 223–227.

[45] W. Jarzyna, “Terms of the turbine and generator choice of wind power stations,” *Rynek Energii*, no. 4, pp. 102–106, 2011.

[46] E. A. De la Breteque, “Thermal aspects of c-si photovoltaic module energy rating,” *Solar Energy*, vol. 83, no. 9, pp. 1425–1433, 2009.

[47] H. Van den Akker and R. F. Mudde, *Fysische transportverschijnselen I*. Delft University Press, 1998.

[48] EngineeringToolbox. The prandtl number for air.

[49] M. K. Fuentes, “A simplified thermal model for flat-plate photovoltaic arrays,” Sandia National Labs., Albuquerque, NM (USA), Tech. Rep., 1987.

[50] A. Jones and C. Underwood, “A thermal model for photovoltaic systems,” *Solar energy*, vol. 70, no. 4, pp. 349–359, 2001.

[51] M. Muller, B. Marion, and J. Rodriguez, “Evaluating the iec 61215 ed. 3 nmot procedure against the existing noct procedure with pv modules in a side-by-side configuration,” in *2012 38th IEEE Photovoltaic Specialists Conference*. IEEE, 2012, pp. 000 697–000 702.

[52] “Largest solar park in the netherlands, chint,” https://www.chintsolar.nl/en/projects/midden-groningen/, accessed: 2020-07-04.

[53] K. Mongird, V. V. Viswanathan, P. J. Balducci, M. J. E. Alam, V. Fotedar, V. S. Koritarov, and B. Hadjerioua, “Energy storage technology and cost characterization report,” Pacific Northwest National Lab.(PNNL), Richland, WA (United States), Tech. Rep., 2019.

[54] L. Goldie-Scot, “A behind the scenes take on lithium-ion battery prices,” *Bloomberg New Energy Finance*, 2019.

[55] H. Keshan, J. Thornburg, and T. S. Ustun, “Comparison of lead-acid and lithium ion batteries for stationary storage in off-grid energy systems,” 2016.

[56] J. Jonkman, S. Butterfield, W. Musial, and G. Scott, "Definition of a 5-mw reference wind turbine for offshore system development," National Renewable Energy Lab.(NREL), Golden, CO (United States), Tech. Rep., 2009.

[57] T. R. Oke, *Boundary layer climates.* Routledge, 2002.

[58] V. Okulov and G. A. van Kuik, "The betz-joukowsky limit for the maximum power coefficient of wind turbines," *International scientific journal for alternative energy and ecology*, no. 9, pp. 106–111, 2009.

[59] H. Hao, Z. Mu, S. Jiang, Z. Liu, and F. Zhao, "Ghg emissions from the production of lithium-ion batteries for electric vehicles in china," *Sustainability*, vol. 9, no. 4, p. 504, 2017.

[60] T. Powerwall, "Ac datasheet, tesla, inc, usa, 2016," 2.

[61] D. Jovcic, D. Van Hertem, K. Linden, J.-P. Taisne, and W. Grieshaber, "Feasibility of dc transmission networks," in *2011 2nd IEEE PES International Conference and Exhibition on Innovative Smart Grid Technologies.* IEEE, 2011, pp. 1–8.

[62] M. E. El-Hawary, "The smart grid—state-of-the-art and future trends," *Electric Power Components and Systems*, vol. 42, no. 3-4, pp. 239–250, 2014.

[63] T. Brand, "Connexxion - arnhems trolleybusnet onderzoek bovenleidingnet," 2012.

Appendices

Appendix A: Comparison between AC and DC power distribution

Back in the day of Nikola Tesla and Thomas Edison the debate between AC or DC voltage systems for power distribution was settled. In the end Tesla's AC system won the battle, because of several reasons [61, 62]:

1. Without modern power electronics it is difficult to increase the voltage of DC distribution lines, resulting in high currents which lead to large resistive losses. On the other hand, for AC power simple transformers could be used to boost the voltage.

2. The loads of the 19$^{\text{th}}$ century where primarily electric motors and light bulbs, both are AC operated.

3. Traditional electricity plants - like coal or gas plants - use steam generators that produce AC power.

For these reasons it made sense that an AC power grid would be installed. However, in the present day our use and generation of power has changed dramatically. Researchers are now interested in using DC power grids to overcome some of the drawbacks that AC power grids have.

Drawbacks of AC power distribution

In AC power lines, the voltage and current are phase-shifted by some degree. Voltage and current without any phase-shift produce so-called *active* power and 180°-shifted voltage and current signals produce *reactive* power, this is shown in figure A.1a and figure A.1b.

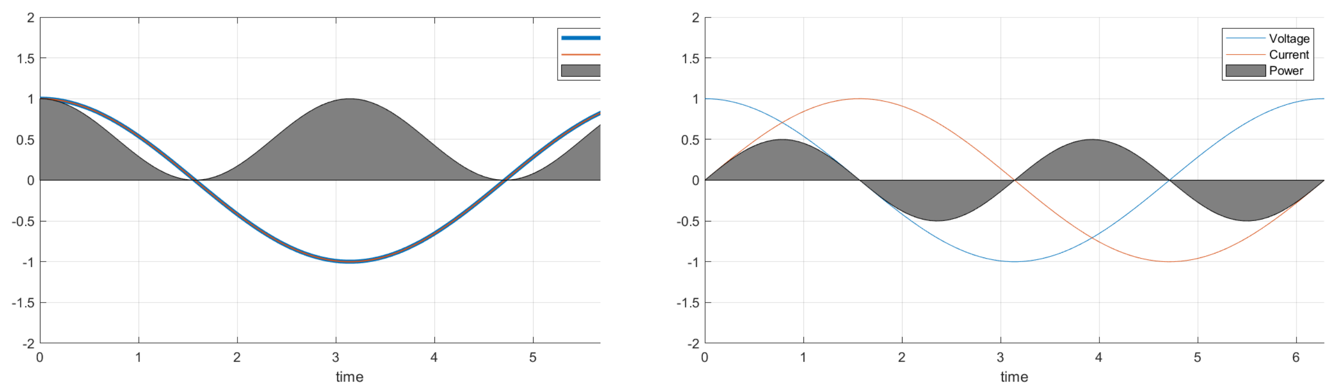

(a) Voltage and current 0°phase-shifted

(b) Voltage and current 180°phase-shifted

It should be noted that the amount of power does not change. However, reactive power cannot be used to do work. To increase the amount of usable power, the phase-shift between the voltage and the current must be minimized. This is where the power factor is introduced. Completely reactive power can equivalently be expressed as having a power factor of zero and active power has a power factor of one. To get the power factor closer to unity a power factor correction (PFC) unit needs to be installed, this power factor correction unit adds to the cost of the system and reduces the overall efficiency.

Moreover, a single-phase AC system may experience large power fluctuations at lower frequencies. As the polarity changes, the voltage and consequently the current change direction also. Therefore, there must be point where the output power is zero. The lower the frequency of the AC power, the larger this power fluctuation will be. To achieve a more stable output power, multiple wires with AC power phase-shifted with regards to each other may be added. In practice a 3-phase system, with each phase shifted 120°with respect to each other is used. This was found to be the economical optimum configuration. Figure A.2 shows the difference in power output between three single phases and 3-phase power.

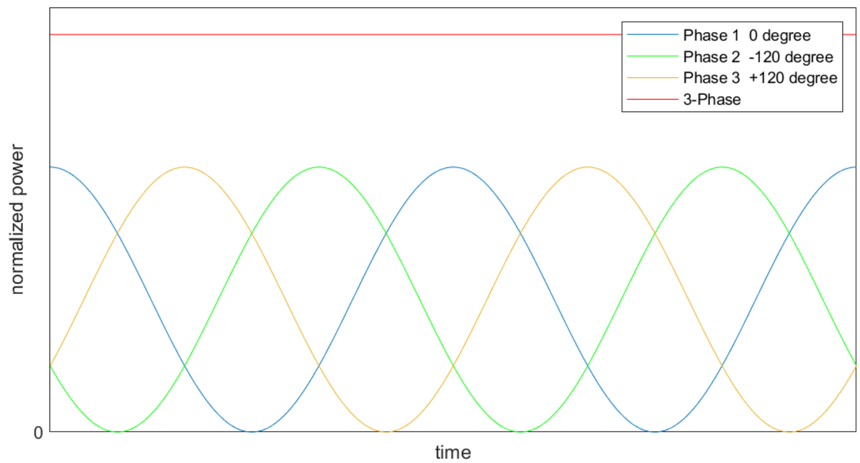

Figure A.2: Single phase AC versus 3-Phase AC; power output

There is one more practical reason to use a 3-phase AC system: Because the currents in each wire are shifted by 120°, the superposition of these currents is - under ideal conditions - always zero. In other words; if one wire is powering the load, the other wires will form the return path for the current, see figure A.3. A 3-phase system would - therefore - in principle need only three wires to operate. However, in practice four wires are often used to enable a return path if the wires are out of sync. In conclusion, AC power distribution requires three or four wires, while DC power distribution only requires two wires. AC distribution cables will thus be heavier and more expensive.

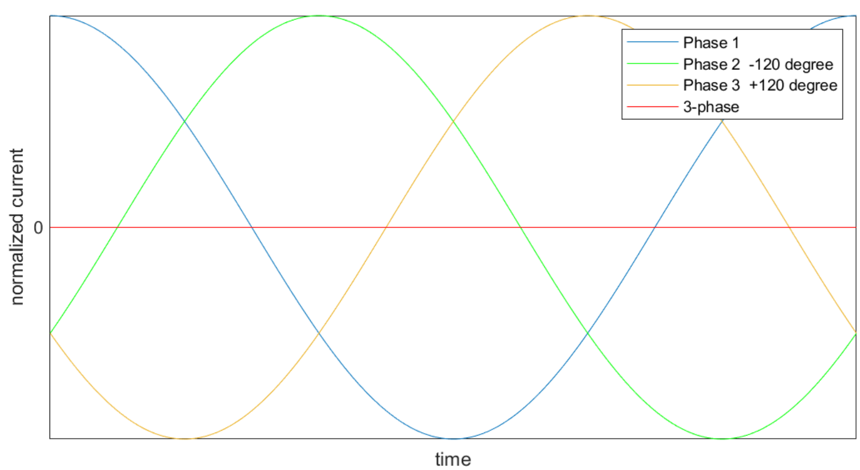

Figure A.3: Single phase AC versus 3-Phase AC; current output

Drawbacks of DC power distribution

One drawback of DC power is in the system protection. Both DC and AC systems are protected by mechanical system breakers. If the system does not operate within the design specifications (eg. high currents), the system breakers will open the system and stop the current flow to protect the system.

In AC systems this will be done as close as possible to the *zero voltage crossing*. At this point, there is little to no current flowing and the breaker can open without much heat generation. In DC systems, the voltage - and therefore - the current are not periodic (see figures A.4a and A.4b). Therefore there will never be a moment when the breakers can open when there is no voltage. Opening the circuit will result in a large charge build up in the breaker, the voltage on the breaker will then rise to the voltage of the source. If the voltage is large and the distance between the breaker and the circuit is not too large, the breaker could discharge using the circuit by ionizing the surrounding air. These arcs generate a lot of heat and could - in the worst case - make the breakers catch fire.

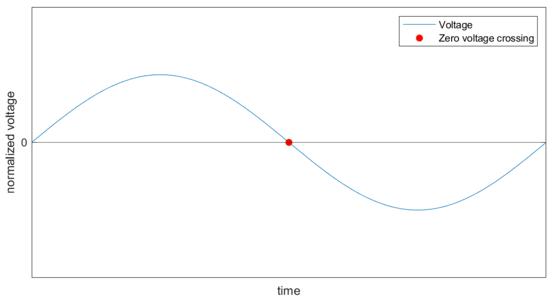

(a) Voltage in AC power flow

(b) Voltage in DC power flow

Appendix B: The power-induced voltage problem

The main challenge in trolley grids is the power induced voltage problem.

To move a trolleybus along a section, the substation has to provide power. If only one bus is on the section, this can be illustrated with the equivalent circuit shown in figure B.1.

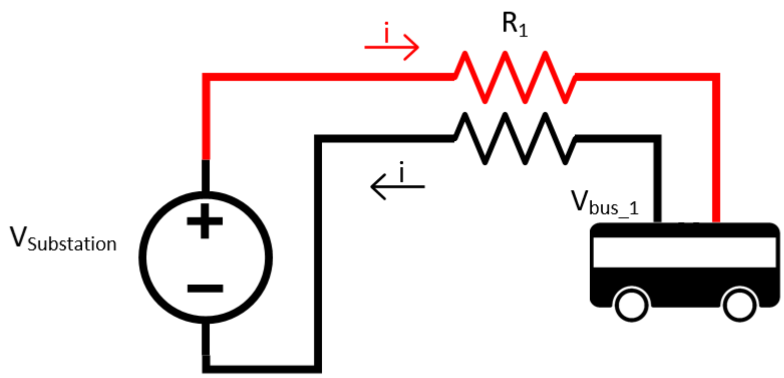

Figure B.1: Equivalent circuit with one bus

Here the line is modelled as a resistance, this assumption is valid because the reactive part of the impedance is negligible. The electric power demanded by the bus can be expressed as follows:

$$P_{\text{bus}} = I_{\text{bus}} * \Delta V_{\text{bus}} \tag{B.1}$$

Where I_{bus} is the current flowing from the substation to the bus and ΔV_{bus} is the voltage drop across the bus. By considering Ohm's law, ΔV_{bus} can be equivalently be written as:

$$\Delta V_{\text{bus}} = V_{\text{substation}} - I_{\text{bus}} * 2R_{\text{line}} \tag{B.2}$$

R_{line} can be rewritten as:

$$R_{\text{line}} = \rho * \frac{l}{A} \tag{B.3}$$

Where ρ is the resistivity of the line in ohm times meters is the line length in meters and A is the cross-sectional area of the wires in meters squared. From this relation, it is obvious that the resistance of the line is proportional to the length of the line. If we then substitute equation B.3 into equation B.2 we get:

$$\Delta V_{\text{bus}} = V_{\text{substation}} - I_{\text{bus}} * 2(\rho * \frac{l}{A}) \tag{B.4}$$

From this equation it can be concluded that the voltage drop across the bus depends *linearly* on the current to the bus and the distance that this current needs to travel to reach the bus. Since the voltage is low (700Vdc) and the power can be high (300kW for a single bus), the current can spike. This results in large voltage drops. Therefore acceleration of a bus far from the substation yield the worst-case scenario for a section with a single bus. If multiple buses are on the same section at the same time the voltage drop would be worse, see figure B.2 for the electrical representation of a section with n buses.

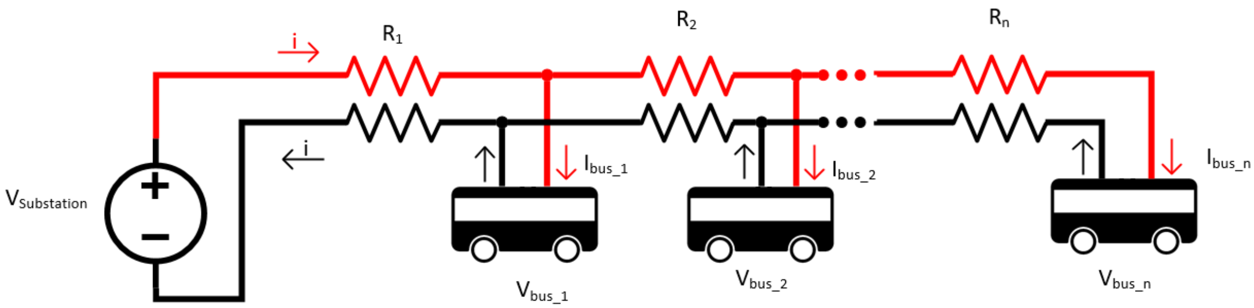

Figure B.2: Equivalent circuit with n buses

The voltage across the n'ed bus can be expressed as:

$$V_{\mathrm{bus_n}} = V_{\mathrm{substation}} - 2[\sum_{i=1}^{n} I_{\mathrm{bus_i}} R_1 + \sum_{i=2}^{n} I_{\mathrm{bus_i}} R_2 + ... + I_{\mathrm{bus_n}} R_n] \tag{B.5}$$

To accentuate the significance of the voltage drop in the overhead lines, an example from the Arnhem trolleybus grid is illustrated in figure B.3. The average voltage on this section is around 660V, however it was found that the voltage drops to 525V during measurements on this particular section. The power to the buses is limited when the voltage on the line drops below 500V. In a report by Liandon it was found that this happened multiple times in the trolley bus grid of Arnhem, the Netherlands. [63].

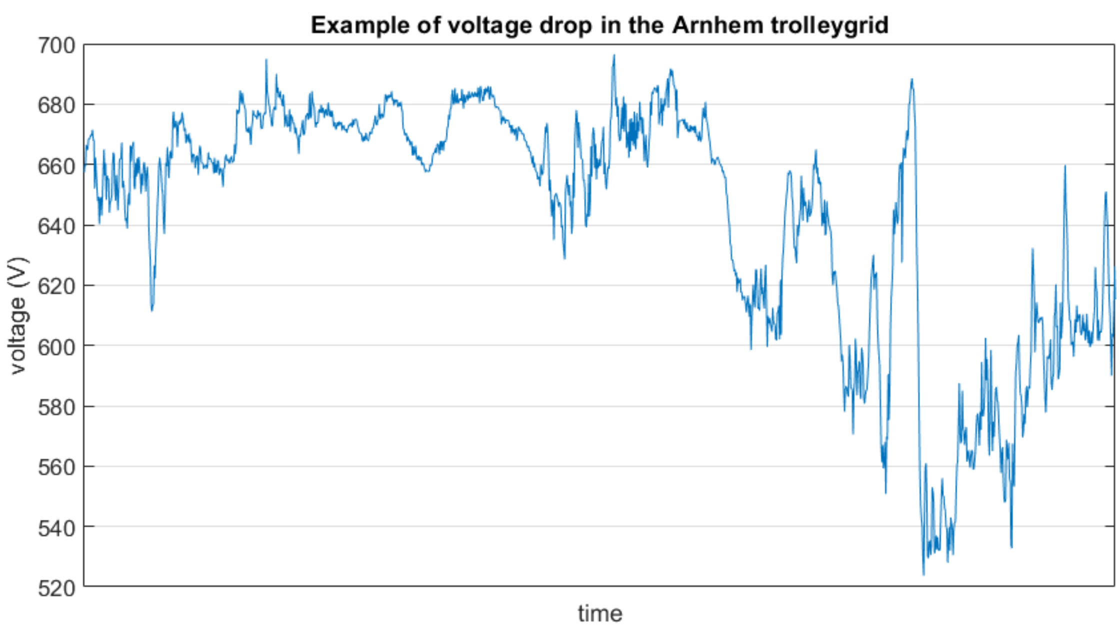

Figure B.3: Voltage drop example from Arnhem trolley grid - with kind permission of Arnhem University of Applied Sciences

Now that it is clear that large voltage drops do occur it is essential to explain why this is important. Large voltage drops could give problems for the grid for various reasons:

1. Large losses, due to the large currents.

2. Low voltage transmission requires high currents; these could exceed the maximum current of the overhead lines. This forces the circuit breakers to break the circuit until the current is reduced.

3. Problems with voltage operation range of the DC/DC converter for other grid applications.

Appendix C: Section lengths Arnhem

In this appendix the section lengths for the Arnhem grid are presented. These lengths are obtained by measuring the bus routes - in both directions - using the measurement tool of Google Maps. The lengths are used to divide the buses from each line into the individual sections.

INSTRUCTIONS **Relative numbers** are the lengths of the sections on the route
Absolute numbers are the absolute lengths of the sections
X0 is the starting point of the section

Xs is the feed-in-point of the section - if this value is orange then the feed-in-point is not in-line with the bus route on that section (eg. For section 7 the feed-in-point is not on route). The location of this feed-in-point is determined by looking at where the bus enters the section

X1 is the end point of the section
Bus location is where the bus starts on the first section and stops at the last section (sometimes the sections are longer than where the bus starts/stops, this is not the case of line 1)
Vs is the voltage of the substation
Voeding is the feed-in-point number
Substation is the substation number
Start tells you the location where the buses start
Stop tells you the location where the buses stop
Split at tells you at which point the section splits (for the main bus route and the feed-in-point) (eg. For Section 7 this is 200m coming from oosterbeek and

Line 1 - Velp to Oosterbeek

RELATIVE			ABSOLUTE								
X0	**Xs**	**X1**	**X0**	**Xs**	**X1**	**Bus location**	**Vs**	**Voeding**	**Substation**	**Points on route**	
0	277	1579	0	277	1579	1579	716	22	10	**starts**	**0**
1580	2760	2819	0	1180	1239	2819	700	18	5		
2820	2860	3809	0	40	989	3809	700	17	5		
3810	3950	4679	0	140	869	4679	698	16	2		
4680	5760	5789	0	1080	1109	5789	630	12	3	**Split at**	**900**
5790	6220	6239	0	430	449	6239	660	6	4		
6240	6390	7179	0	150	939	7179	660	5	4		
7180	8030	8119	0	850	939	8119	698	3	1		
8120	8200	9389	0	80	1269	9389	698	2	1		
9390	10160	10199	0	770	809	10199	686	23	12		
10200	10260	11700	0	60	1499	11650	686	24	12	**final stop**	**11650**

Line 1 - Oosterbeek to Velp

RELATIVE			ABSOLUTE								
X0	**Xs**	**X1**	**X0**	**Xs**	**X1**	**Bus location**	**Vs**	**Voeding**	**Substation**	**Points on route**	
0	1310	1390	0	1310	1390	1390	686	24	12	**starts**	**0**
1391	1471	2241	0	80	850	2241	686	23	12		
2242	3452	3542	0	1210	1300	3542	698	2	1		
3543	3618	4423	0	75	880	4423	698	3	1		
4424	5144	5434	0	720	1010	5434	660	5	4		
5435	5465	5915	0	30	480	5915	660	6	4		
5916	6256	7016	0	340	1100	7016	630	12	3	**split at**	**200**
7017	7737	7917	0	720	900	7917	698	16	2		
7918	8868	8948	0	950	1030	8948	700	17	5		
8949	8999	10129	0	50	1180	10129	700	18	5		
10130	11560	11720	0	1430	1590	11660	716	22	10	**final stop**	**11660**

Line 2 - Arnhem Central to Zuid-Laren

RELATIVE			ABSOLUTE								
X0	**Xs**	**X1**	**X0**	**Xs**	**X1**	**Bus location**	**Vs**	**Voeding**	**Substation**	**Points on route**	
0	60	260	0	60	260	260	685	5	4	**starts**	**0**
261	1000	709	0	19	449	709	685	6	4		
710	1760	1109	0	360	400	1109	630	12	3		
1110	1608	1827	0	498	718	1827	660	9	6		
1828	?	2687	0	?	860	2687	660	9	3		
2688	3721	3907	0	160	1220	3907	630	36	3		
4614	5653	4408	0	1160	501	4408	628	41	14	**split at**	**230**
5124	6253	5602	0	1129	1194	5602	705	42	16		
6324	6373	6320	0	49	718	6320	705	43	16		
7044	7053	7998	0	9	1678	7998	?	48	?		
8724	9873	9186	0	1149	1188	8436	659	31	11	**final stop**	**8436**

Line 2 - Zuid-Laren to Arnhem Central

RELATIVE			ABSOLUTE								
X0	**Xs**	**X1**	**X0**	**Xs**	**X1**	**Bus location**	**Vs**	**Voeding**	**Substation**	**Points on route**	
0	100	1360	0	100	1360	605	659	31	11	**starts**	**755**
1361	2941	3001	0	1580	1640	2246	?	48	?		
3002	3642	3737	0	640	735	2982	705	43	16		
3738	3813	4918	0	75	1180	4163	705	42	16		
4919	6119	5469	0	1200	550	4714	628	41	14	**split at**	**320**
5470	6450	6670	0	980	1200	5915	630	36	3		
6671	?	7491	0	?	820	6736	660	9	3		
7492	7672	8212	0	180	720	7457	660	9	6		
8213	8288	8628	0	75	415	7873	630	12	3		
8629	9004	9084	0	375	455	8329	685	6	4		
9085	9485	9370	0	400	285	8514	685	5	4	**final stop**	**9269**

Line 3 - Burgers' Zoo - Duifje										
RELATIVE			**ABSOLUTE**							
X0	**Xs**	**X1**	**X0**	**Xs**	**X1**	**Bus location**	**Vs**	**Voeding**	**Substation**	**Points on route**
0	1460	1580	0	1460	1580	1580	700	19	8	**starts 0**
1581	2470	3240	0	840	1659	3240	700	13	8	
3241	4500	4670	0	50	1320	4670	698	14	2	
4671	4721	4771	0	50	100	4771	698	8	4	
4772	5022	4950	0	250	320	4950	698	6	4	
4951	5281	5360	0	330	660	5360	698	5	4	
5361	5431	5801	0	70	440	5801	698	6	4	
5802	6202	6262	0	400	460	6262	630	12	3	
6263	6728	6940	0	465	677	6940	660	9	6	
6941	?	7801	0	?	860	7801	660	?	?	
7802	7962	8582	0	160	780	8582	630	36	3	
8583	9383	9533	0	800	950	9533	724	20	7	
9534	9584	10594	0	50	1060	10594	724	21	7	**final stop 10594**

Line 3 - Duifje - Burgers' Zoo										
RELATIVE			**ABSOLUTE**							
X0	**Xs**	**X1**	**X0**	**Xs**	**X1**	**Bus location**	**Vs**	**Voeding**	**Substation**	**Points on route**
0	120	1000	0	970	1000	1000	724	21	7	**starts 0**
1001	2351	1961	0	190	960	1961	724	20	7	
1962	3411	2402	0	240	440	2402	630	36	3	
2403	4721	3223	0	?	820	3223	660			
3224	4700	3944	0	180	720	3944	660	9	6	
3945	5030	5125	0	75	1180	5125	630	12	3	
5126	5731	5581	0	375	455	5581	685	6	4	
5582	5862	6252	0	400	670	6252	698	5	4	
6253	6475	6553	0	50	300	6553	698	6	4	
6554	6634	6704	0	80	150	6704	698	8	4	
6554	8422	7814	0	1240	1260	7814	698	14	2	
7815	8733	9485	0	785	1670	9485	700	13	8	
9486	10544	10746	0	150	1260	10745	700	13	8	**final stop 10745**

Line 5 -Schuyfgraaf - Presikchaaf (via centraalspoor)										
RELATIVE			**ABSOLUTE**							
X0	**Xs**	**X1**	**X0**	**Xs**	**X1**	**Bus location**	**Vs**	**Voeding**	**Substation**	**Strange points on rout**
0	60	1240	0	60	1240	380	700	45	18	**starts 860**
1241	2170	2200	0	929	959	1340	696	46	19	
2201	2250	3490	0	49	1289	2630	698	47	19	
3491	4790	4090	0	1299	599	3230	700	44	18	**split at 60**
4091	4960	4980	0	869	889	4120	659	30	11	**split at 430**
4981	6030	6050	0	1049	1069	5190	673	29	13	
6051	6090	7020	0	39	969	6160	673	28	13	
7021	8010	8030	0	989	1009	7170	628	27	14	
8031	8130	9150	0	99	1119	8290	628	26	14	
9151	9930	9970	0	779	819	9110	677	25	9	
9971	10150	10540	0	330	520	9680	685	5	4	
10541	10570	11010	0	29	469	10150	685	6	4	
11011	11350	11390	0	339	379	10530	630	12	3	
11391	11930	12250	0	539	859	11390	660	9	6	
12251	12290	13310	0	39	1059	12450	660	32	6	
13311	14370	14420	0	1059	1109	13560	684	33	15	
14421	14470	15050	0	49	629	14190	684	34	15	
15051	14451	16400	0	-600	1349	15370	684	34	15	**final stop 16230**

Line 5 - Presikchaaf - Schuyfgraaf (via koningskers)										
RELATIVE			**ABSOLUTE**							
X0	**Xs**	**X1**	**X0**	**Xs**	**X1**	**Bus location**	**Vs**	**Voeding**	**Substation**	**Points on route**
0	1800	1200	0	1800	1200	1080	684	34	15	**starts 120**
1201	1701	1801	0	500	600	1681	684	34	15	
1802	1852	2942	0	50	1140	2822	684	33	15	
2943	3953	4003	0	1010	1060	3883	660	32	6	
4004	4474	4684	0	470	680	4564	660	9	6	**split at 300**
4685	4760	5105	0	75	420	4985	630	12	3	
5106	5481	5561	0	375	455	5441	685	6	4	
5562	5862	6092	0	300	530	5972	685	5	4	
6093	6168	7073	0	75	980	6953	677	25	9	
7074	7824	8074	0	750	1000	7954	628	26	14	
8075	8135	9075	0	60	1000	8955	628	27	14	
9076	9906	9966	0	830	890	9846	673	28	13	
9967	10017	11067	0	50	1100	10947	673	29	13	
11068	11958	11938	0	890	870	11818	659	30	11	**split at 430**
11939	13259	13339	0	1320	1400	13219	700	44	18	
13340	13460	14560	0	120	1220	14059	700	45	18	**final stop: 14179**

We have no measured data from HAN for these routes

Line 5 -Schuyfgraaf - Presikchaaf (via koningskers)										
RELATIVE			**ABSOLUTE**							
X0	**Xs**	**X1**	**X0**	**Xs**	**X1**	**Bus location**	**Vs**	**Voeding**	**Substation**	**Strange points on rout**
0	60	1220	0	60	1220	850	700	45	18	**starts 370**
1221	2170	2700	0	929	1480	2330	696	44	19	
2701	4960	3589	0	869	889	3219	659	30	11	**split at 430**
3590	6030	4658	0	1049	1069	4288	673	29	13	
4659	6090	5627	0	39	969	5257	673	28	13	
5628	8010	6636	0	989	1009	6266	628	27	14	
6637	8130	7755	0	99	1119	7385	628	26	14	
7756	9930	8574	0	779	819	8204	677	25	9	
8575	10150	9094	0	330	520	8724	685	5	4	
9095	10570	9563	0	29	469	9193	685	6	4	
9564	11350	9942	0	339	379	9572	630	12	3	
9943	11930	10801	0	539	859	10431	660	9	6	**split at 500**
10802	12290	11860	0	39	1059	11490	660	32	6	
11861	14370	12969	0	1059	1109	12599	684	33	15	
12970	13019	13598	0	-1402	629	13228	684	34	15	
13599	?	14947	0	?	1349	14407	684	34	15	**final stop 14777**

Line 5 - Presikchaaf - Schuyfgraaf (via centraalspoor)										
RELATIVE			**ABSOLUTE**							
X0	**Xs**	**X1**	**X0**	**Xs**	**X1**	**Bus location**	**Vs**	**Voeding**	**Substation**	
0	?	1200	0	?	1200	1080	684	34	15	**starts 120**
1201	1701	1800	0	500	600	1680	684	34	15	
1801	1851	2940	0	50	1140	2820	684	33	15	
2941	3951	4000	0	1010	1060	3880	660	32	6	
4001	4471	4680	0	470	680	4560	660	9	6	**split at 300**
4681	4756	5100	0	75	420	4980	630	12	3	
5101	5476	5555	0	375	455	5435	685	6	4	
5556	5856	6085	0	300	530	5965	685	5	4	
6086	6161	7065	0	75	980	6945	677	25	9	
7066	7816	8065	0	750	1000	7945	628	26	14	
8066	8126	9065	0	60	1000	8945	628	27	14	
9066	9896	9955	0	830	890	9835	673	28	13	
9956	10006	11055	0	50	1100	10935	673	29	13	
11056	11946	11925	0	890	870	11805	659	30	11	**split at 430**
11926	13225	12524	0	1299	599	12404	700	44	18	
12525	13765	13813	0	1240	1289	13693	700	47	18	
13814	13844	14772	0	30	959	14652		46		
14773	15953	16061	0	1180	1289	15012		45		**final stop 15132**

We have no measured data from HAN for these routes

Line 5 -Schuyfgraaf - Presikchaaf (via koningskers)										
RELATIVE			**ABSOLUTE**							
X0	**Xs**	**X1**	**X0**	**Xs**	**X1**	**Bus location**	**Vs**	**Voeding**	**Substation**	**Strange points on rout**
0	60	1220	0	60	1220	850	700	45	18	**starts 370**
1221	2170	2700	0	929	1480	2330	696	44	19	
2701	4960	3589	0	869	889	3219	659	30	11	**split at 430**
3590	6030	4658	0	1049	1069	4288	673	29	13	
4659	6090	5627	0	39	969	5257	673	28	13	
5628	8010	6636	0	989	1009	6266	628	27	14	
6637	8130	7755	0	99	1119	7385	628	26	14	
7756	9930	8574	0	779	819	8204	677	25	9	
8575	10150	9094	0	330	520	8724	685	5	4	
9095	10570	9563	0	29	469	9193	685	6	4	
9564	11350	9942	0	339	379	9572	630	12	3	
9943	11930	10801	0	539	859	10431	660	9	6	**split at 500**
10802	12290	11860	0	39	1059	11490	660	32	6	
11861	14370	12969	0	1059	1109	12599	684	33	15	
12970	13019	13598	0	-1402	629	13228	684	34	15	
13599	?	14947	0	?	1349	14407	684	34	15	**final stop 14777**

Line 5 - Presikchaaf - Schuyfgraaf (via centraalspoor)										
RELATIVE			**ABSOLUTE**							
X0	**Xs**	**X1**	**X0**	**Xs**	**X1**	**Bus location**	**Vs**	**Voeding**	**Substation**	
0	?	1200	0	?	1200	1080	684	34	15	**starts 120**
1201	1701	1800	0	500	600	1680	684	34	15	
1801	1851	2940	0	50	1140	2820	684	33	15	
2941	3951	4000	0	1010	1060	3880	660	32	6	
4001	4471	4680	0	470	680	4560	660	9	6	**split at 300**
4681	4756	5100	0	75	420	4980	630	12	3	
5101	5476	5555	0	375	455	5435	685	6	4	
5556	5856	6085	0	300	530	5965	685	5	4	
6086	6161	7065	0	75	980	6945	677	25	9	
7066	7816	8065	0	750	1000	7945	628	26	14	
8066	8126	9065	0	60	1000	8945	628	27	14	
9066	9896	9955	0	830	890	9835	673	28	13	
9956	10006	11055	0	50	1100	10935	673	29	13	
11056	11946	11925	0	890	870	11805	659	30	11	**split at 430**
11926	13225	12524	0	1299	599	12404	700	44	18	
12525	13765	13813	0	1240	1289	13693	700	47	18	
13814	13844	14772	0	30	959	14652		46		
14773	15953	16061	0	1180	1289	15012		45		**final stop 15132**

Line 6 -De Laar-West - Elsweide

RELATIVE			ABSOLUTE								
X0	**Xs**	**X1**	**X0**	**Xs**	**X1**	**Bus location**	**Vs**	**Voeding**	**Substation**	**Points on Route**	
0	1810	1830	0	1810	1830	560	659	31	11	**starts**	**1270**
1831	1881	2781	0	50	950	1511	659	30	11		
2781	3870	3920	0	1089	1139	2650	673	29	13		
3921	3970	4780	0	49	859	3510	673	28	13		
4781	5810	5860	0	1029	1079	4590	628	27	14		
5861	5961	6800	0	100	939	5530	628	26	14		
6801	7720	7770	0	919	969	6500	677	25	9		
7771	8101	8291	0	330	520	7021	685	5	4		
8292	8342	8751	0	50	459	7481	685	6	4		
8752	9121	9171	0	369	419	7901	630	12	3		
9172	9722	10072	0	550	900	8802	660	9	6	**split at**	**430**
10073	10132	11132	0	59	1059	9862	660	32	6		
11133	12222	12272	0	1089	1139	11002	684	33	15		
12273	12323	12862	0	50	589	11592	684	34	15		
12863	13553	13553	0	690	690	12273	700	35	5	**final stop**	**13543**

Line 6 -Elsweide - De Laar-West

RELATIVE			ABSOLUTE								
X0	**Xs**	**X1**	**X0**	**Xs**	**X1**	**Bus location**	**Vs**	**Voeding**	**Substation**	**Points on route**	
0		700	0	0	700	520	700	35	5	**starts**	**180**
701	1221	1291	0	520	590	1111	684	34	15		
1292	1342	2432	0	50	1140	2252	684	33	15		
2433	3443	3493	0	1010	1060	3313	660	32	6		
3494	3964	4174	0	470	680	3994	660	9	6	**split at**	**300**
4175	4250	4595	0	75	420	4415	630	12	3		
4596	4971	5051	0	375	455	4871	685	6	4		
5052	5352	5582	0	300	530	5402	685	5	4		
5583	5658	6563	0	75	980	6383	677	25	9		
6564	7314	7564	0	750	1000	7384	628	26	14		
7565	7625	8565	0	60	1000	8385	628	27	14		
8566	9396	9456	0	830	890	9276	673	28	13		
9457	9507	10557	0	50	1100	10377	673	29	13		
10558	11448	11558	0	890	1000	11378	659	30	11		
11559	11609	12869	0	50	1310	12098	659	31	11	**final stop**	**12278**

Line 7 -Rijkerswoerd - Geitenkamp

RELATIVE			ABSOLUTE								
X0	**Xs**	**X1**	**X0**	**Xs**	**X1**	**Bus location**	**Vs**	**Voeding**	**Substation**	**Points on route**	
0	?	40	0	?	40	40	?	?	?	**starts**	**0**
41	1400	1430	0	1359	1389	1430	?	49	?		
1431	2040	2090	0	609	659	2090	705	43	16		
2091	2140	3310	0	49	1219	3310	705	42	16		
3311	4470	4520	0	1159	1209	4520	628	41	14		
4521	4780	4830	0	259	309	4830	628	27	14		
4831	4931	5770	0	100	939	5770	628	26	14		
5771	6690	6740	0	919	969	6740	677	25	9		
6741	7071	7261	0	330	520	7261	685	5	4		
7262	7312	7721	0	50	459	7721	685	6	4		
7722	8091	8822	0	369	1100	8822	630	12	3	**split at**	**200**
8823	9563	9543	0	740	720	9543	698	16	2	**split at**	**580**
9544	10019	10664	0	475	1120	10664	698	15	2		
10665	11715	11795	0	1050	1130	11795	728	39	17		
11796	11836	12716	0	40	920	12716	728	40	17	**final stop**	**12716**

Line 7 - Geitenkamp - Rijkerswoerd

RELATIVE			ABSOLUTE								
X0	**Xs**	**X1**	**X0**	**Xs**	**X1**	**Bus location**	**Vs**	**Voeding**	**Substation**	**Points on route**	
0		800	0	700	800	800		40	17	**starts**	**0**
801	861	1951	0	60	1150	1951		39	17		
1952	2582	3032	0	630	1080	3032		15	2		
3033	3233	3783	0	200	750	3783		16	2	**split at**	**100**
3784	4864	4893	0	1080	1109	4893	630	12	3	**split at**	**900**
4894	5324	5343	0	430	449	5343	660	6	4		
5344	5644	5844	0	300	500	5844		5	4		
5845	5945	6705	0	100	860	6705		25	9		
6706	7456	7706	0	750	1000	7706	628	26	14		
7707	7837	8007	0	130	300	8007		27	14		
8008	8118	9318	0	110	1310	9318		41	14		
9319	10448	10513	0	1129	1194	10513	705	42	16		
10514	10563	11232	0	49	718	11232	705	43	16		
11233	11273	12613	0	40	1380	12613	?	49	?		
12614	?	12739	0	?	125	12648	?	?	?	**final stop**	**12648**

Appendix D: Bus traffic for all bus schedules

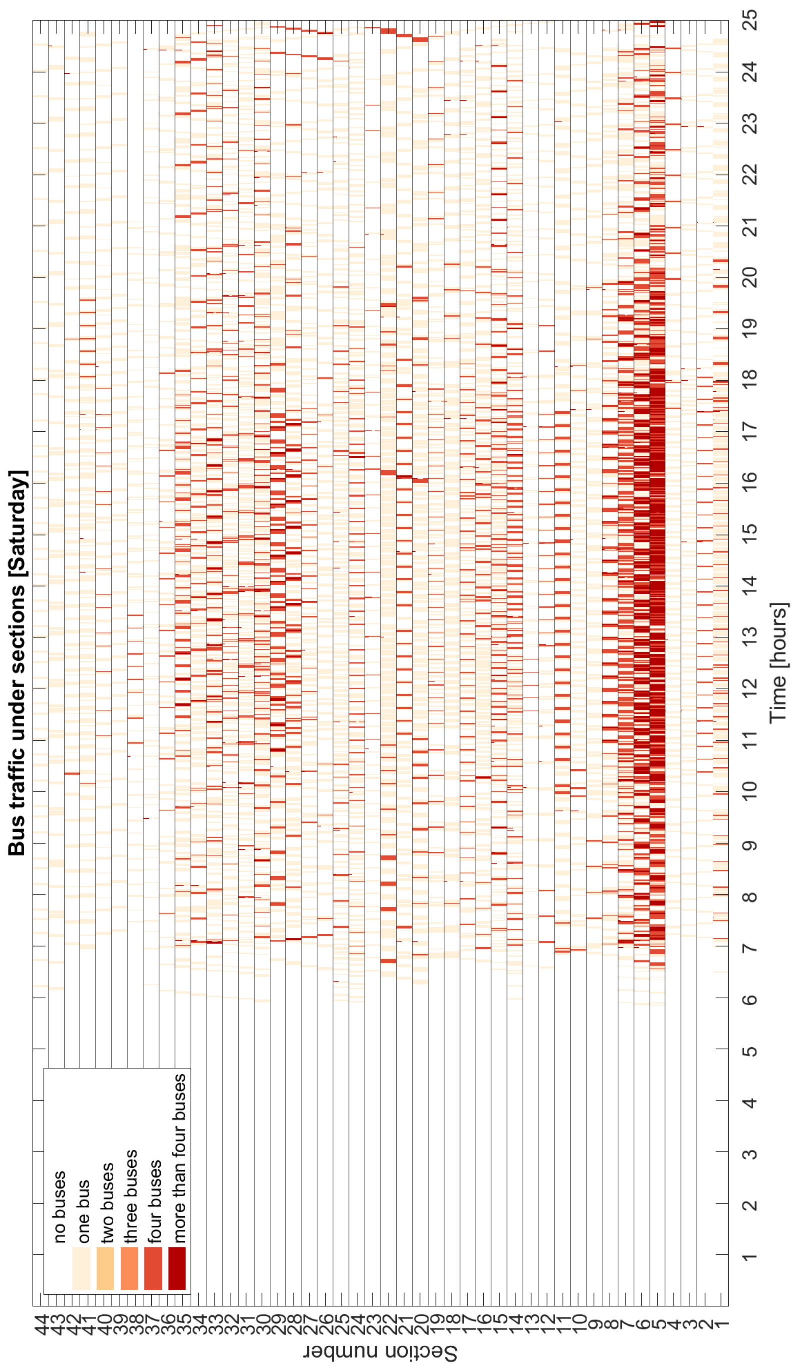
Bus traffic under sections [Saturday]
no buses
one bus
two buses
three buses
four buses
more than four buses
Section number
Time [hours]

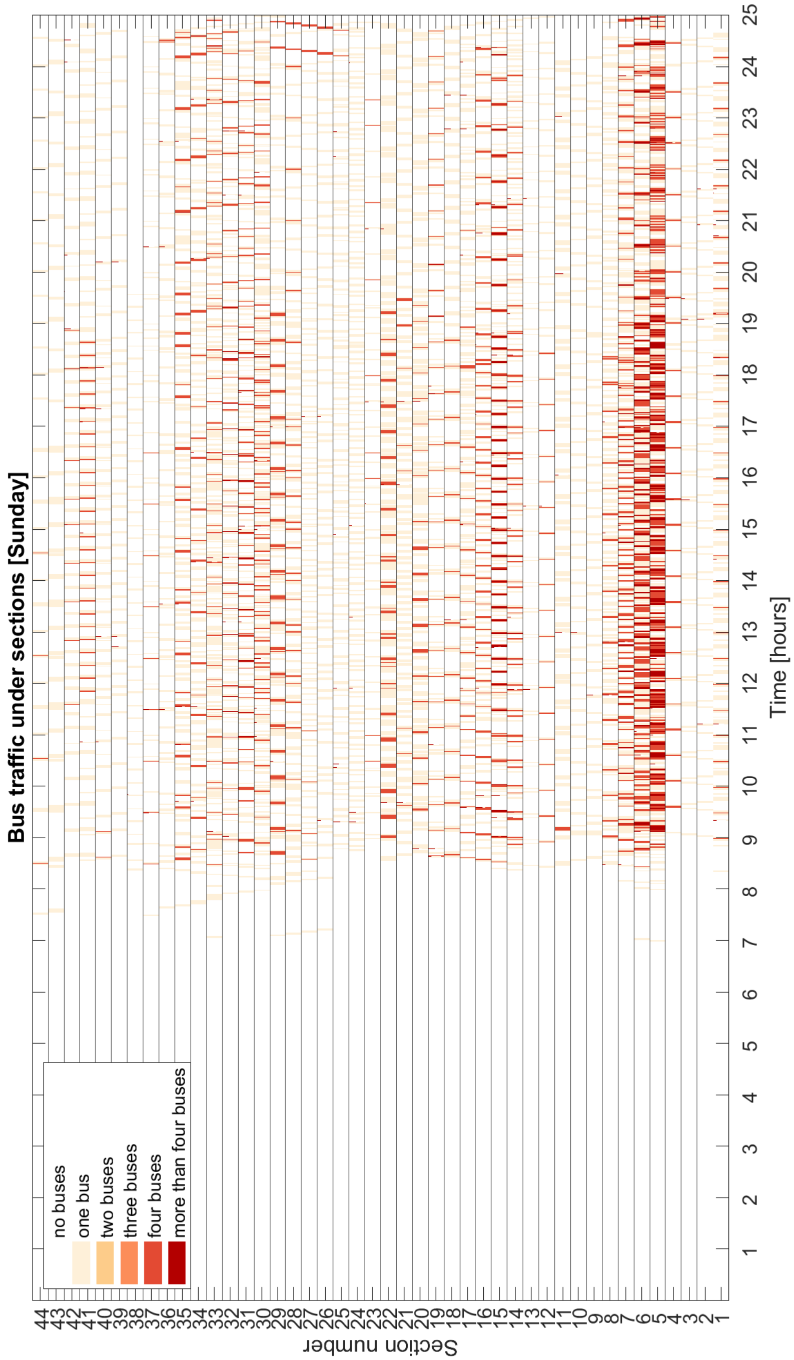

Bus traffic under sections [Sunday]
no buses
one bus
two buses
three buses
four buses
more than four buses
Section number
Time [hours]

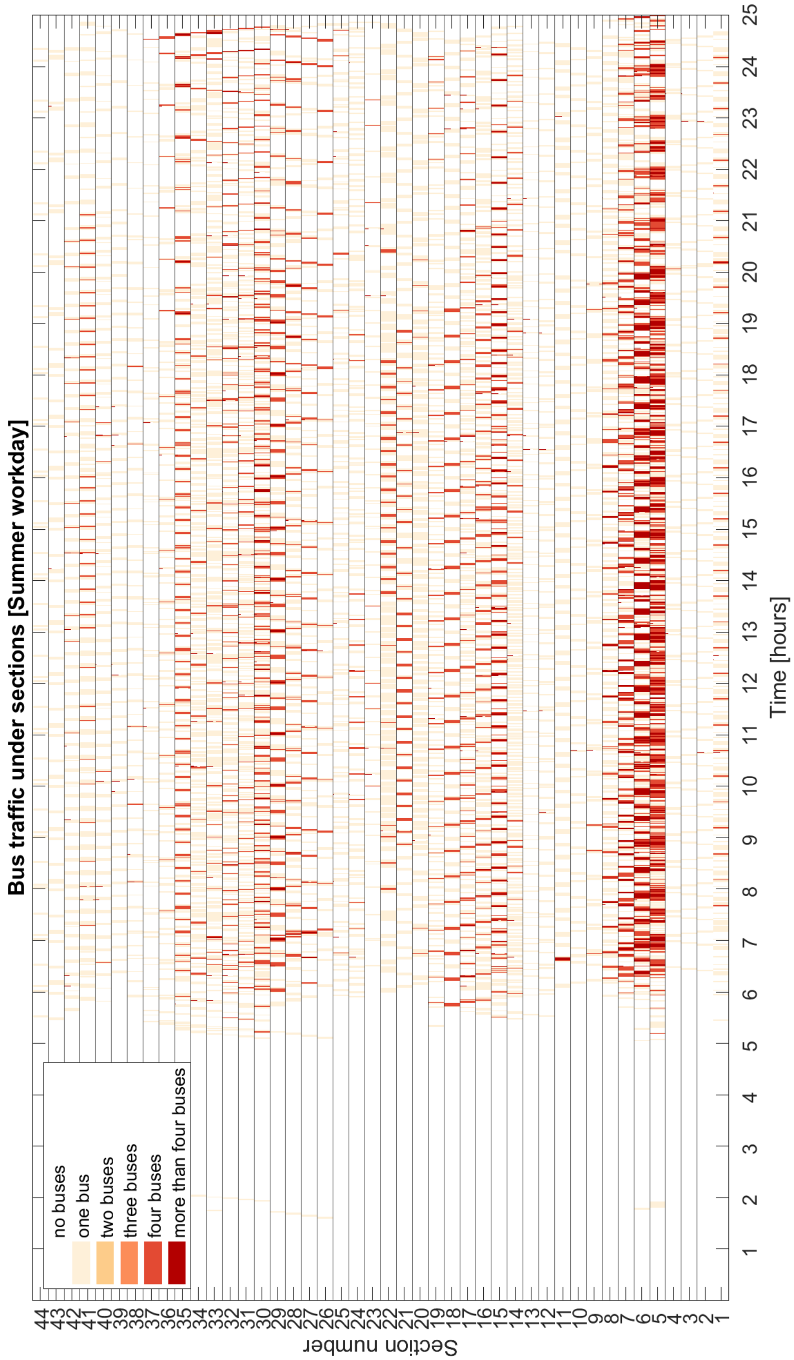

Bus traffic under sections [Summer workday]
Section number
Time [hours]
no buses
one bus
two buses
three buses
four buses
more than four buses

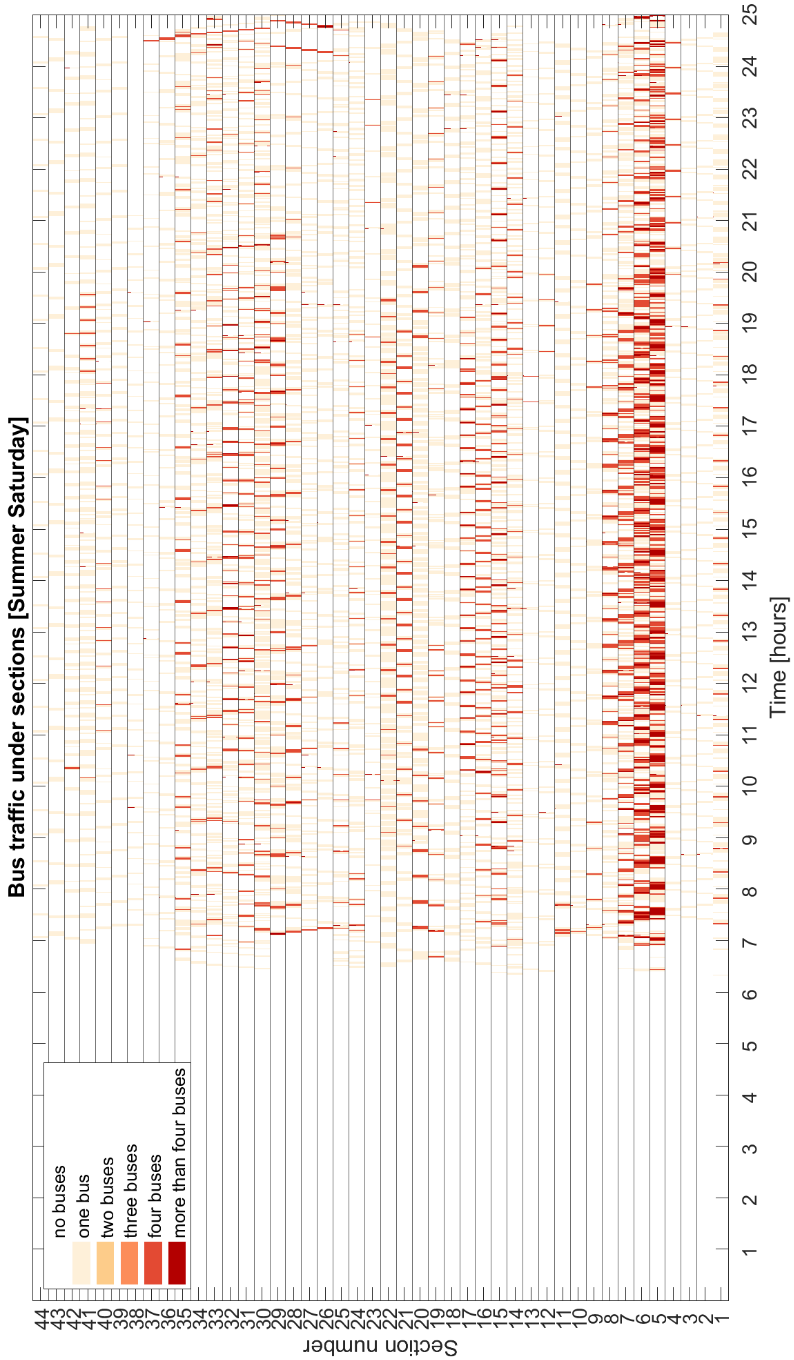

Bus traffic under sections [Summer Saturday]
no buses
one bus
two buses
three buses
four buses
more than four buses
Section number
Time [hours]

Appendix E: Load profiles of sections and substations

These power profiles are important, because they are used for the sizing of the PV. Later on, when the PV is sized, the degree of utilization of the PV will be investigated on the basis of these power profiles. Moreover, the power profiles could show unexpected behaviour on the substations, which would indicate that there are errors in the model.

E.1 Section power profiles

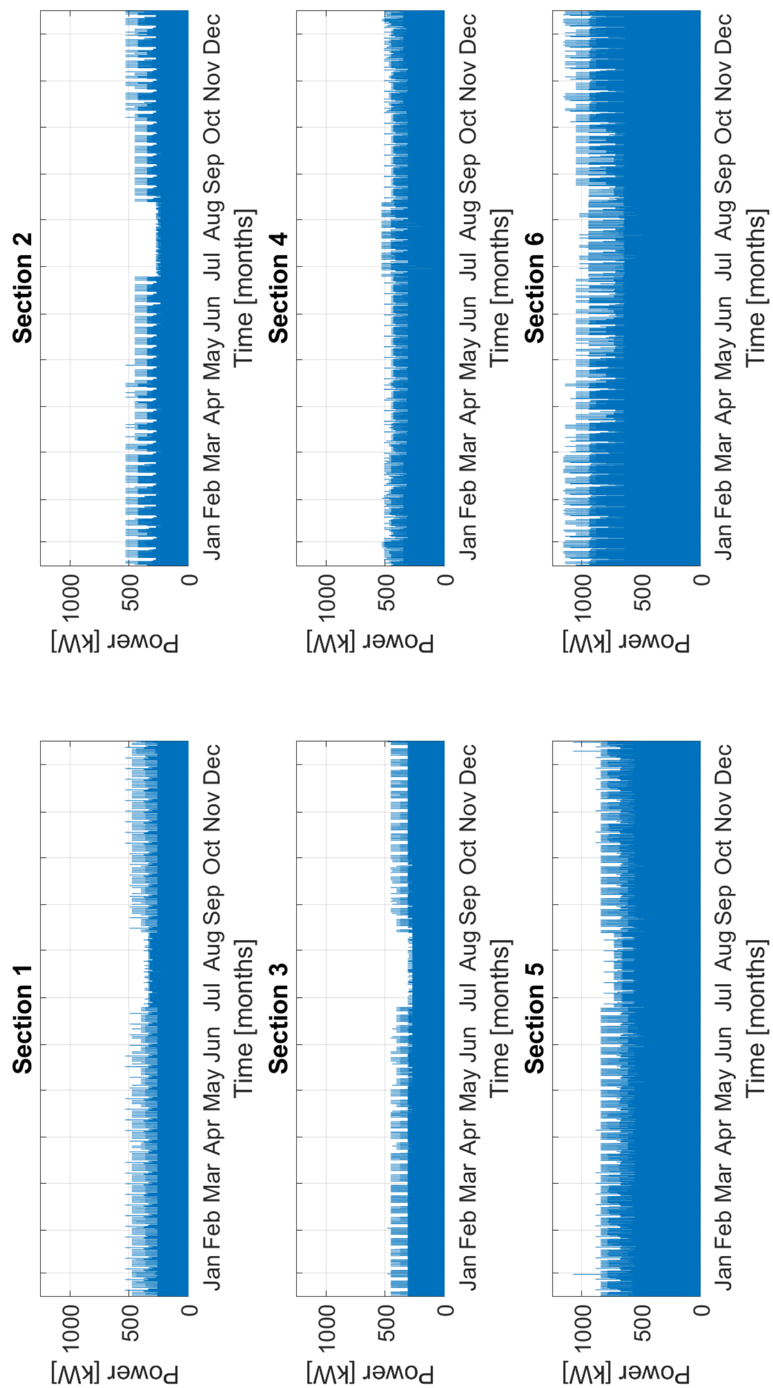
Section 1
Section 2
Section 3
Section 4
Section 5
Section 6
Power [kW]
0
500
1000
Jan Feb Mar Apr May Jun Jul Aug Sep Oct Nov Dec
Time [months]

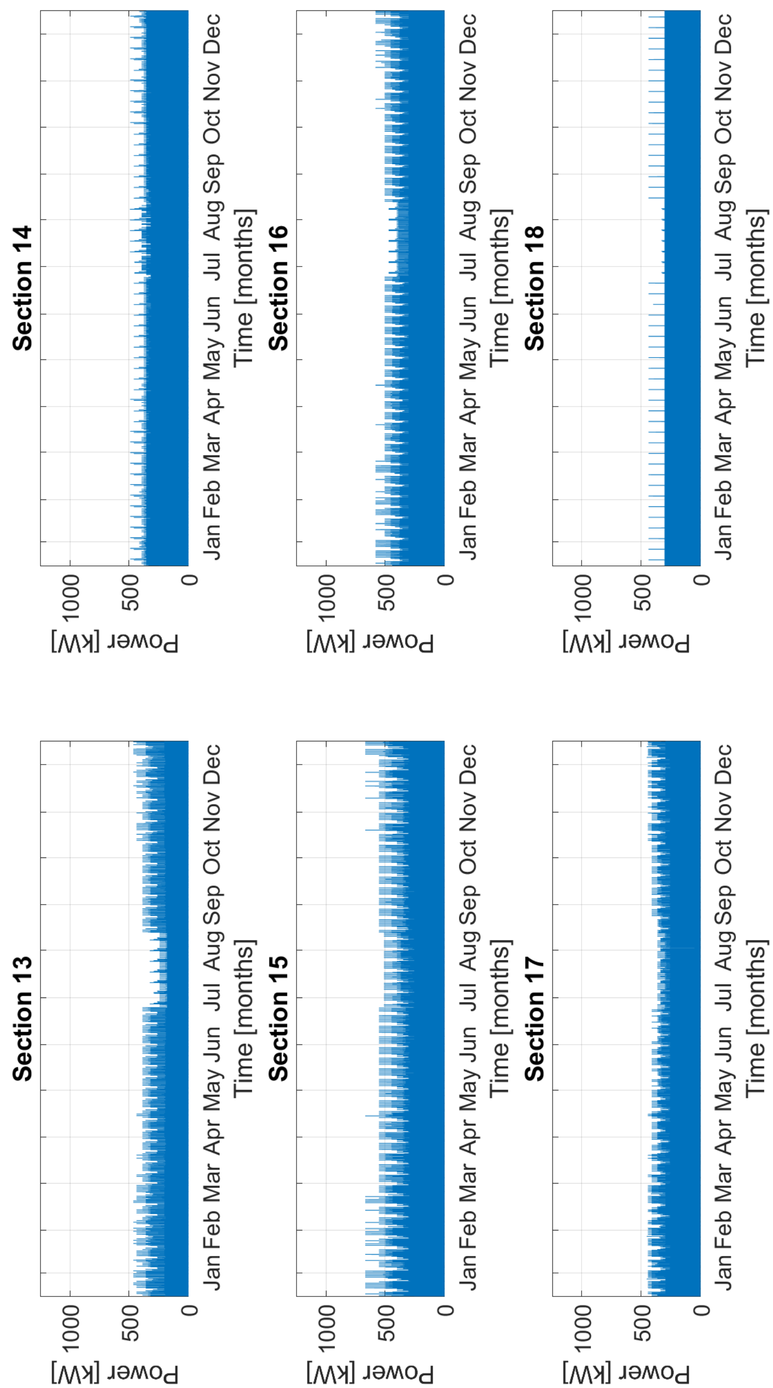
Section 13
Section 14
Section 15
Section 16
Section 17
Section 18
Power [kW]
Time [months]
Jan Feb Mar Apr May Jun Jul Aug Sep Oct Nov Dec

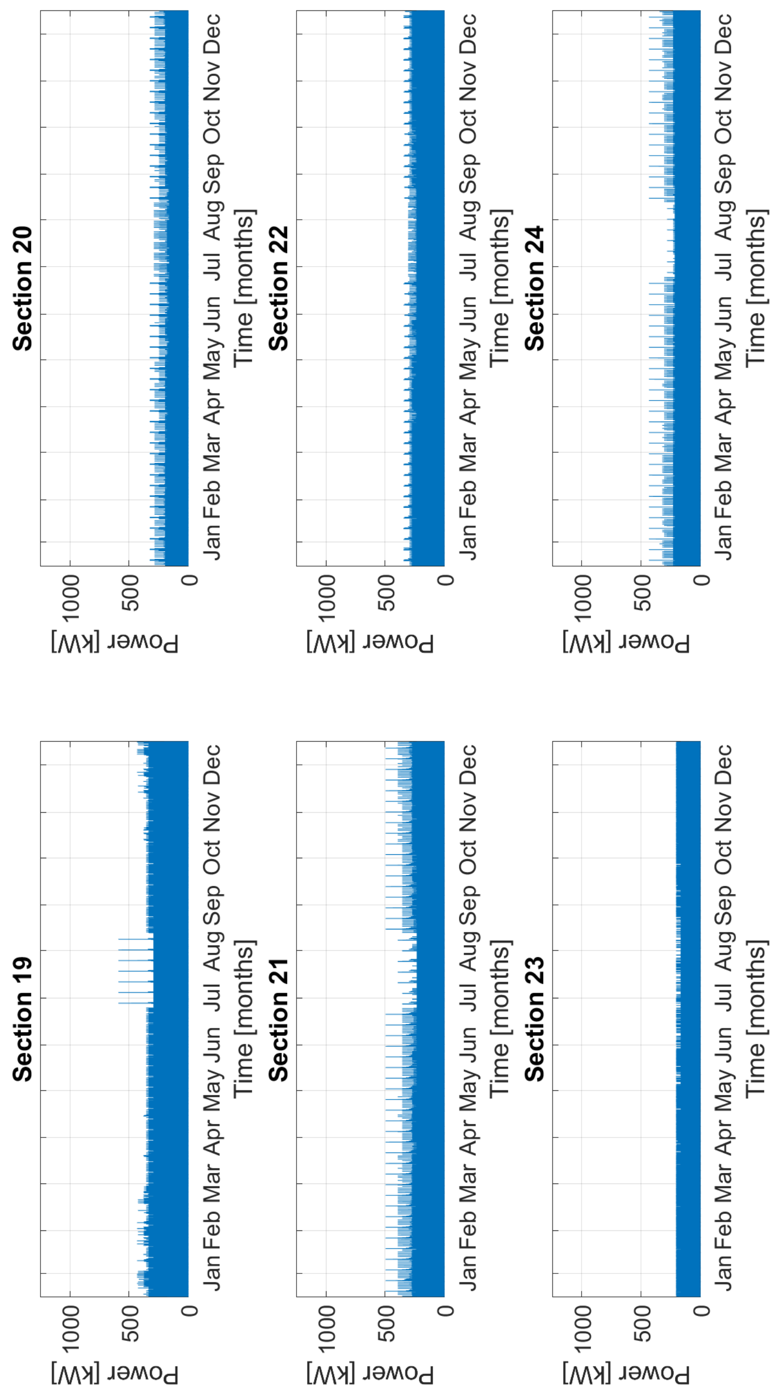
Section 19
Section 20
Section 21
Section 22
Section 23
Section 24
Power [kW]
1000
500
0
Jan Feb Mar Apr May Jun Jul Aug Sep Oct Nov Dec
Time [months]

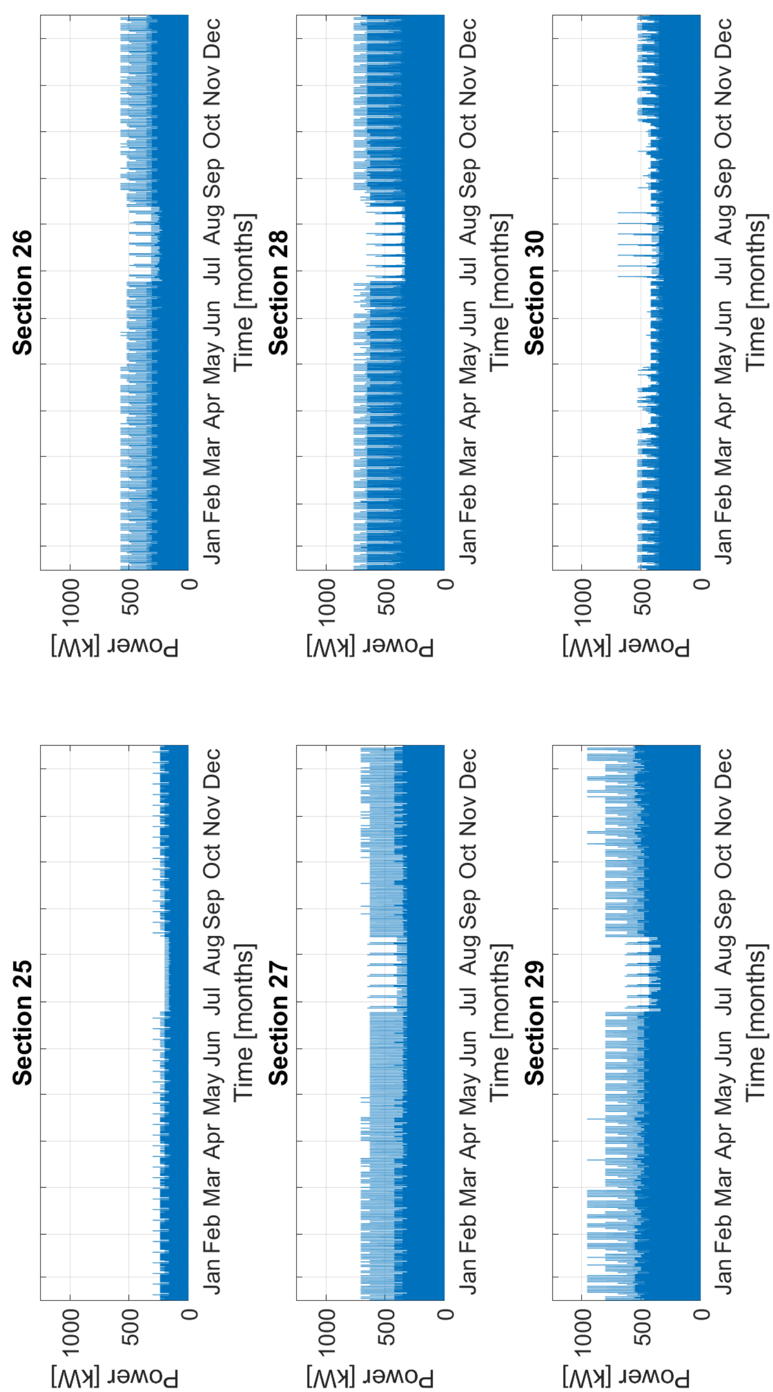
Section 25
Section 26
Section 27
Section 28
Section 29
Section 30
Power [kW]
1000
500
0
Jan Feb Mar Apr May Jun Jul Aug Sep Oct Nov Dec
Time [months]

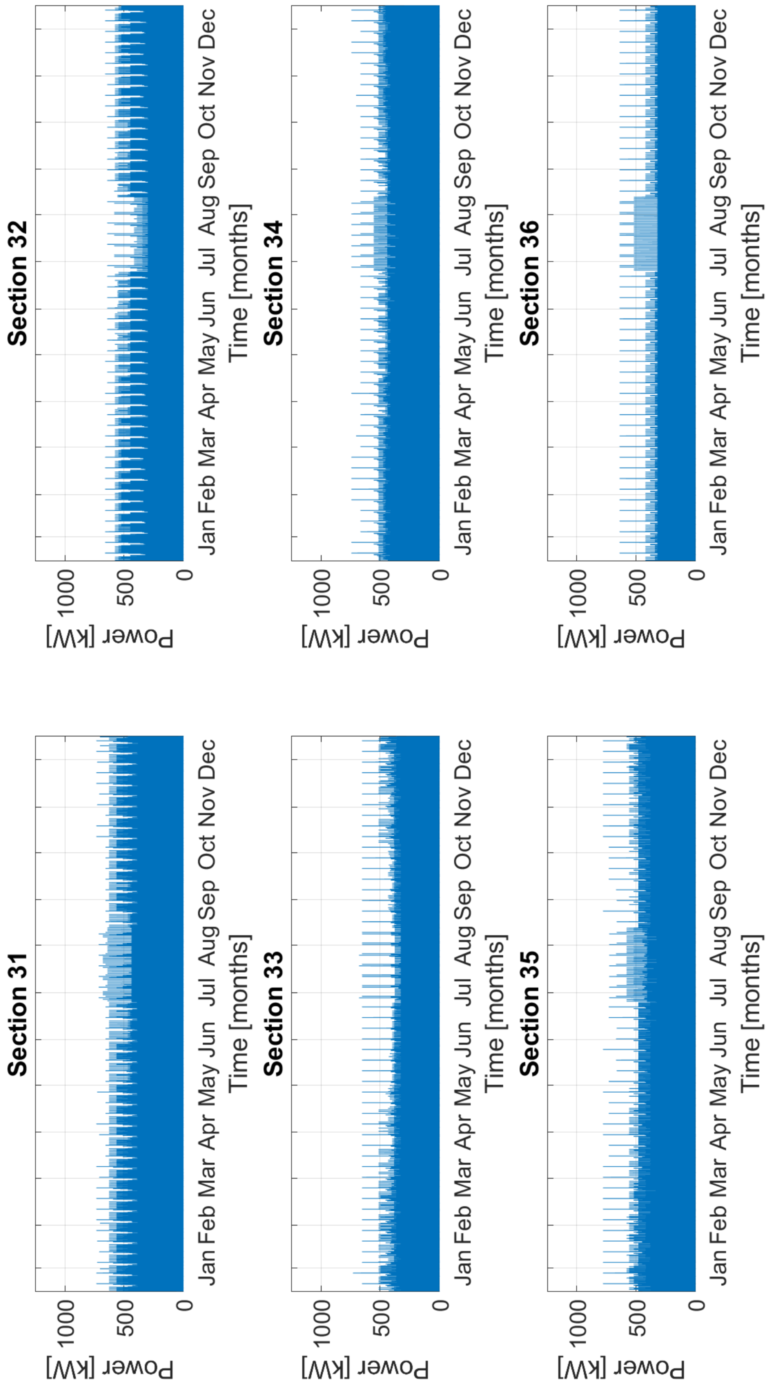

Section 31
Section 32
Section 33
Section 34
Section 35
Section 36
Power [kW]
1000
500
0
Jan Feb Mar Apr May Jun Jul Aug Sep Oct Nov Dec
Time [months]

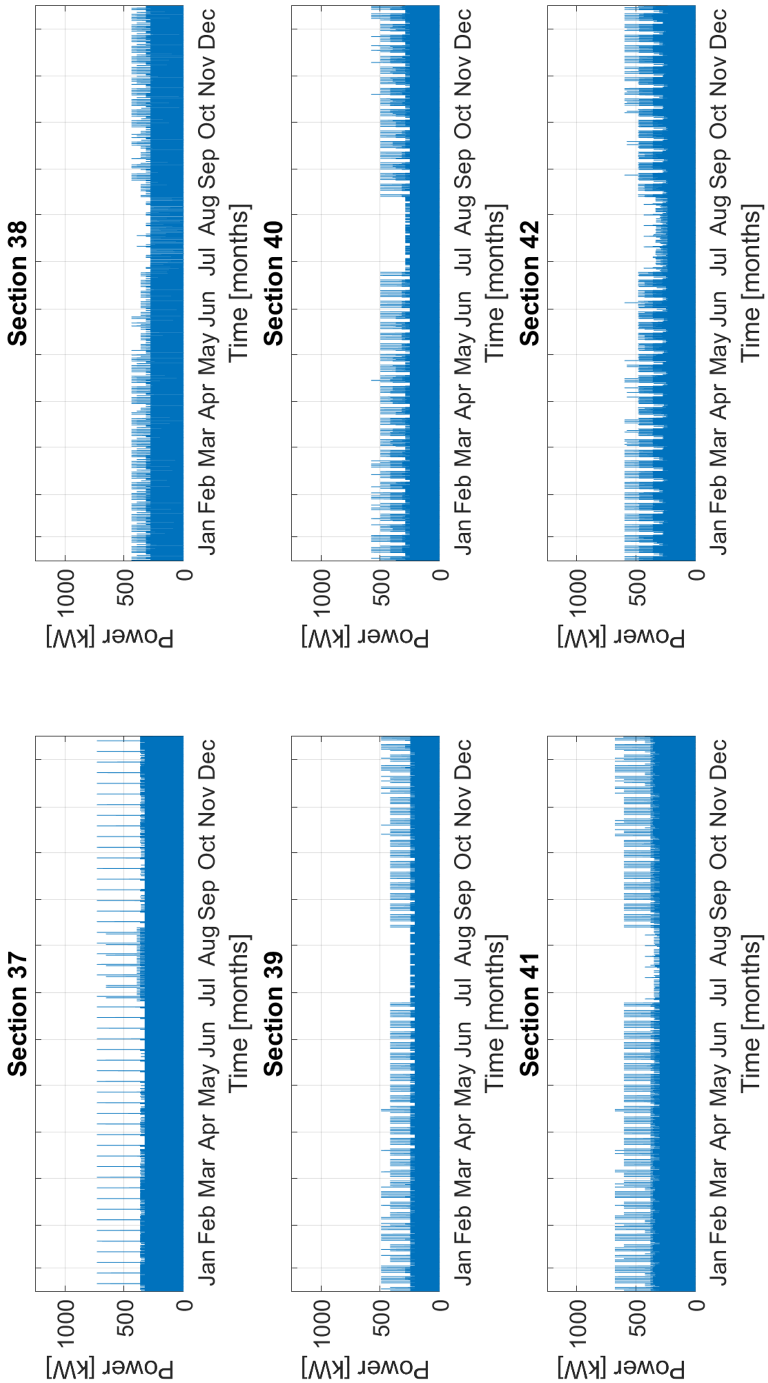
Section 37
Section 38
Section 39
Section 40
Section 41
Section 42
Power [kW]
1000
500
0
Jan Feb Mar Apr May Jun Jul Aug Sep Oct Nov Dec
Time [months]

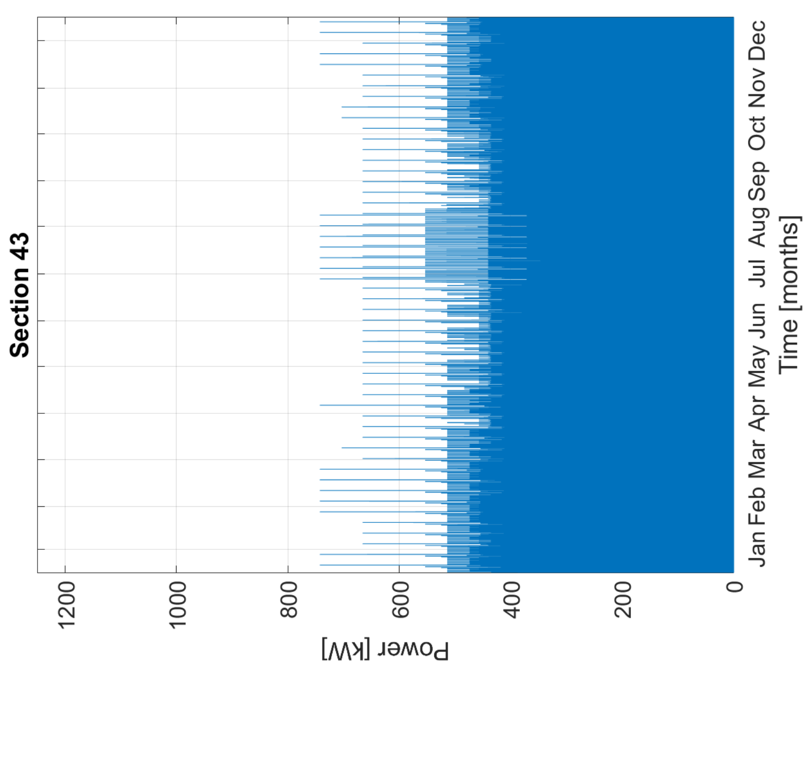

Section 43
Power [kW]
0
200
400
600
800
1000
1200
Jan Feb Mar Apr May Jun Jul Aug Sep Oct Nov Dec
Time [months]

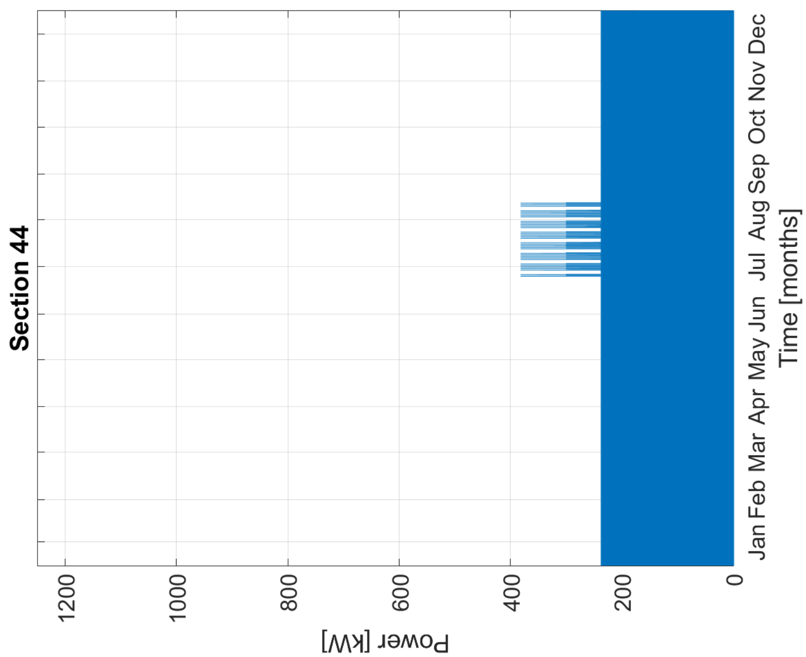

Section 44
Power [kW]
0
200
400
600
800
1000
1200
Jan Feb Mar Apr May Jun Jul Aug Sep Oct Nov Dec
Time [months]

E.2 Substation power profiles

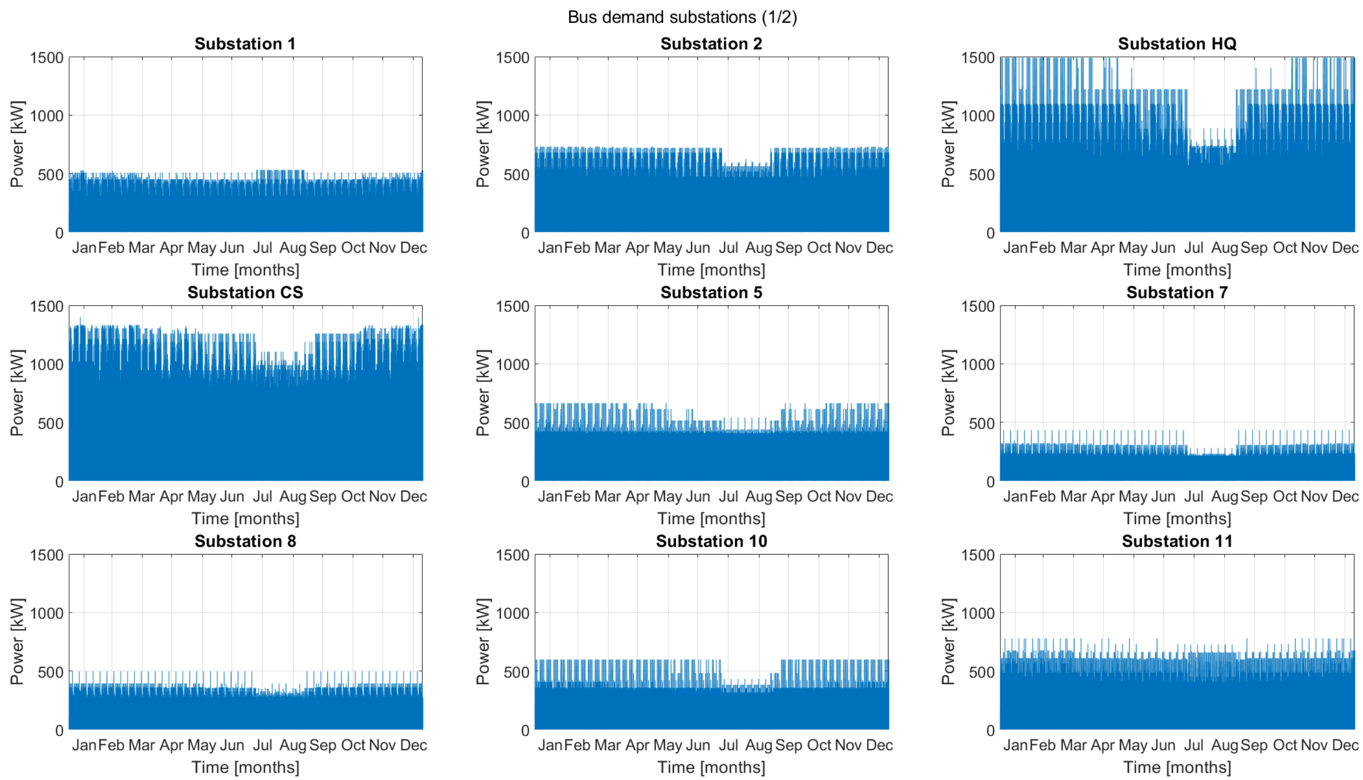
Bus demand substations (1/2)
Substation 1
Substation 2
Substation HQ
Substation CS
Substation 5
Substation 7
Substation 8
Substation 10
Substation 11
Power [kW]
0
500
1000
1500
Jan Feb Mar Apr May Jun Jul Aug Sep Oct Nov Dec
Time [months]

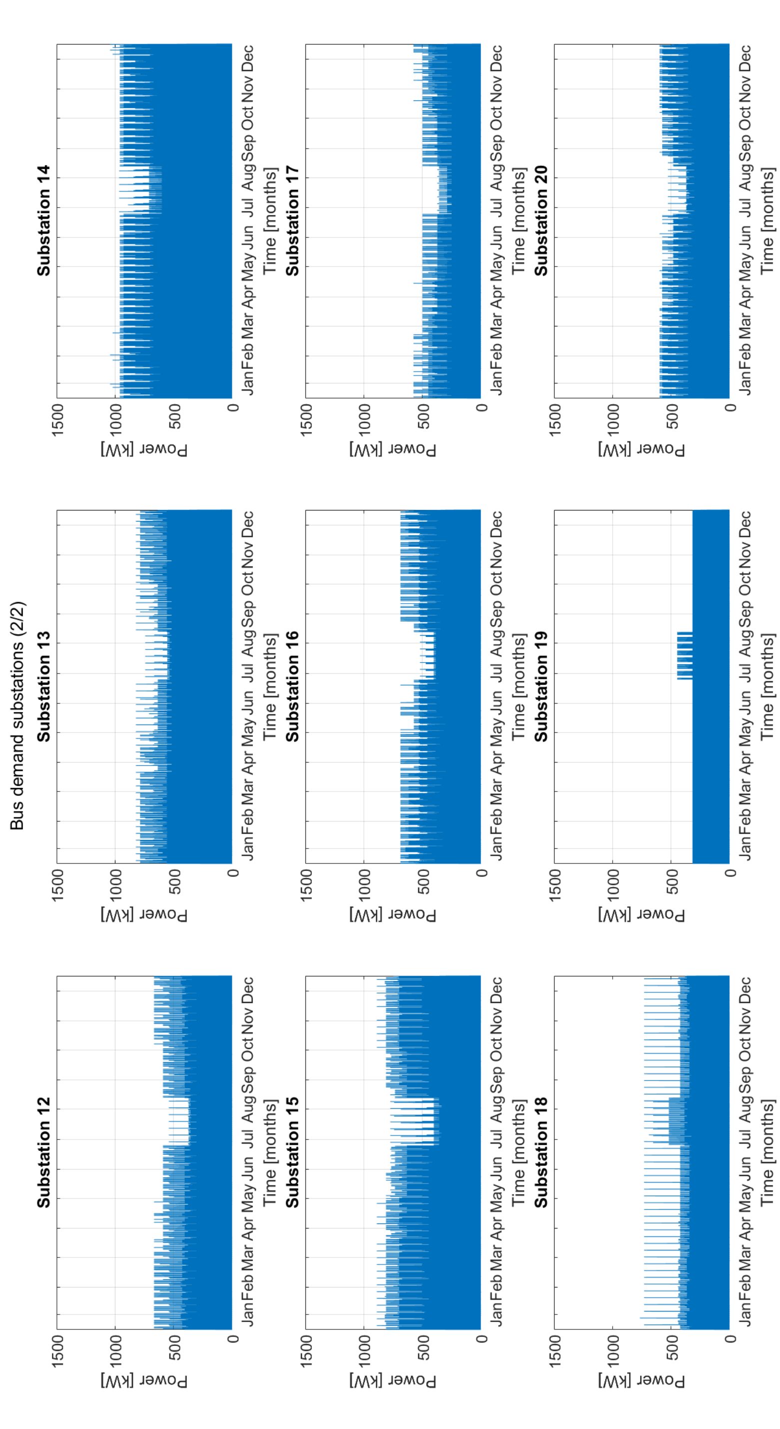
Bus demand substations (2/2)
Substation 12
Substation 13
Substation 14
Substation 15
Substation 16
Substation 17
Substation 18
Substation 19
Substation 20
Power [kW]
Time [months]
Jan Feb Mar Apr May Jun Jul Aug Sep Oct Nov Dec
0
500
1000
1500

Appendix F: Meteorological input parameters

In this appendix the meteorological data that has been used in this work is presented. The radiation data, the locations that were used are; Wageningen(16km, NL), De Bilt(49km, NL), Bocholt (48km, DE), Cabauw(65km, NL), Bochum(113km, DE) and Osnabrueck (151km, DE). For the temperature data, the following locations have been used: Deelen (7km, NL), Kalkar (39km, DE), Soesterberg (45km, NL), Volkel (41km, NL), De Bilt and Hupsel (53km, NL). The selection of stations and the interpolation has been automatically carried out by Meteonorm. Furthermore, the data ha a resolution of one minute and is based on a data set from 2000 to 2009 for temperature variables and 1991 to 2010 for the irradiance data. Meteonorm generates realistic data by applying a stochastic model to the data.

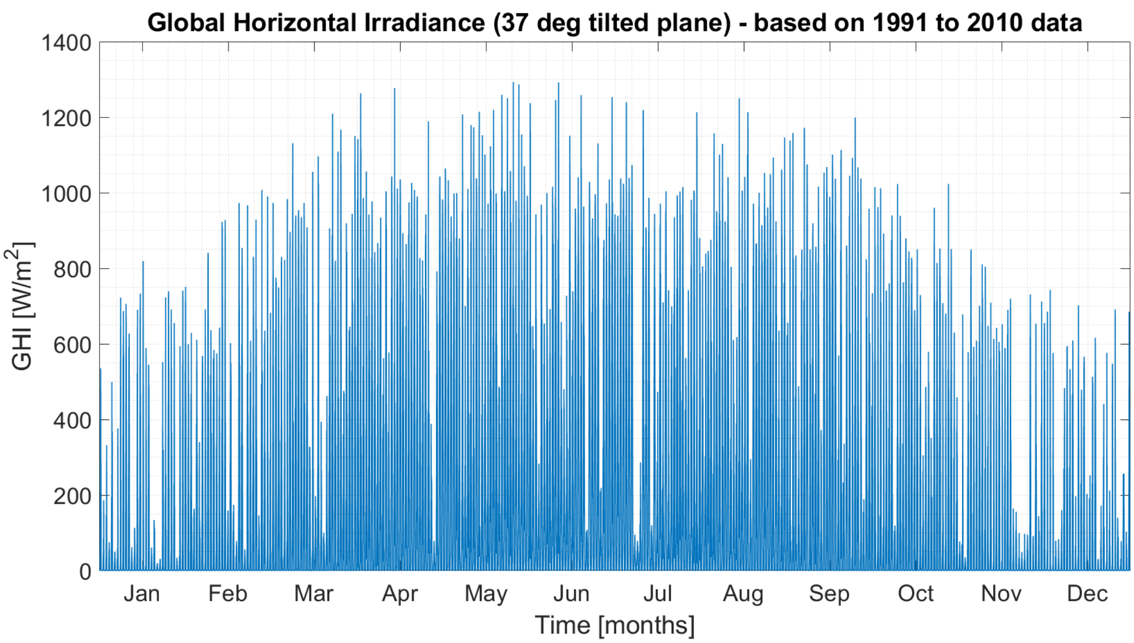

Figure F.1: GHI Arnhem - based on 1991 to 2010 data

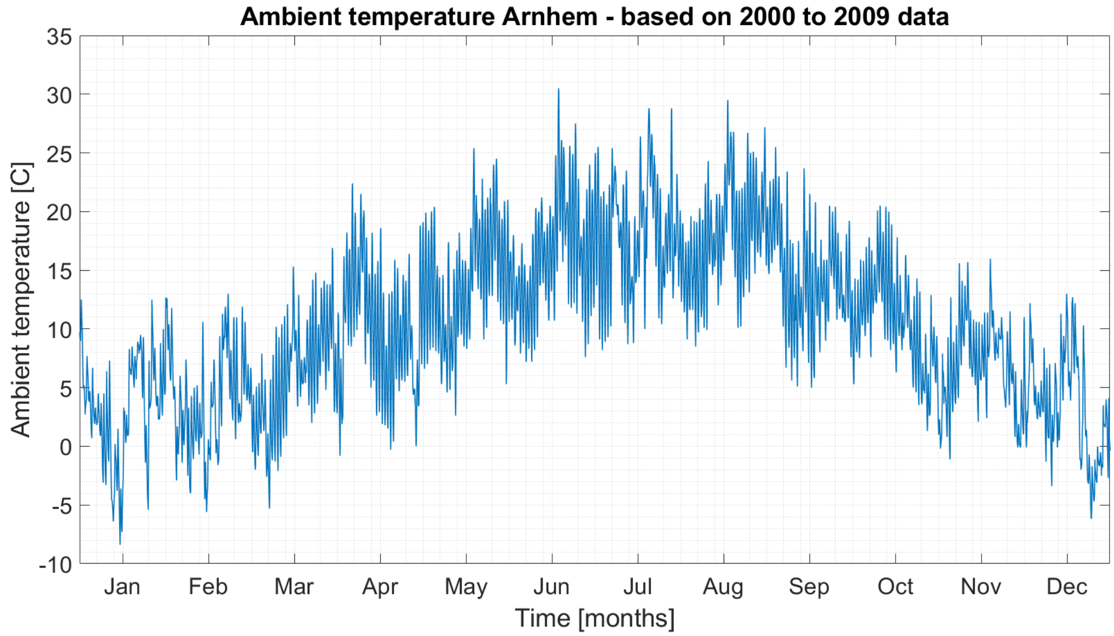

Figure F.2: Ambient temperature Arnhem - based on 2000 to 2009 data

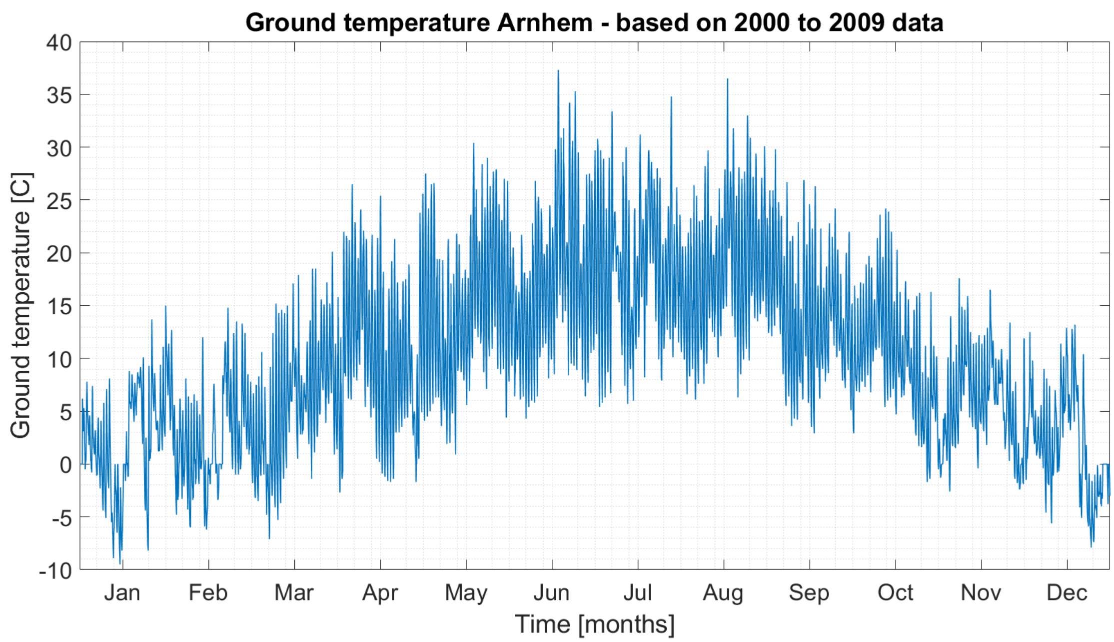

Figure F.3: Ground temperature Arnhem - based on 2000 to 2009 data

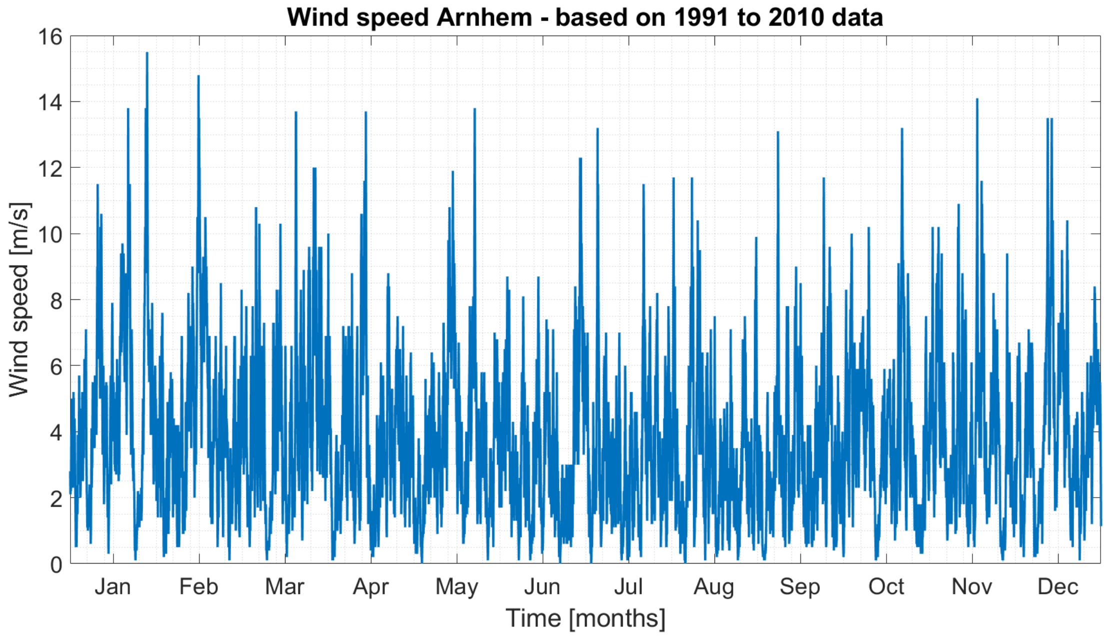

Figure F.4: Wind speed Arnhem - based on 1991 to 2010 data

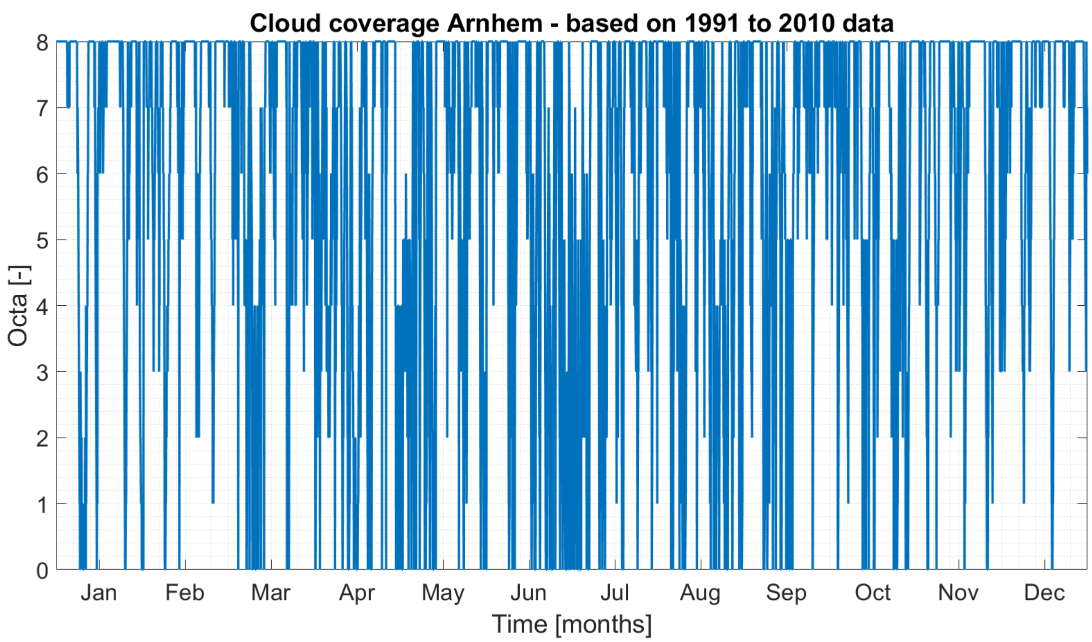

Figure F.5: Cloud coverage Arnhem - based on 1991 to 2010 data

The next plot shows the wind speed scaled with the log and power law from 10m to 60m to 90m.

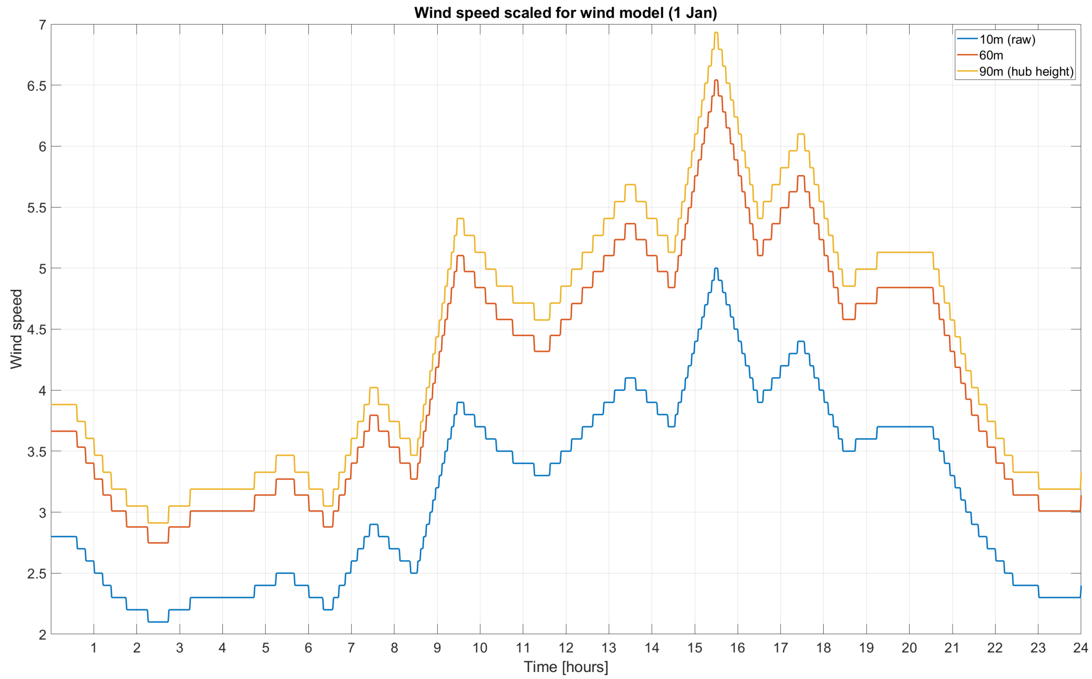

Figure F.6: Example of wind speed at 10m, 60m and 90m

Appendix G: PV module specification sheet

AstroSemi™

Incredible Power for Small Body

355W~365W

Monocrystalline PV Module

CHSM60M(BL)-HC Series (166)

Tier 1	No.1		DNV GL
Bloomberg	PHOTON	Underwritten by International Insurer	2020 TOP Performance

12-year Warranty for Materials and Processing

25-year Warranty for Extra Linear Power Output

(1st year ≤ 2.0%, 2nd~25th years ≤ 0.55% / year)

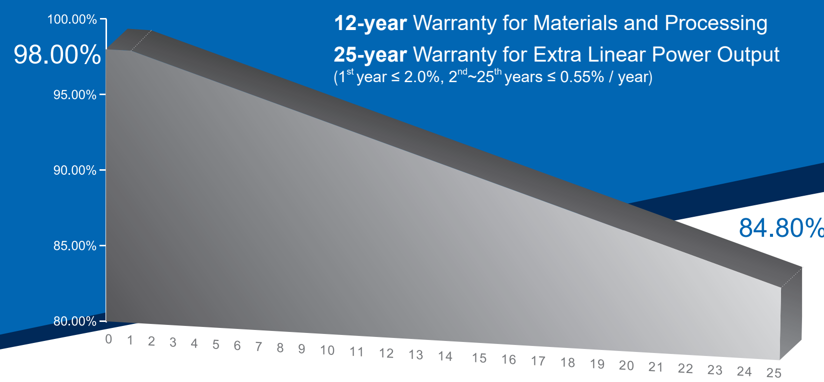

KEY FEATURES

+5W **OUTPUT POSITIVE TOLERANCE**
Guaranteed 0~+5W positive tolerance ensures power output reliability.

INNOVATIONAL HALF-CELL TECHNOLOGY
Improves the module output, decreases the risk of mirco-crack, enhances the module reliability.

PERC **INNOVATIVE PERC CELL TECHNOLOGY**
Excellent cell efficiency and output.

REDUCE SHADOW LOSS
Effectively reduces the effect of shadow on the module surface.

REDUCE INTERNAL MISMATCH LOSS
Reduces mismatch loss and improves output.

THE-STATE-OF-THE-ART APPEARANCE
Full black designed for a better aesthetic appearance and building integration.

Anti PID **PID RESISTANCE**
Excellent PID resistance at 96 hours (@85℃ /85%) test, and also can be improved to meet higher standards for the particularly harsh environment.

COMPREHENSIVE CERTIFICATES

TÜVRheinland CERTIFIED | CE | ISO 9001 | ISO 14001 | OHSAS 18001

CNAS | SATELLITE Intertek | TÜV NORD IEC TS 62941

First solar company which passed the TUV Nord IEC/TS 62941 certification audit.

For Global Market

ASTRONERGY
A CHNT COMPANY

ELECTRICAL SPECIFICATIONS

STC rated output (P_{mpp})*	355 Wp	360 Wp	365 Wp
Rated voltage (V_{mpp}) at STC	33.24 V	33.49 V	33.73 V
Rated current (I_{mpp}) at STC	10.68 A	10.75 A	10.82 A
Open circuit voltage (V_{oc}) at STC	39.80 V	40.14 V	40.41 V
Short circuit current (I_{sc}) at STC	11.15 A	11.21 A	11.29 A
Module efficiency	19.2%	19.5%	19.7%
Rated output (P_{mpp}) at NMOT	264.7 Wp	268.5 Wp	272.2 Wp
Rated voltage (V_{mpp}) at NMOT	30.99 V	31.22 V	31.45 V
Rated current (I_{mpp}) at NMOT	8.54 A	8.60 A	8.65 A
Open circuit voltage (V_{oc}) at NMOT	37.42 V	37.74 V	37.99 V
Short circuit current (I_{sc}) at NMOT	8.97 A	9.02 A	9.08 A
Temperature coefficient (P_{mpp})	- 0.34%/°C		
Temperature coefficient (I_{sc})	+0.04%/°C		
Temperature coefficient (V_{oc})	- 0.27%/°C		
Nominal module operating temperature (NMOT)	44±2°C		
Maximum system voltage (IEC/UL)	$1000V_{DC}$		
Number of diodes	3		
Junction box IP rating	IP 68		
Maximum series fuse rating	20 A		

STC: Irradiance 1000W/m^2, Cell Temperature 25°C, AM=1.5
NMOT: Irradiance 800W/m^2, Ambient Temperature 20°C, AM=1.5, Wind Speed 1m/s

CURVE

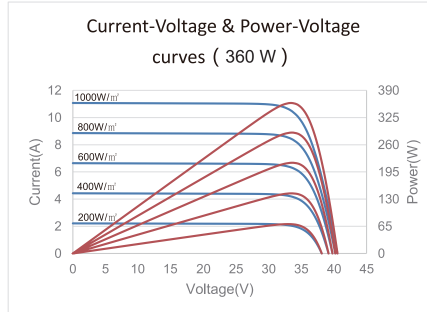

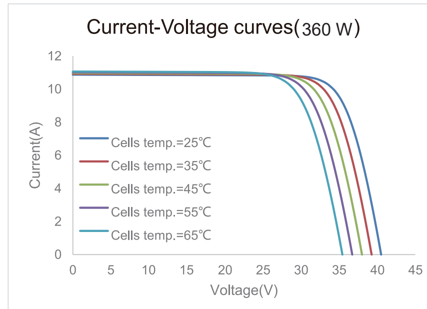

MECHANICAL SPECIFICATIONS

Outer dimensions (L x W x H)	1765 x 1048 x 35 mm
Frame technology	Aluminum, black anodized
Module composition	Glass / EVA / Backsheet (black)
Front glass thickness	3.2 mm
Cable length (IEC/UL)	Portrait: 350 mm Landscape: 1200 mm
Cable diameter (IEC/UL)	4 mm² / 12 AWG
① Maximum mechanical test load	5400 Pa (front) / 2400 Pa (back)
Fire performance (IEC/UL)	Class C (IEC) or Type 1 (UL)
Connector type (IEC/UL)	MC4 compatible

① Refer to Astronergy crystalline installation manual or contact technical department.
Maximum Mechanical Test Load=1.5×Maximum Mechanical Design Load.

PACKING SPECIFICATIONS

① Weight (module only)	20.0 kg
② Packing unit	31 pcs / box
Weight of packing unit (for 40'HQ container)	661 kg
Number of modules per 40'HQ container	806 pcs

① Tolerance +/- 1.0kg
② Subject to sales contract

MODULE DIMENSION DETAILS

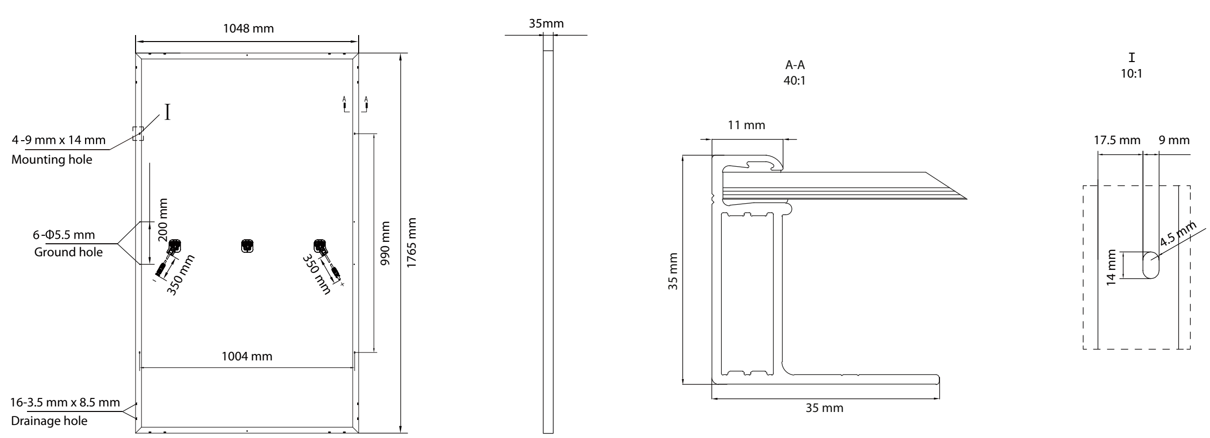

Appendix H: Future work insights

H.1 Literature

Trolley grids experience voltage drops due to the large peaks in loads and the low voltage of the overhead lines. It is not the aim of this work to improve the robustness of the overhead lines, but the simulations of the bus load and the bus traffic may be used for this in the future. With this in mind, the following literature may be useful for future work.

A paper by the University of Wuppertal, by M. Wazifehdust et al. goes in depth about the placement of PV into the Solingen grid [22]. First an empty LVDC test grid is modeled, then the substations are added and the PV is added to all nodes that can support PV. Afterwards the bus traffic is simulated according to the timetables. Then the 'zone of influence' (ZoI) of the PV panels is determined. ZoI is non-specifically defined by the authors as *To what 'extend' a solar PV panel can power a load.* The ZoI is determined in three different ways;

1. Based on a set distance between the solar PV and the load (max 500m).
2. Based on a maximum voltage difference between the solar PV and the loads
3. Based on maximum power losses that may occur between the solar PV and the loads.

The first way of calculating the ZoI is rather simplistic, but this method does not take into account the cross-sectional area of the overhead lines. The cross-sectional area influences the resistance that the lines have and therefore affect the losses of the power. See Equation H.1, for a reminder of this relation.

$$R_{\text{wires}} = \rho * \frac{l}{A} \tag{H.1}$$

Where R_{wires} is the resistance of the wires, ρ is the specific resistance of the cable in ohm per meter, l is the length of the wires and A is the cross-sectional area of the wires.

The problems with this simple method are that the losses of the PV to the load may differ for each 500m and that the sections in the Arnhem grid are at most 1.5km. Therefore, this method would allow too few places to put the solar PV and thus yield a poor optimization.

Method two and three take the resistance into account, but determine this resistance in different ways.

In the second method, first the current coming from the solar panels during rated performance is calculated.

$$I_{\text{PV}} = \frac{P_{\text{PV}}}{V_{\text{PV}}} \tag{H.2}$$

Then the maximum allowable voltage difference between the solar PV and the loads is arbitrarily established. The maximum resistance is then calculated by dividing this voltage difference by the maximum current from the PV panels. See equation H.3.

$$R = \frac{\Delta V}{I_{\text{PV}}} \tag{H.3}$$

In the third method, the ZoI is determined based on the maximum allowable losses.

First the maximum current from the PV panels is calculated (see equation H.2. Then the maximum relative losses (ν) are arbitrarily defined. The maximum lost power can then be calculated by multiplying ν with the power through wires. See equation H.4.

$$P_{\text{losses}} = P * \nu \tag{H.4}$$

Finally, the maximum resistance can then be calculated by dividing the maximum power losses by the maximum current squared.

$$R = \frac{P_{\text{losses}}}{{I_{\text{PV}}}^2} \tag{H.5}$$

After establishing the ZoI of the solar PV, the theoretical power that nodes can deliver determined. This was done by comparing the *ideal PV power profile* with the feed-in-power of the nodes (which depends on the ZoI). The lower the resistance (or distance for method 1), the higher the feed-in-potential of the PV. Finally, the nodes were selected to which the PV should be connected. This was done by summing the Feed-In-Power (FIP) of the nodes for each ZoI and then checking which node has the largest feed-in-potential.

The authors then proceeded to size the solar PV. They did this with the objective of maximizing the utilization of the PV. First, they summed all the FIP's for a ZoI for all nodes. This is the ideal amount of power that all nodes can deliver within a specfic ZoI, refered to as the feed-in-power profile of a ZoI. Then the PV sizes of each node were changed. This was done to change the feed-in-power profile in such a way that most of the power in that ZoI was delivered by the PV instead of the substation. To determine the relative input of PV to the total input, a utilization factor was introduced. See equation H.6.

$$U = \frac{P_{\text{PV}}}{P_{\text{Total}}} \tag{H.6}$$

Here U is the utilization factor. The sizes of all PV nodes were iterated, so that U is maximized.

This seems like a promising approach, however the validation of their model is lacking, since the authors do not show the timetable of the buses or the power coming from each node. They only conclude that a utlization factor of 90% could be reached with a total PV size of 100kWp. Moreover, the effects of the PV on the grid characteristics are not discussed.

In [24] the team goes in-depth in finding the optimal placement for stationary storage with integrated solar PV. A case study on the trolleybus grid of Solingen is conducted to validate the model. Storage is necessary for the Solingen grid, because the grid - just like the Arnhem grid - is unidirectional. This means that no excess energy can be fed into the MVAC grid. First the powerflows in the grid are computed, by executing their Adapted Newton Raphson power flow algorithm (ANR). [40]. The outputs of the ANR are the voltages of all the nodes in the network and the branch resistances. The current between storage node x and node k can be calculated by dividing the differences between the node voltages by the resistance of the branch, see equation H.8.

$$I_{xk} = \frac{\Delta V_{xk}}{R_{xk}} \tag{H.7}$$

The authors go on to establish the maximum current that may be caused by operation of the storage by subtracting the current I_{xk} from the maximum allowed current on that branch $I_{xk,\max}$.The actual current coming from the storage is limited by the branch with the lowest current margin ($\Delta I_{\min}$).

$$\Delta I_{xk} = I_{xk,\max} - I_{xk} \tag{H.8}$$

The authors then used this calculated current to perform a sensitivity analysis, instead of performing an additional ANR. First they checked the voltage of node k. If this voltage was at least 5% higher than the nominal voltage, the storage medium is discharging and if the voltage is at least 5% lower than the nominal voltage, the storage medium is charging. Within the 5% ranges, the storage medium is assumed to be not operating. The voltage change of node k is determined by multiplying the current moving from or towards the node by the *sensitivity matrix*. This is the inverse of the *admittance matrix*. The sensitivity matrix is basically the resistance of the branches and the nodes connected to node k.

$$\Delta V_k = \mathbf{S} * \Delta I_k \tag{H.9}$$

where

$$\Delta I_k \leq \Delta I_{xk,\min} \tag{H.10}$$

By adding ΔV_k to V_k, $V_{k,\text{new}}$ was established. This new voltage should of course remain below the rated voltage and above the minimum voltage. The power from or to node k can be calculated by multiplying the new voltage with the current.

$$P_{k,\text{storage}} = V_{k,\text{new}} * \Delta I_k \tag{H.11}$$

Finally, the authors introduce two constraints to optimize the storage. Constraint **A** is the maximization of the usage of the storage medium. This is done by maximizing the absolute energy that flows in and out of the storage medium by integrating the power flow for all simulation times. Constraint **B** minimizes the difference between the overall energy flowing in to the storage and out of the storage. This constraint was necessary to have a similar *state of charge* at the beginning and end of the simulation. The state of charge is how much the storage medium is charged as a fraction of the maximum energy that the medium can store. Since the model cannot be optimal for both constraints at the same time, weights were introduced.

$$\textbf{A} \text{ maximize } E_{k,\text{abs}} = \sum_0^t \left| P_{k,\text{storage}(t))} \right| \tag{H.12}$$

$$\textbf{B} \text{ minimize } E_{k,\text{nom}} = \sum_0^t \left| P_{k,\text{storage}(t))} \right| \tag{H.13}$$

This article gives interesting insights in the placement methodologies for the storage. Furthermore, the constraints can be used to approximate the power from or towards the storage medium. This is interesting, when the utilization of the storage medium is to be minimized. The approach proposed here could be interesting for the storage placement on the DC-side. Especially, if the PV and the storage are not at the same location and the overhead lines have to be shared for power transfer. However - for the AC-side placement - line sharing does not occur. The storage sizing constraints could still prove useful for the AC-side placement.

PV in LVDC may give fluctuations in voltage, if the MPPT response time is too quickly.

H.2 Approach for relating storage size to time scale

In figure H.1 and 5.6 this is shown for substation HQ (high traffic) and substation 10 (low traffic), respectively. The system sizes are shown in table H.1.

Table H.1: PV system sizes for substation HQ (high traffic) and substation 10 (low traffic)

Size	Substation HQ (kWp)	Substation 10 (kWp)
1.0 EN	746	120
0.9 EN	671	108
0.8 EN	596	96
0.7 EN	522	84
0.6 EN	448	72
0.5 EN	373	60

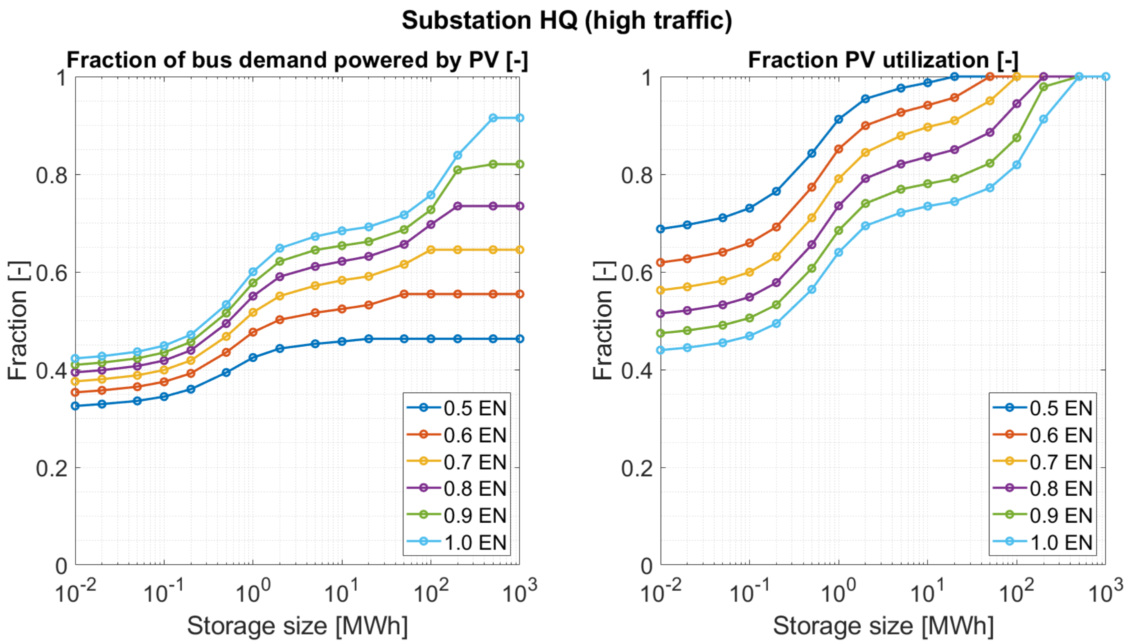

Figure H.1: PV impact as a function of PV size and storage size - substation HQ

What is interesting from both plots are the two knee points that occur at different storage sizes. This raised the question if these storage sizes can be related to time scales of the mismatch between PV generation and bus load. The time that storage can be used depends on the magnitude of the mismatch between generation and load. However, in this work, average storage sizes for a range of time scales are approximated. Moreover, the analysis is limited to the energy neutral PV systems.

Since the annual energy output of the PV system is by design equal to the annual load of the buses. It is not possible to take the mean of an average for a time period for the whole year, since this will be zero. To work around this, we could define a relevant time window in the year for which the storage system is sized. In this work, this time window is found by taking the average from PV generation minus bus load with an average per day for the whole year. The result is shown in figure H.2.

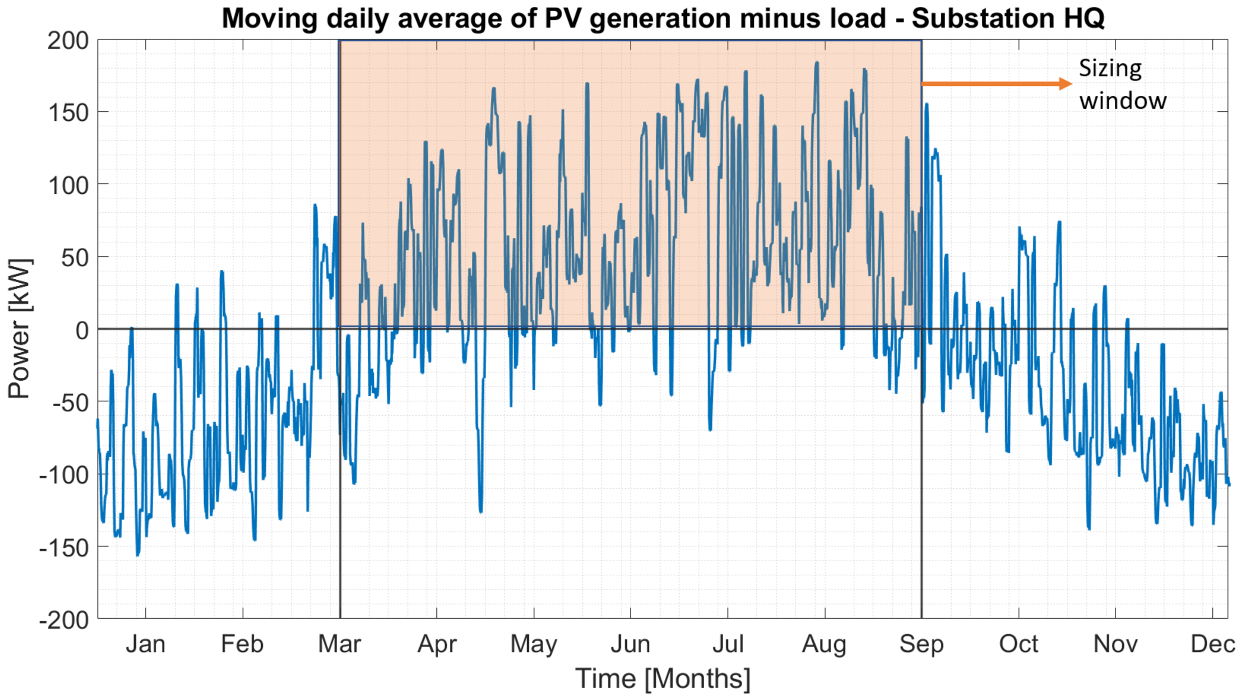

Figure H.2: Moving daily average PV generation minus load - Substation HQ

From the figure it can be approximated that the time that PV generation is larger than the bus load is from mid March till mid September. Since the purpose of the storage is to store the excess energy of the PV, the storage window is between mid March and Mid September. Next, the average storage energy for the following time scales *second, minute, hour, day, week and month* is approximated with equation H.14.

$$\mathrm{E}_{\mathrm{storage}} = \frac{\mathrm{mean}(\mathrm{PV}_{\mathrm{subs}} \bar{-} \mathrm{Load}_{\mathrm{subs}}) \cdot t}{0.375 \cdot 3.6 * 10^6} \tag{H.14}$$

Here $\mathrm{mean}(\mathrm{PV}_{\mathrm{subs}} \bar{-} \mathrm{Load}_{\mathrm{subs}})$ denotes the mean of the mismatch of the average of the time scale within the time window. For example, for the minute time scale, first the average for the minute mismatch between mid March and mid September is calculated, then the mean of this average is taken. To get the mismatch per minute this mismatch needs to be multiplied by 60. Now we have the energy that should be stored in kJ. The final two steps are to convert it to MWh and divide it by 0.375. This division by 0.375 is done because of the assumption that the storage system is half full at the beginning of charging (LL = 0.2, UL = 0.95, SoC = 0.575). The result is an approximation of the average storage size required to store the mismatch between generation and load for one minute. This process is repeated for the other time scales and the results are shown on the top x-axis in figure H.3 for energy neutral PV systems. The top x-axis therefore does not show time, but it shows the average time that the storage could sustain the bus load in the sizing window. The storage size is shown on the bottom x-axis. The aim of these plots is to identify for what time range the PV should be installed, in this time range the variation in load and the variation in PV are minimal and the storage is optimally utilized.

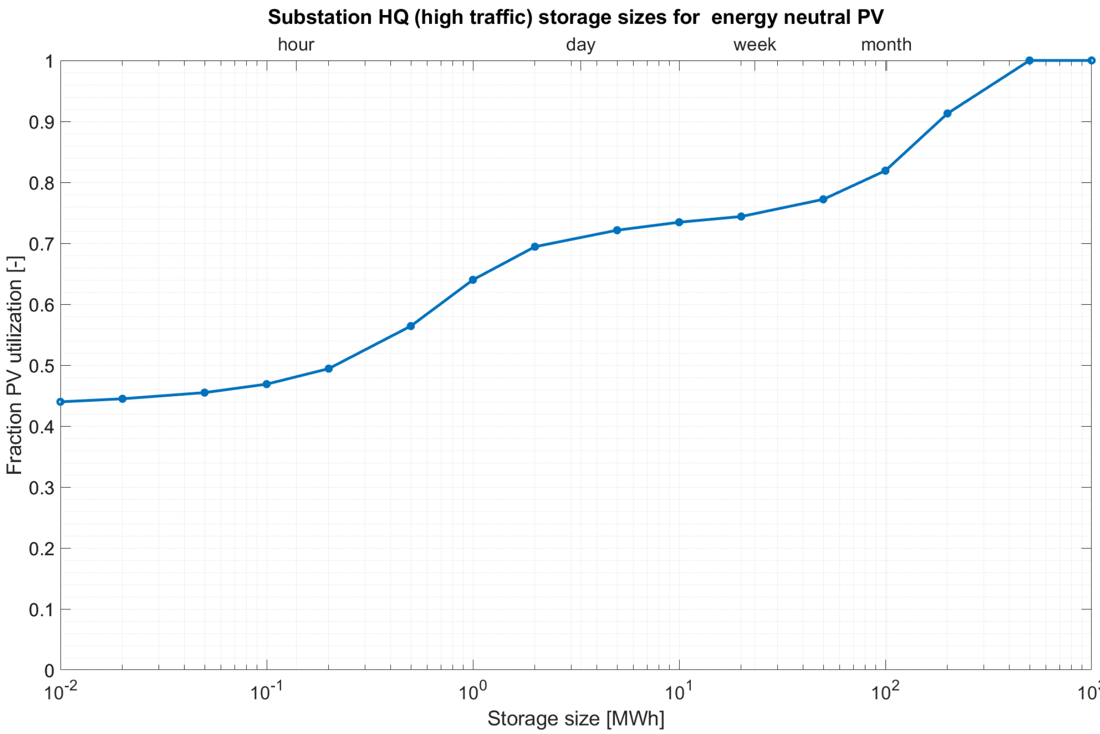

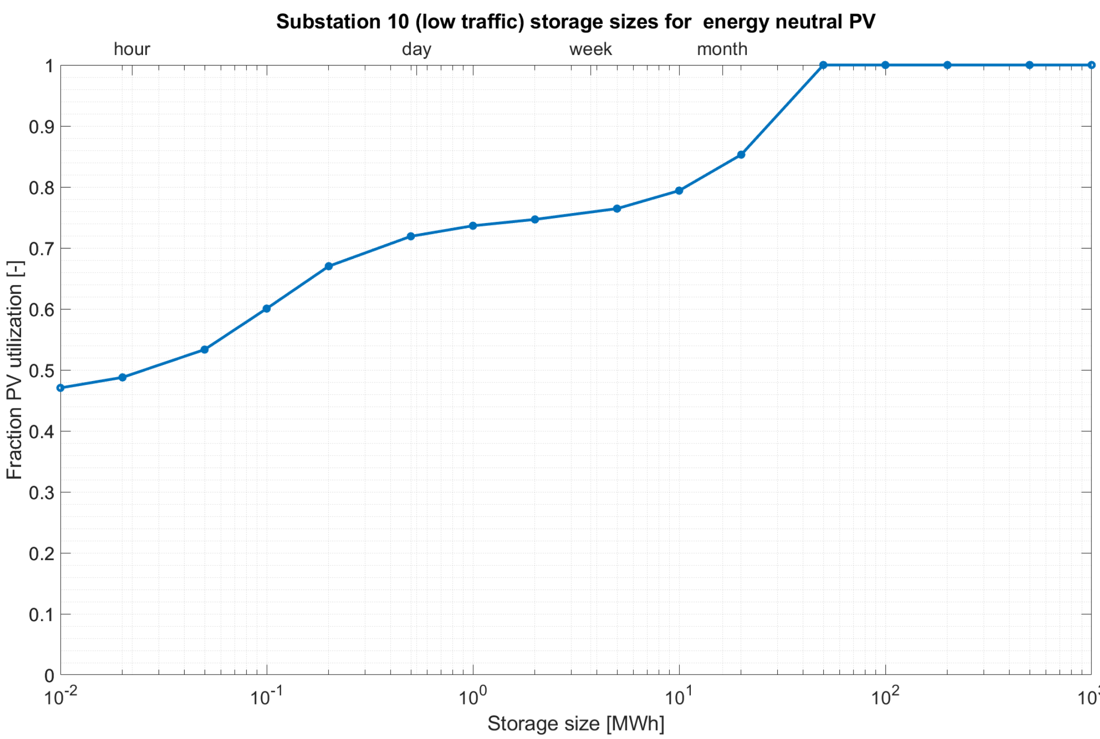

Figure H.3: Storage sizes for energy neutral PV systems

In both plots there are two areas for storage sizes that are promising. One is in the hour-day range, this is because the hourly generation of the PV and the bus load are relatively constant throughout the year. Therefore storage in this size range may be used throughout large parts of the year. Another area is in the month storage range. For small PV systems this may be an option, but for large PV systems investing in these storage sizes is too expensive.